Studies on the Dynamics of Solvation and Rotational Relaxation of Some Well-known Dipolar Fluorescent Probes in Room Temperature Ionic Liquids

BY

SUDHIR KUMAR DAS
CHEM07201004004

National Institute of Science Education and Research
Bhubaneswar, Odisha-751005

A thesis submitted to the
Board of Studies in Chemical Sciences
In partial fulfillment of requirements
For the degree of

DOCTOR OF PHILOSOPHY

of

HOMI BHABHA NATIONAL INSTITUTE

April, 2014

Name : Mr. SUDHIR KUMAR DAS ; HBNI REGISTRATION NO.: CHEM07201004004

Title : " STUDIES ON THE DYNAMICS OF SOLVATION AND ROTATIONAL RELAXATION OF SOME WELL-KNOWN DIPOLAR FLUORESCENT PROBES IN ROOM TEMPERATURE IONIC LIQUIDS"

Homi Bhabha National Institute[1]

Recommendations of the Viva Voce Committee

As members of the Viva Voce Committee, we certify that we have read the dissertation prepared by <Candidate Name> entitled <" Title" > and recommend that it may be accepted as fulfilling the thesis requirement for the award of Degree of Doctor of Philosophy.

Prof. A. SRINIVASAN
Chairman - <Name>   Date: 19.06.14

Dr. MOLOY SARKAR
Guide / Convener - <Name>   Date: 19.06.14

_____
Co-guide - <Name> (if any)   Date: 19.06.14

Prof. ANUNAY SAMANTA
Member 1 - <Name>   Date: 19.06.14

Dr. SUDIP BARMAN
Member 2- <Name>   Date: 19.06.14

Dr. ARINDAM GHOSH
Member N - <Name>   Date: 19.06.14

_____

Final approval and acceptance of this thesis is contingent upon the candidate's submission of the final copies of the thesis to HBNI.

I/We hereby certify that I/we have read this thesis prepared under my/our direction and recommend that it may be accepted as fulfilling the thesis requirement.

Date: 19.06.2014

Place: Bhubaneswar   <Signature>   <Signature>

                         Co-guide (if applicable)   Guide

_____
[1] This page is to be included only for final submission after successful completion of viva voce.

STATEMENT BY AUTHOR

This dissertation has been submitted in partial fulfillment of requirements for an advanced degree at Homi Bhabha National Institute (HBNI) and is deposited in the Library to be made available to borrowers under rules of the HBNI.

Brief quotations from this dissertation are allowable without special permission, provided that accurate acknowledgement of source is made. Requests for permission for extended quotation from or reproduction of this manuscript in whole or in part may be granted by the Competent Authority of HBNI when in his or her judgment the proposed use of the material is in the interests of scholarship. In all other instances, however, permission must be obtained from the author.

Sudhir Kumar Das

DECLARATION

I, hereby declare that the investigation presented in the thesis has been carried out by me. The work is original and has not been submitted earlier as a whole or in part for a degree / diploma at this or any other Institution / University.

Sudhir Kumar Das

List of Publications

1. *Solvation and rotational relaxation of coumarin153 and 4-aminophthalimide in a new hydrophobic ionic liquid: Role of N–H. . . F interaction on solvation dynamics. **Das, S. K.**; Sarkar, M. *Chem. Phys. Lett.* **2011**, *515*, 23-28.

2. Investigating the interaction of a nitrobenzoxadiazole derivative with metal ions: photophysical and theoretical (DFT) study. **Das, S. K.**; Patra, A. S.; Jose, D.; Sarkar, M. *Chem. Phys. Lett.* **2012**, *528*, 11-15.

3. Photophysical and density functional studies on the interaction of a new nitrobenzoxadiazole derivative with anions. **Das, S. K.**; Mishra, S. S.; Sahu, P. K.; Nijamudheen, A.; Mohan, V.; Sarkar, M. *Chem. Phys. Lett.* **2012***, 546*, 90-95.

4. *Studies on the solvation dynamics of coumarin153 in 1-ethyl-3-methylimidazolium alkylsulfate ionic liquids: Dependence on alkyl chain length. **Das, S. K.**; Sarkar, M. *ChemPhysChem* **2012**, *13*, 2761-2768.

5. Ion interactions with a new ditopic naphthalimide-based receptor: A photophysical, NMR and theoretical (DFT) Study. Mohan, V.; Nijamudheen, A.; **Das, S. K.**; Sahu, P. K.; Kar, U. P. ; Rahaman, A.; Sarkar, M. *ChemPhysChem* **2012**, *13*, 3882-3892.

6. *Rotational dynamics of coumarin-153 and 4-aminophthalimide in 1-ethyl-3-methylimidazolium alkylsulfate ionic liquids: effect of alkyl chain length on the rotational dynamics. **Das, S. K.**; Sarkar, M. *J. Phys. Chem. B* **2012***, 116*, 194-202.

7. *Steady-state and time-resolved fluorescence behavior of coumarin-153 in a hydrophobic ionic liquid and ionic liquid–toluene mixture. **Das, S. K.**; Sarkar, M. *J. Mol. Liq.* **2012**, *165*, 38-43.

8. *Solvation and rotational relaxation of coumarin 153 in a new hydrophobic ionic liquid: An excitation wavelength dependence study. **Das, S. K.**; Sarkar, M. *J. Lumin.* **2012***, 132*, 368-374.

9. *Diffusion−viscosity.decoupling in solute rotation and solvent relaxation of coumarin153 in ionic liquids containing fluoroalkylphosphate (FAP) Anion: A thermophysical and photophysical study. **Das, S. K.**; Sahu, P. K.; Sarkar, M. *J. Phys. Chem. B* **2013**, *117*, 634-647.

10. Synthesis, photophysics, live Cell imaging and aggregation behaviour of some structurally similar alkyl chain containing bromonaphthalimide systems: influence of alkyl chain length on the aggregation behaviour. Soni, M.; **Das, S. K.**; Sahu, P. K.; Kar, U. P.; Rahaman, A.; Sarkar, M. *J. Phys. Chem. C* **2013**, *117*, 14338-14347.

11. Picosecond solvation dynamics of coumarin153 in bis(1-methyl-1H-imidazol-3-ium-3-yl)dihydroborate cation containing room temperature ionic liquid and ionic liquid-DMF mixtures. Sahu, P. K.; **Das, S. K.**; Sarkar, M. *J. Ap. Sol. Chem. & Mod.* **2013**, *2*, 47-56.

12. *Probing the microscopic aspects of 1-butyl-3-methylimidazolium trifluoroacetate ionic liquid and its mixture with water and methanol: A photophysical and theoretical (DFT) study. **Das, S. K.**; Sahu, P. K.; Sarkar, M. *J. Fluoresc.* **2013**, *2*, 1217-1227.

13. Towards understanding solute-solvent interaction in room-temperature mono and dicationic ionic liquids: A combined fluorescence spectroscopy and mass spectrometry analysis. Sahu, P. K.; **Das, S. K.**; Sarkar, M. *J. Phys. Chem. B* **2014**, *118*, 1907-1915.

14. *Probing solute-solvent interaction in 1-ethyl-3-methylimidazolium-based room temperature ionic liquids: A time-resolved fluorescence anisotropy study. **Das, S. K.**; Sarkar, M. *J. Fluoresc.* **2014**, *24*, 455.

15. Fluorescence response of a dipolar organic solute in a dicationic ionic liquid (IL): Is the behavior of dicationic IL different from that of usual monocationic IL? Sahu, P. K.; **Das, S. K.**, Sarkar, M. *Phys. Chem. Chem. Phys.* **2014**, *16*, 12918.

*pertaining to the present thesis.

Conferences

1. "National Seminar on Frontiers in Chemistry", November 11-14, 2010, conducted at School of Chemical Sciences, National Institute of Science Education and Research (NISER), Bhubaneswar, India.

2. "Symposium in Chemistry", Chemical Research Society of India (CRSI-2011), February 4-6, 2011, conducted at Kalinga Institute of Industrial Technology (KIIT), Bhubaneswar, India.

3. "Indo-European Symposium on Frontiers of Chemistry", November 10-12, 2011, conducted at School of Chemical Sciences, National Institute of Science Education and Research (NISER), Bhubaneswar, India.

4. Symposium on "Radiation and Photochemistry (NSRP – 2011)", March 04-07, 2011, organised by "Indian Society for Radiation and Photochemical Sciences (ISRPS), Jodhpur, Rajasthan, India. Presented a poster entitled "Solvation and rotational relaxation of coumarin 153 and 4-aminophthalimide in a new hydrophobic ionic liquid: Role of N–H. . .F interaction on solvation dynamics".

5. "Trombay Symposium on Radiation and Photochemistry (TSRP-2012)", January 03-07, 2012, organised by "Indian Society for Radiation and Photochemical Sciences" (ISRPS), Mumbai, India. Presented a poster entitled "Studies on the solvation dynamics of coumarin 153 in 1-ethyl-3-methylimidazolium alkylsulfate ionic liquids: Dependence on alkyl chain length".
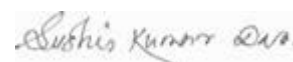
Sudhir Kumar Das

Dedicated to……

My Parents

ACKNOWLEDGEMENTS

CONTENTS

Chapter 3

Fluorescence Response of Coumarin 153 and 4-Aminophthalimide in Room Temperature Ionic Liquids: A Probe and Alkyl Chain Length Dependence Study

Chapter 4

Effect of Anions and Alkyl Chain Length on the Rotational Relaxation of Coumarin153 and 4-Aminophthalimide in Room Temperature Ionic Liquids

Chapter 5

Effect of Nonpolar and Polar Cosolvents on the Solute Rotation and Solvation Dynamics in Room Temperature Ionic Liquids

Chapter 6

Solute Rotation and Solvent Relaxation of Coumarin153 in Moderate and High Viscous Room Temperature Ionic Liquids: An Excitation Wavelength Dependence Study

SYNOPSIS

Room temperature ionic liquids (RTILs) have come up as a class of novel compounds primarily because of their interesting physicochemical properties like very low vapour pressure, wide liquid range, moderate to high viscosity, high ionic conductivity etc.[1-3] It has been observed that intermolecular interactions have profound influence on many physicochemical properties of liquids and solutions.[4] It is, therefore, important to have in-depth understanding of the various interactions that exist between the constituents of the RTILs and also their interaction with the added solutes so that they can be used to their full potential. In this context, studies on dynamics of solvation[5-13] and rotational relaxation of solutes[14, 15] have found to be quite useful in providing such information about medium. The main objective of the present thesis work is to explore solvation dynamics and rotational relaxation studies in a systematic manner in a variety of RTILs such that a comprehensive and quantitative understanding of the relationship among structure, intermolecular interaction and dynamics in ionic liquids is obtained.

Organization of thesis

The results obtained from different studies during current research investigations have been presented and discussed in this thesis, to be submitted to the Homi Bhabha National Institute for Ph.D. degree. For convenience of presentation, different aspects of the present thesis work have been discussed in a systematic manner in six different chapters. The contents of the different chapters of the present thesis are briefly described below.

Chapter 1: Introduction

This chapter starts with a brief description of RTILs and their different physicochemical properties. Applications of RTILs in chemical and biological sciences are also presented. A detailed discussion on different photophysical studies such as solvation dynamics, rotational relaxation dynamics and photoinduced electron transfer reactions in RTILs have been

described. The objective of the present work has also been discussed at the end of this chapter.

Chapter 2: Instrumentations and Methods

Brief descriptions of different instrumental techniques which have been used during the present investigation have been provided in this chapter. Working principle of the time-correlated single photon counting (TCSPC) technique has been demonstrated in details. Basic principles of the other instrumental techniques used in the present studies, such as absorption spectrophotometry, steady state spectrofluorimetry, have also been described briefly in this chapter. Various methodologies employed in the present study, such as data analysis procedure for construction of the time-resolved emission spectra from the decay curves, estimation of the solvation times and position of the time zero spectrum have also been discussed. Solvent purification techniques and experimental error limit are also provided in this chapter.

Chapter 3: Fluorescence Response of Coumarin 153 and 4-Aminophthalimide in Room Temperature Ionic Liquids: A Probe and Alkyl Chain Length Dependence Study

This chapter begins by discussing the effect of probe molecules on solvation dynamics.[7] Solvation dynamics being a solvent property is expected to be independent of the probe molecules used. However, there are significant variations of the solvation time depending on the probe.[8] One of the possible reasons for the probe dependent solvation dynamics may be specific solute-solvent interaction which affects the solvent reorganization time around the photoexcited probe. To understand the effect of solute-solvent interaction on solvation dynamics, we have carried out temperature dependent fluorescence response of Coumarin153 and 4-aminophthalimide in MOEMPLFAP (Chart 1).

Average solvation times for AP have been found to be six times higher than that of C153 (Figure1). Rotational coupling constants obtained from the rotational relaxation times also show a higher value for AP as compared to the same for C153. Theoretical investigation

15

reveals that N-H....F interaction between AP and anionic moiety of RTIL is primarily responsible for the slow solvation dynamics for AP.[16]

(A) Coumarin153 (C153)

(B) 4-aminophthalimide (AP)

(C) 1-(2-methoxyethyl)-1-methylpyrrolidinium tris(pentafluoroethyl)trifluorophosphate (MOEMPLFAP)
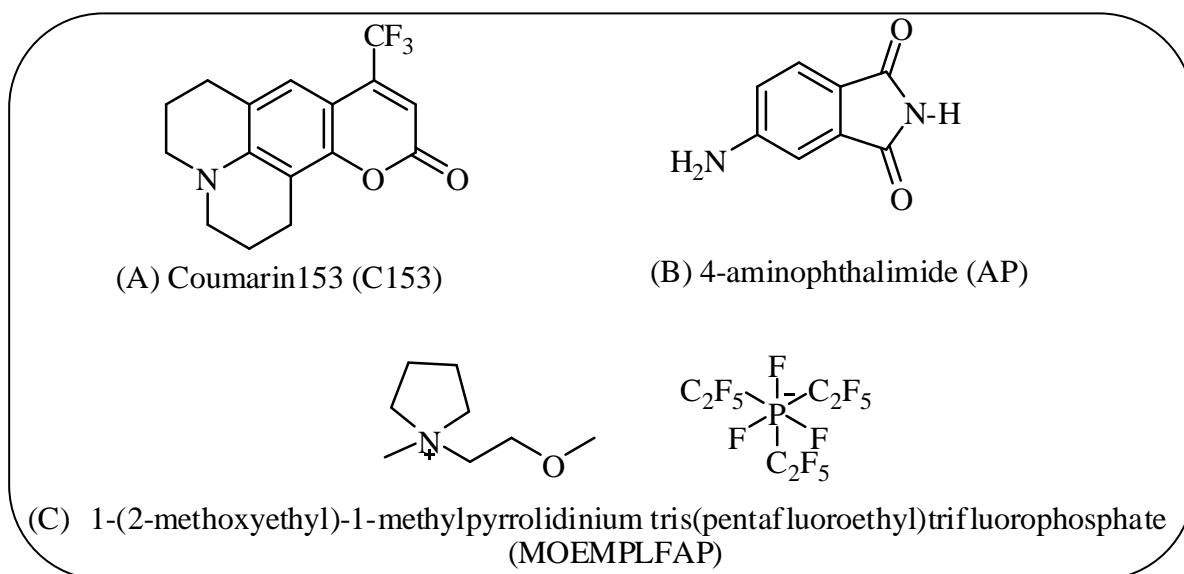
Chart 1. Molecular diagrams of (a) Coumarin153, (b) 4-aminophthalimide and (c) MOEMPLFAP.
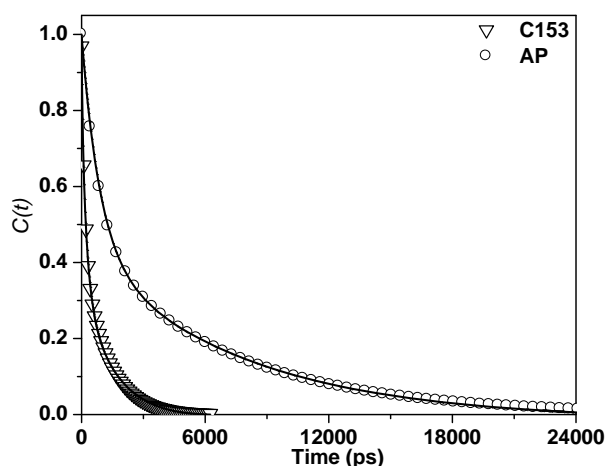
Figure 1. Decay of the spectral shift correlation function, *C(t),* of C153 and AP in MOEMPLFAP RTIL at 298 K at $\lambda_{exc.}$=375 nm. In both cases, symbols denote the experimental data points and solid lines represent the bi-exponential fit to the data points.

Although a large number of reports are available on solvation dynamics[5-13], limited number of studies on these aspects have been performed where systematic variations of the ionic constituents are made. To understand the effect of anionic alkyl chain length on the dynamics of solvation in RTILs, we have carried out studies on solvation dynamics in a series of 1-ethyl-3-methylimidazolium alkylsulfates (Chart 2) where chain length in the anion varied from butyl to octyl.

From the steady state behaviour, it has been found that C153 experiences more nonpolar character with increasing anionic alkyl chain length. A steady blue shift of the time-zero maximum of the time-resolved emission spectrum has also been found with increasing alkyl chain length which indicates that the probe molecule experiences a less polar microenvironment in the early part of the dynamics on going from butyl to octyl analogue. The average solvation time increases with increasing length of the alkyl side chain, and this is attributed to the increase in bulk viscosity of the RTILs with increasing alkyl chain length (Table 1).[17]

Table 1. Summary of the solvent relaxation parameters of C153 in 1-ethyl-3-methylimidazolium alkylsulfates at 298K.

RTILs	Vis.(cP)[a]	a_1	τ_1(ns)	a_2	τ_2(ns)	$\langle \tau_s \rangle$ (ns)[a]
EMIMBSU	141	0.70	0.42	0.30	1.39	0.71
EMIMHSU	284	0.65	0.43	0.35	2.48	1.15
EMIMOSU	453	0.61	0.42	0.39	2.98	1.42

[a]experimental error 5%.

Chapter 4. Effect of Anions and Alkyl Chain Length on the Rotational Relaxation of Coumarin153 and 4-Aminophthalimide in Room Temperature Ionic Liquids

This chapter describes the effect of various anions on the rotational relaxation dynamics of organic solutes. Specifically, the effects of H-bond basicity and alkyl chain lengths of anions on the rotational diffusion behavior of two well known fluorescent dipolar probes, C153 and AP (Chart 2, 3), have been discussed in this chapter.

1-ethyl-3-methylimidazolium (EMIM)   alkylsulfate

R= C_2H_5 (EMIMESU)
= C_4H_9 (EMIMBSU)
= C_6H_{13} (EMIMHSU)
= C_8H_{17} (EMIMOSU)
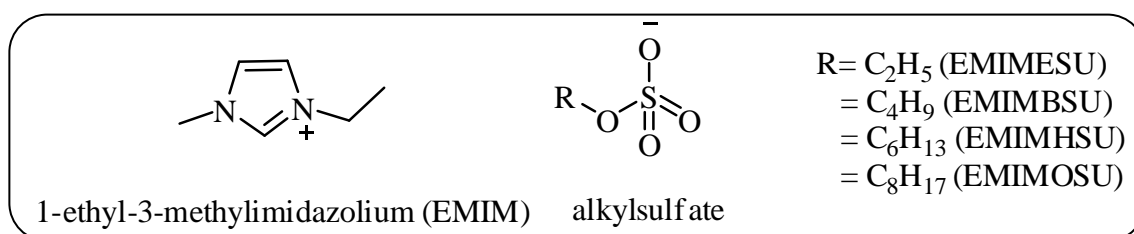
Chart 2. Molecular diagrams of 1-ethyl-3-methylimidazolium alkylsulfates.

The results obtained from the rotational diffusion measurements indicate two distinct rotational environments for these two different probes. The rotational dynamics of C153 lie between stick and slip boundary condition in the ethyl analogue and finally reaches the

subslip condition in the case of octyl substituent. The rotational dynamics of C153 becomes faster with an increase in the alkyl chain length, primarily because of the fact that larger solvent molecules offer lower friction to the rotating solute (Figure 2). We have also observed fractional viscosity dependency on the rotation of C153 in these RTILs. The observation indicates a significant diffusion−viscosity (d-η) decoupling during rotational relaxation of C153 in these RTILs. The decoupling is analyzed through fractional viscosity dependence of the measured rotational times $\langle \tau_r \rangle$: $\langle \tau_r \rangle \propto (\eta/T)^p$ (p is the exponent, and T is the temperature). The fractional viscosity dependency (p = 0.76 to 0.48) increases with increasing anionic alkyl chain length of the anions from butyl to octyl. Generally, fractional viscosity dependence arises due to diffusion-viscosity decoupling during the solute rotation in highly organized and microheterogeneous medium.[18, 19] From d-η decoupling, it can be concluded that structural organization and heterogeneity increases with increase in anionic alkyl chain length in these RTILs.[17, 20]

For AP, hydrodynamic behavior changes from superstick to stick with the increase of the alkyl chain length. Superstick behavior has been attributed to the strong solute-solvent H-bonding interaction between AP and the ionic liquid. Rotational coupling constant values have been found to decrease with increasing length of alkyl side chains. Theoretical calculation (DFT) shows that charge density of sulphate moiety decreases with increasing alkyl chain length of anion in RTILs.
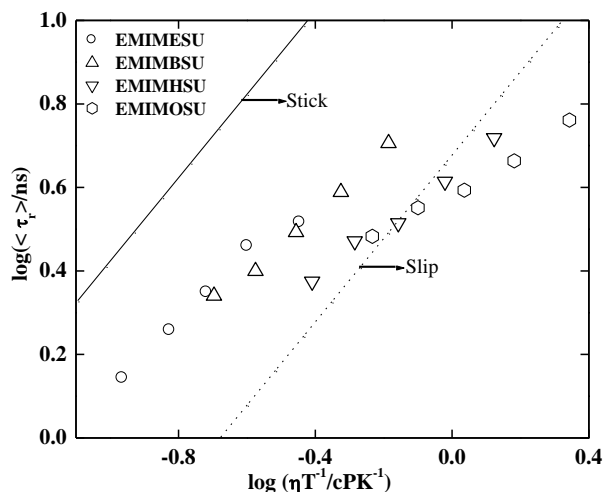
Figure 2. log-log plots of average rotational relaxation time of C153 vs. η/T in different 1-ethyl-3-methylimidazolium alkylsulfate RTILs with slip and stick boundary condition parameters. Symbols denote the experimental data points.

The second part of this chapter discusses the role of solute-solvent H-bonding interaction during the rotational diffusion of organic solutes. To find a correlation between H-bond basicity of anions and average rotational relaxation time of solute, we have investigated rotational diffusion of AP and C153 in several RTILs (Chart 3) that differ in their H-bond basicity. Among the solutes AP is known to form H-bond with H-bond acceptors.[20] While the reorientation times of C153 depends upon the viscosity of the ionic liquids and follows normal hydrodynamics, rotational diffusion of AP has been found to be significantly influenced by H-bond basicity of anions. AP shows superstick behavior in EMIMESU and EMIMTFA and follows stick hydrodynamics in EMIMTFB and EMIMTCB (Figure 3). The superstick behavior is attributed to the strong specific solute solvent interaction. Rotational coupling constant values for AP are found to decrease in the order TFA>ESU>TCB>TFB. The variation in the rotational coupling constants, the measure of extent of departure from the normal hydrodynamics behavior due to specific solute-solvent interaction, is explained by considering the H-bond basicity of the anionic moiety of the corresponding RTILs.[21]
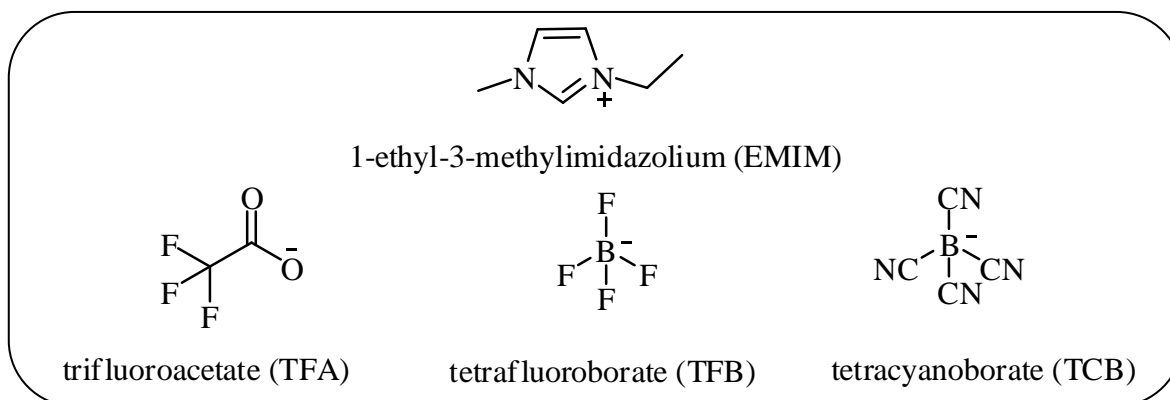
Chart 3. Molecular diagrams of RTILs used under the present study.
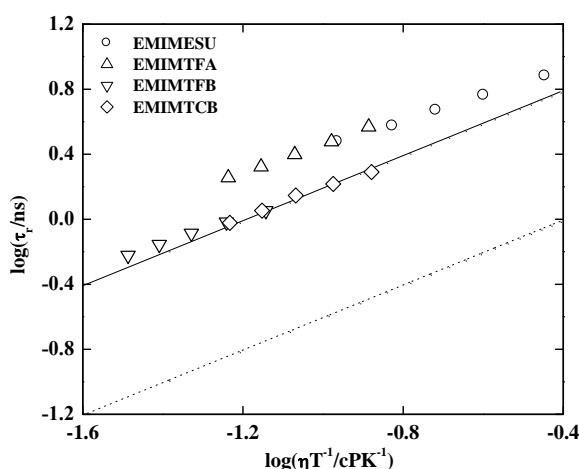
Figure 3. log-log plots for τ_r vs. η/T for AP in different RTILs. Computed data are with stick (——), slip (----) boundary conditions and experimentally measured data are shown by symbol.

Chapter 5. Effect of Nonpolar and Polar Cosolvents on the Solute Rotation and Solvation Dynamics in Room Temperature Ionic Liquids

This chapter attempts to demonstrate the role of various cosolvents toward solvation and rotational relaxation dynamics of C153 in RTIL. The present work is undertaken, keeping in mind the potential of mixed ionic liquid-cosolvent system in real application. To study the effect of nonpolar cosolvent, we have explored the solvation and rotational relaxation behavior of C153 in a hydrophobic IL, MOEMPLFAP and IL-toluene mixture.

Time-resolved fluorescence anisotropy measurements show that the rotational diffusion of the probe becomes faster in presence of toluene. Solvation dynamics in ionic liquid–toluene mixtures is found to be biphasic, and the average solvation time is found to decrease with the addition of nonpolar cosolvent to the ionic liquid. A significant blue shift of the

time-zero maximum of time-resolved fluorescence spectrum upon addition of toluene indicates a more nonpolar environment around C153 at the initial stage of dynamics in the mixed solvent system. A comparison of the dynamics of solvation data in ionic liquid and ionic liquid–toluene mixture suggests that toluene can effectively penetrate into the ionic liquid-rich cybotactic region of the probe. This behaviour is explained in terms of favourable hydrophobic interaction between ionic liquid and toluene.[22]

Again in order to understand the effect of polar solvent on solute rotation and solvation dynamics, we have carried out the fluorescence response of C153 in 1-butyl-3-methylimidazolium trifluoroacetate (BMIMTFA) (Chart 4), and also its mixture with water, methanol. Steady state absorption and emission maxima of C153 has found to be unaffected (no blue or red shift) by the addition of these cosolvents. Solvation as well as solute rotational relaxation times is found to be faster due to the lowering viscosity of the medium only. Theoretical calculations (DFT studies) have been performed on ground state structure of neat BMIMTFA, BMIMTFA-H_2O and BMIMTFA-CH_3OH systems to rationalize the experimental observations.[23]

1-ethyl-3-methylimidazolium (EMIM)   trifluoroacetate (TFA)
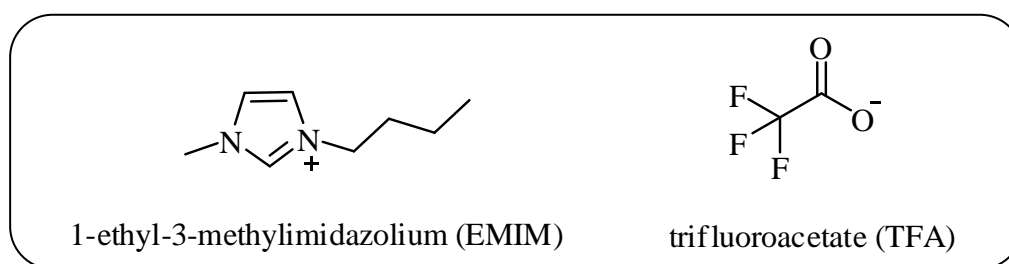
Chart 4. Molecular diagram of BMIMTFA

Chapter 6. Solute Rotation and Solvent Relaxation of Coumarin153 in Moderate and High Viscous Room Temperature Ionic Liquids: An Excitation Wavelength Dependence Study

Some recent studies depicts that RTILs are microheterogeneous in nature[5, 6, 24, 25]. Again, recent literature reports reveal that the solute rotation and solvation dynamics in deep eutectic melts are decoupled from the medium viscosity due to heterogeneity of the medium.[18, 19] Thus, it is expected that this microheterogeneous behaviour of the medium may

contribute significantly towards the solvent reorganization. To investigate whether microheterogeneous nature of the media has any bearing on solvation and solute relaxation dynamics, we have carried out the temperature as well as excitation wavelength dependence solvation and rotational relaxation of C153 in a highly viscous MOEMMOFAP and moderately MOEMPLFAP (Chart 5).

1-(2-methoxyethyl)-1-methylmorpholinium tris(pentafluoroethyl)trifluorophosphate (MOEMMOFAP)
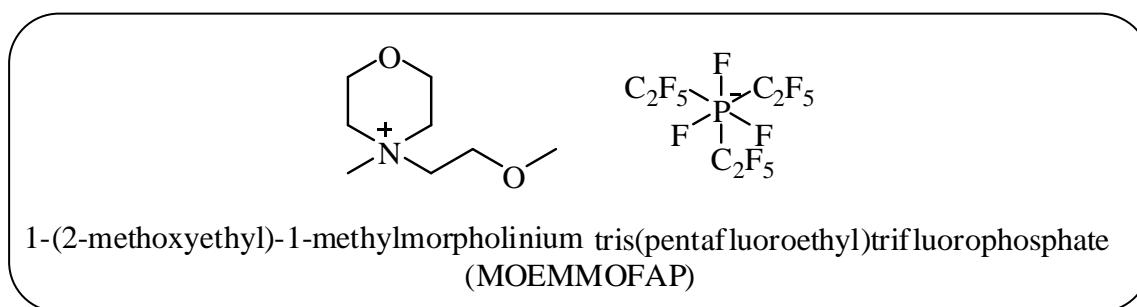
Chart 5. Molecular diagram of MOEMMOFAP used in the present study.

The average solvation times are found to depend on the excitation wavelengths. In case of a more viscous, morpholinium cation containing ionic liquid, the solvation and rotational relaxation times are found not to be as slow as are expected from the bulk viscosity of the medium. The breakdowns of both Stokes-Einstein (SE) and Stokes-Einstein-Debye (SED) relationships have been observed. The observation indicates a significant viscosity-diffusion decoupling during solvation and rotational relaxation of C153 in highly viscous IL. The observation seems to suggest that both static and dynamic heterogeneity may play an important role for the observed viscosity-diffusion (d-η) decoupling in highly viscous ionic liquid (Figure 4).[26, 27]
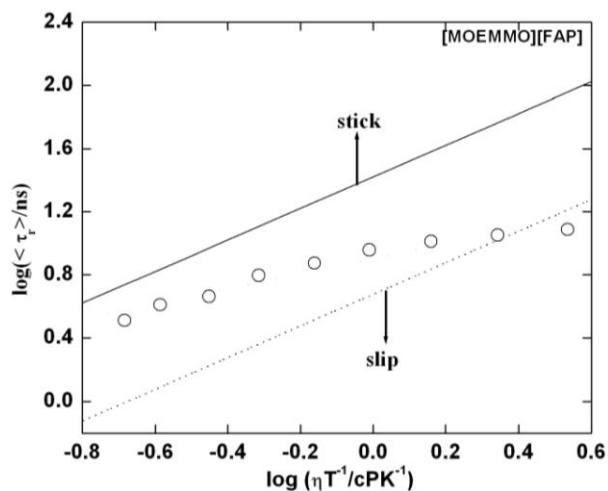
Figure 4. log-log plots of average rotational relaxation time of C153 in MOEMMOFAP with slip and stick boundary condition parameters. Symbols denote the measured rotational data points.

In conclusion, solvation and rotational relaxation dynamics of some well known organic dipolar probes have been investigated in several RTILs. Many interesting features with regard to understanding the fundamentals of solvation and rotational dynamics have come out from the present study. (1) Specific solute-solvent interaction even though weak in nature can influence the solvation dynamics in RTILs. (2) Rotational relaxation of organic solute becomes faster with the increase of alkyl chain length in anion because larger solvent molecules offer lower friction to the rotating solute. (3) Hindered rotational motion of organic solute (capable of H-bond formation) can be correlated with the hydrogen bond basicity of anion. (4) Trace amount of cosolvents can affect the solvation and rotational relaxation dynamics in RTILs in a significant manner. (5) The highly organised and heterogeneous nature of RTILs is revealed through diffusion-viscosity decoupling (d-η).

The future prospect and challenges are outlined at the end of the thesis.

References

1. *Ionic liquids industrial applications for green chemistry*; Rogers, R. D.; Seddon, K. R.; Eds.; ACS Symposium Series 818; American Chemical Society: Washington, DC, 2002.

2. *Ionic liquids as green solvent.* Rogers, R. D.; Seddon, K. R. Eds.; ACS Symposium Series 856; American Chemical Society: Washington, DC, 2003; Chapter 12.

3. *Ionic Liquids IIIA: Fundamentals, progress, challenges, and opportunities: Properties and structure.* Rogers, R. D.; Seddon, K. R., Eds.; American Chemical Society: Washington, DC, 2005, Vol. 901.

4. Dutt, G. B. *ChemPhysChem* **2005**, *6*, 413.

5. Samanta, A. *J. Phys. Chem. B* **2006**, *110*, 13704.

6. Samanta, A. *J. Phys. Chem. Lett.* **2010**, *1*, 1557.

7. Khara, D. C.; Samanta, A. *J. Phys. Chem. B* **2012**, *116*, 13430.

8. Ito, N.; Arzhantsev, S.; Maroncelli, M. *Chem. Phys. Lett.* **2004**, *396*, 83.

9. Zhang, X. X.; Liang, M.; Ernsting, N. P.; Maroncelli, M. *J. Phys. Chem. Lett.* **2013**, *4,* 1205.

10. Pramanik, R.; Rao, V. G.; Sarkar, S.; Ghatak, C. ; Setua, P.; Sarkar, N. *J. Phys. Chem. B* **2009**, *113*, 8626.

11. Sarkar, S.; Pramanik, R.; Ghatak, C.; Setua, P.; Sarkar, N. *J. Phys. Chem. B* **2010**, *114*, 2779.

12. Daschakraborty, S.; Biswas, R. *J. Phys. Chem. B* **2011**, *115*, 4011.

13. Daschakraborty, S.; Biswas, R. *Chem.Phys. Lett.* **2011**, *510*, 202.

14. Khara, D. C.; Samanta, A. *Phys. Chem. Chem. Phys.* **2010**, *12*, 7671.

15. Fruchey, K.; Fayer, M. D. *J. Phys. Chem. B* **2010**, *114*, 2840.

16. Das, S. K.; Sarkar, M. *Chem. Phys. Lett.* **2011**, *515*, 23.

17. Das, S. K.; Sarkar, M. *ChemPhysChem* **2012**, *13*, 2761.

18. Pal, T.; Biswas, R. *Chem. Phys. Lett.* **2011**, *517*, 180.

19. Guchhait, B.; Daschakraborty, S.; Biswas, R. *J. Chem. Phys.* **2012**, *136*, 11847.

20. Das, S. K.; Sarkar, M. *J. Phys. Chem. B* **2012**, *116*, 194.

21. Das, S. K.; Sarkar, M. *J. Fluoresc.* **2014**, *24*, 455.

22. Das, S. K.; Sarkar, M. *J. Mol. Liq.* **2012**, *165*, 38.

23. Das, S. K.; Sahu, P. K.; Sarkar, M. *J. Fluoresc.* **2013**, *23*, 1217.

24. Wang, Y.; Voth, G. A. *J. Am. Chem. Soc.* **2005**, *127*, 12192.

25. Lopes, J.N.A.C.; Padua, A.A.H. *J. Phys. Chem. B* **2006**, *110*, 3330.

26. Das, S. K.; Sarkar, M. *J. Lumin.* **2012**, *132*, 368.

27. Das, S. K.; Sahu, P. K.; Sarkar, M. *J. Phys. Chem. B* **2013**, *117*, 636.

reference 135. (ii) Plot of weighted solvation time-components vs. bulk viscosity of ILs at 293 K. The symbol represents data points and solid line represents linear fit to the data. (a) EMIMBSU, (b) EMIMHSU and (c) EMIMOSU.

31

system with slip and stick boundary condition parameters. Dashed and dotted lines represent the slip and stick boundary condition for C153. Symbols denote the experimental data points and solid lines represent the fit to the data points respectively.

methylimidazolim cation containing RTILs at different
temperatures

Glossary of Acronyms

RTILs	room temperature ionic liquids
ILs	ionic liquids
NaCl	sodium chloride
Tf_2N	bis(trifluoromethanesulfonyl)imide
BF_4^-	tetrafluoroborate
PF_6^-	hexafluorophophate
FAP	fluoroalkylphosphate
Cl^-	chloride ion
TFA	trifluoroacetate
HF	hydrofluoric acid
T_d	thermal decomposition
T_g	glass transition temperature
PI-TOFMS	photoionization time-of-flight mass spectrometry
VFT	Vogel-Tammann-Fulcher
n_D	refractive index
ε	static dielectric constant
NMR	nuclear magnetic resonance
OHD-RIKES	Optical heterodyne-detected Raman induced Kerr effect spectroscopy
MD	molecular dynamics
BASIL	biphasic acid scavenging ionic liquids
UV	ultra-violet
MALDI-MS	matrix-assisted laser desorption/ionization mass spectrometry
PEMFCs	polymer membrane fuel cells

TSILs	task specific ionic liquids
TDFSS	time-dependent fluorescence Stokes shifts
ns	nanoseconds
ps	picoseconds
fs	femtoseconds
C153	coumarin153
AP	4-aminophthalimide
C480	coumarin480
PRODAN	6-propionyl-2-dimethylaminonaphthalene
PET	photoinduced electron transfer
REES	red edge excitation shift
REE	red edge effect
BMIMBF$_4$	1-butyl-3-methylimidazolium tetrafluoroborate
BMIMPF$_6$	1-butyl-3-methylimidazolium hexafluorophosphate
DMABN	4-(N, N' dimethylamino)benzonitrile
ANF	2-amino-7-nitroflurene
DMA	N, N-dimethylaniline
k_{diff}	diffusion controlled rate constant
FCS	fluorescence correlation spectroscopy
BMIMTFA	1-butyl-3-methylimidazolium trifluoroacetate
MOEMPLFAP	1-(2-methoxyethyl)-1-methylpyrrolidinium tris(pentafluoroethyl)trifluorophosphate
MOEMMOFAP	1-(2-methoxyethyl)-1-methylmorpholinium tris(pentafluoroethyl)trifluorophosphate
EMIMESU	1-ethyl-3-methylimidazolium ethylsulfate

EMIMBSU	1-ethyl-3-methylimidazolium butylsulfate
EMIMHSU	1-ethyl-3-methylimidazolium hexylsulfate
EMIMOSU	1-ethyl-3-methylimidazolium octylsulfate
EMIMTFA	1-ethyl-3-methylimidazolium trifluoroacetate
EMIMTCB	1-ethyl-3-methylimidazolium tetracyanoborate
EMIMTFB	1-ethyl-3-methylimidazolium tetrafluoroborate
A	absorbance
ε_λ	molar extinction coefficient
C	concentration
PMT	photomultiplier tube
TCSPC	time-correlated single photon counting
CFD	Constant Fraction Discriminator
TAC	Time to Amplitude Converter
MCA	Multichannel Analyzer
ADC	Analog-to-Digital Converter
FWHM	full width at half maximum
NLLS	nonlinear least squares
TRES	time-resolved emission spectra
MC	missing component
DFT	density functional theory
η	viscosity
ρ	density
EMIMTf$_2$N	1-ethyl-3-metylimidazolium bis(trifluoromethylsulfonyl)imide
BMIMTf$_2$N	1-butyl-3-metylimidazolium bis(trifluoromethyl)sulfonyl)imide
BMPYTf$_2$N	1-butyl-1-methylpyrrolidinium bis(trifluoromethylsulfonyl)imide

IR spectroscopy   infra red spectroscopy

C_{rot} rotational coupling constants

BTBP   N,N′-bis(2,5-di-tert-butylphenyl)-3,4,9,10-

        perylenecarboximide(BTBP)

MPTS   sodium 8-methoxypyrene-1,3,6-sulfonate

DMDPP   2, 5-dimethyl-1, 4-dioxo-3, 6-diphenylpyrrolo [3,4-*c*] pyrrole

Introduction

1.1. Room Temperature Ionic Liquids

Room temperature ionic liquids (RTILs) are the class of salts, which are liquids at ambient temperature (20–30°C) and pressure (1 bar). They consist of bulky organic cations and anions, usually inorganic. Due to the relatively large size of their cations and the nature of the chemical substituents of the anions, the charges on the ions of these salts are usually diffuse. As a result, there is a reduction of electrostatic forces between the ionic constituents of RTILs. The steric constraint of ionic constituents and their low charge density on them make it difficult for RTILs to form a regular crystalline structure, and therefore, they are found as liquids even though at room temperature. The term 'ionic liquid' differs from 'molten salt', the latter usually represents high melting salts like NaCl with strong electrostatic interactions between cations and anions.[1] The lowest melting point reported for RTILs till date is -96°C.[2] These liquids have interesting physicochemical properties such as low volatility, negligible vapour pressure, non-flammability, thermal stability, broad electrochemical window and miscibility with organic compounds. Production methods of RTILs are also, in some cases, considered to be more eco-friendly when compared to the same for conventional solvents.[3-18]

Although the first RTIL, ethylammonium nitrate, was identified in 1914[19], significant attentions towards these systems were given in early 1980s when Wilkes and his coworkers[20, 21] developed chloroaluminate anions ($AlCl_4^-$ or $Al_2Cl_7^-$) based systems. Later on, many cations such as (i) imidazolium, (ii) ammonium, (iii) phosphonium, (iv) piperdinium, (v) pyrrolidinium, (vi) morpholinium, (vii) pyridinium were used along with anions such as tetrafluoroborate (BF_4^-), hexafluorophosphate (PF_6^-), nitrate (NO_3^-) etc to develop RTILs

(Chart 1.1). In most of the cases, anion plays a vital role in determining the hydrophilic and hydrophobic characters of RTILs.[12] RTILs are generally classified in to three categories.

tetraalkylammonium   tetraalkylphosphonium BF_4^- PF_6^-
                                                 tetrafluoroborate   hexafluorophosphate

1,3-dialkylimidazolium   N-alkylpyridinium NO_3^- $(CF_3SO_2)_2N^-$
                                                 nitrate   bis(trifluoromethanesulfonyl)imide
                                                            (Tf_2N)

N,N-dialkylpyrrollidinium   N,N-dialkylmorphilinium $CF_3CO_2^-$ $CH_3CO_2^-$
                                                          trifluoroacetate   acetate

R = alkyl group
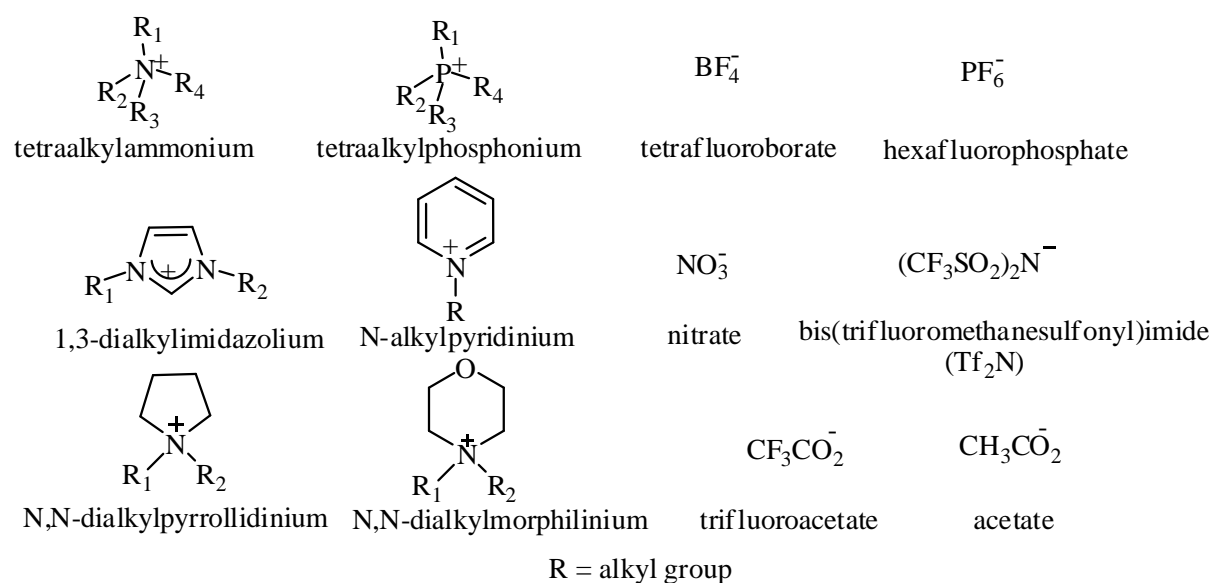
Chart 1.1. Molecular diagrams of different cations and anions

First generation RTILs: They are based on chloroaluminate ($AlCl_4^-$ or $Al_2Cl_7^-$) anions. They are highly hygroscopic in nature. Due to the high reactivity of these RTILs towards water, there is limitation of their applications in practical purposes.

Second generation RTILs: The draw backs in first generation RTILs, lead to development of "second generation RTILs", which are mostly composed of air stable anion[5], such as BF_4^-, PF_6^-. However, these are highly viscous and produce detectable amount of HF acid formed by hydrolysis in the presence of trace amount of water.[22]

Third generation RTILs: They are composed of perfluorinated anion containing RTILs such as Tf_2N, fluoroalkylphosphate (FAP) and address the problem of second generation RTILs. These are mostly hydrophobic in nature and characterized with low melting points, low viscosity, and low conductivity. However, RTILs composed of these anions are more expensive and show stronger binding ability towards the Lewis acid metal ions. Due to the presence of fluorine which is toxic and harmful for human beings, disposal of these RTILs become more complicated.[22-24] This problem leads to the realization of non-fluorinated

44

orthoborate, carborane anion containing RTILs which are low coordinating and cheaper than other RTILs.[25, 26]

Recently, task specific RTILs with specific functional groups, are also developed for a particular task[27-30]. For example, thiol functionalized RTILs have been used to synthesize gold nanoparticles[29] and stabilize nanocrystal quantum dots[30]. Recently developed amino acid based, RTILs are being extensively used for different biological applications.[31, 32]

1.1.1. *Properties of RTILs*

RTILs have attained considerable interest from academic as well as industrial communities across the globe due to their inherent and unique properties such as negligible vapor pressure, ability to dissolve a large variety of organic and inorganic substances, high thermal and chemical stability, wide liquidous range, wide electrical conductivity, moderate to high polarity, non-flammable nature and the advantage of recyclability.[3-15, 33-35] Since, these properties of RTILs are found to depend on ionic constituents, by appropriate combination and permutation of cations and anions, there is a possibility to design and develop RTILs having desired properties. Because of this they are also known as "designer solvents"[3]. Molecular diagrams of some well known common imidazolium based RTILs are depicted in Chart 1.2 and physical properties of some common imidazolium based RTILs are given in Table 1.1.

Melting points: The melting point is a fundamental physical property of compounds. For RTILs, melting point is especially significant because RTILs have a wide liquidus range determined by their low melting points as well as high decomposition points. Moreover, solubility of RTILs in water or organic solvents are also strongly correlated with their melting points. Melting happens when the molecules or ions fall out of their crystal structures, and become disordered liquid. Melting point values of most of RTILs are uncertain as they can undergo supercooling.[12] Phase transfer temperature on RTILs depends on whether the RTIL

is heated or cooled. As the properties of the RTILs depend on the structure, attempts have been made to correlate the melting point of the RTILs to the nature of their cation or anion.[36, 37] ILs with symmetric cation exhibits the highest melting point; the melting point appear to fall gradually with increasing alkyl chain length. The melting point of RTILs generally decreases with increasing anionic radius of RTILs.[38]

	n =	1	3	5
X= BF_4^-		$EMIMBF_4$	$BMIMBF_4$	$HMIMBF_4$
= PF_6^-			$BMIMPF_6$	
= $CF_3CO_2^-$		EMIMTFA	BMIMTFA	
= Tf_2N		$EMIMTf_2N$	$BMIMTf_2N$	$HMIMTf_2N$
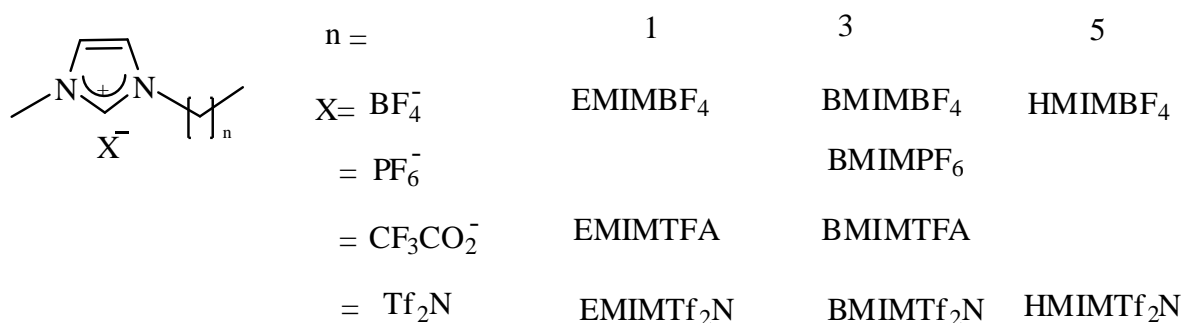
Chart 1.2. Molecular diagrams and abbreviation of some common imidazolium-based RTILs.

Thermal phase behavior: Thermal decomposition (T_d) is strongly dependent on the structures of RTILs. Unlike organic solvents, many kinds of RTILs can be kept in the liquid state above 400 °C (with T_d ranging from 600 to 700 K).[12] Generally, the imidazolium cations tend to be thermally more stable than the tetra-alkyl ammonium cations. High thermal stability is provided by certain kinds of anions such as $[(CF_3SO_2)_2N^-]$, $[(C_2F_5SO_2)_2N^-]$. The relative anion stabilities follows the order $PF_6^- > [(C_2F_5SO_2)_2N^-] > [(CF_3SO_2)_2N^-] > CF_3SO_3^- > BF_4^- > Me\,[(CF_3SO_2)3C]^- >> I^-, Br^-, Cl^-$.[34]

Glass transition temperature: The glass transition temperature (T_g) is an indication of the cohesive energy within the salt, which generally decreases due to repulsive Pauli forces from the overlap of closed electron shells and increases through the attractive Coulomb and van der Waals interactions.[39] Hence, T_g can be decreased by minimizing the cohesive energy within the salt, which is usually achievable through modification of the cationic or anionic components of the RTILs. It has been found that with decreasing cation size and increasing

asymmetry of the cation leads to lower value of T_g through the reduction of packing and cohesive energy of the RTILs.[40]

Thermal stability and volatility: Generally RTILs are thermally stable up to 250°C. Beyond this limit (250°C), it is found that, some of the RTILs are decompose. The decomposition temperature decreases as the hydrophilicity of the anion increases. However, cations have no significant contribution in this regard. The thermal stability of the RTILs comprising different anions decreases in the order $PF6^- > [(C_2F_5SO_2)_2N^-] > \sim BF_4^- > I^-, Br^-, Cl^-$.[34]

Table 1.1. Physical properties of some common imidazolium RTILs

RTILs	T_{mp}(°C)	T_d(°C)	ρ (g/CC)	η (cP)	σ (ms/cm)	$E_T(30)$
EMIMCl	86[a]	-	solid	solid	-	-
BMIMCl	65[a]	-	solid	solid	-	-
EMIMTf$_2$N	-3[b]	-	1.52[b]	34[b]	8.8[b]	47.7[c]
BMIMTf$_2$N	-4[b]	>400[d]	1.43[e]	52[e]	3.9[e]	47.2[c]
EMIMPF$_6$	60[f]	-	solid	solid	5.2[g]	solid
BMIMPF$_6$	-61[h]	-	1.37[i]	371[i]	1.5[j]	52.3[k]
BMIMBF$_4$	-81[h]	435[d]	1.2[i]	154[i]	3.5[d]	48.9[l]

T_{mp}: melting point, T_d: decomposition temperature, η: viscosity, ρ: density, σ: specific conductivity, $E_T(30)$: microscopic solvent polarity parameter. (a) ref[7]; (b) at 20°C, ref[41]; (c) ref[42]; (d) ref[43]; (e) ref[44]; (f) ref[45]; (g) at 25°C, ref[37]; (h) ref[46]; (i) at 20°C, ref[16]; (j) ref[47]; (k) ref[48]; (l) ref[49].

Recent reports have shown that RTILs have non-negligible vapor pressure and thus, they can be distilled under reduced pressure without any thermal decomposition. In this regard, report by Earle and coworkers is noteworthy.[50] They found that by vacuum distillation of RTILs, most of the commonly used aprotic RTILs can be distilled at 200-300°C and low pressure. Later, attempts have been made to separate the mixture of RTILs in pure form, which is also found to be useful for the recyclability of spent RTILs.[51] Though, Earle and coworkers could not provide direct proof of ions in the gas phase of their distillation process, recently Leone et al. by tunable vacuum ultraviolet photoionization time-of-flight

mass spectrometry (PI-TOFMS) identified intact ion pair of 1-butyl-3-methylimidazolium tricyanomethanide.[52]

Density: The density of a material depends on how closely the ions can pack together and, hence, on the size and shape of the ions and ion-ion interactions. So, the density of RTILs depends on the ionic constituents of RTILs. It is observed that the density decreases slowly as the alkyl chain length increases for alkylammonium and alkylimidazolium cations. Tributylammonium nitrate is known to have lowest density because of its bulkier cation.[53, 54] It is expected that primary amines are likely to have higher densities than secondary or tertiary amines. The densities of heterocyclic amine cations are generally higher than those of the alkylammonium cations. For lactum based RTILs with fluorinated anions, it has been seen that with increasing the ring carbon number of the cation, density is decreased. This has been attributed to the modification of the cation-anion interaction due to the increase in the cation size.[55]

Viscosity: The viscosity of RTILs is generally dependent on the columbic i.e. ion-ion interactions, van der Waals interaction and hydrogen bonding interactions within the ionic species. Interactions between ionic constituents lead to higher viscosities. It has been revealed that with the increase of the length of alkyl chains of the cationic moiety viscosity increases and this is due to stronger van der Waals interactions.[41] Similar change in anionic constituents influence viscosity greater than the cationic constituents. Delocalization of the charge on the anion decreases the viscosity by weakening hydrogen bonds.[56] Impurities like halide and water affect the RTILs viscosity considerably.[2, 57] The viscosities of RTILs generally decreases with increasing temperature and it does not follow the Arrhenius behavior but it obeys Vogel-Tammann-Fulcher (VFT) equation which is given below[58]

$$\ln(\eta) = \ln(\eta_0) + \frac{DT_C}{T - T_C}$$

(1.1)

where, η_0 is the viscosity at infinite temperature, D is the fragility parameter and T_C is the characteristic temperature at which viscosity diverges.

Surface tension: Modifications in either the cation or anion structures have a similar effect on surface tension, indicating that both ions are present at the surface of the medium.[59] In general it is observed that surface tension is decreased when the ions have a higher packing efficiency and it is increased when the cohesiveness of the IL increases through ionic interaction or through an increase in the amount of hydrogen bonding interaction.

Refractive index: The refractive index, n_D, of a material can give the idea about its polarity. The n_D values indicate that RTILs can be considered to be moderately polar media like acetonitrile but less polar than short chain alcohol. It has been shown that n_D decreases slowly with increasing alkyl length, while the substitution of a hydroxyl group causes a more significant increase.[59]

Ionic conductivity: The ionic conductivity (specific conductivity) of a medium is generally governed by the ionic mobility of the ions. Ionic mobility depends on the viscosity of the medium and number of charge carriers, which in turn depend on the molecular weight, density, and ion sizes.[41, 54, 56, 60] Any association that may arise due to ion-ion interactions or hydrogen bonding interaction can reduce the ionic conductivity of the medium.[61] The ionic conductivity of RTILs containing alkylammonium and alkylimidazolium cations decreases as the alkyl chain length increases. Larger change in conductivity is observed for short chains (C1-C4) and little change for longer chains (C4-C12).

Polarity: Polarity of the medium is generally expressed by static dielectric constant (ε) of the medium. Dielectric constants of some RTILs are found to vary in a narrow range 9-13 (25°C). These data indicate that RTILs are less polar than acetonitrile ($\varepsilon=35.9$ at 25°C)[62] and similar to pyridine ($\varepsilon=12.3$ at 25°C)[63, 64]. However, these bulk polarity values fail to explain many of the experimental observation in RTILs.[65] Hence, microscopic polarity parameters

such as $E_T(30)$ and E_T^N values which can be obtained from the micropolarity reporter probe such as betaine dye, would be the more appropriate than the dielectric constant (ε).[48, 49, 66, 67] These $E_T(30)$ values are defined as the molar transition energies of standard pyridinium-N-phenoxide betaine dye measured in solvents of different polarity at room temperature and normal pressure. The $E_T(30)$ values for imidazolium cation containing RTILs are generally in the range of 48-52 kcal mol^{-1}. With the increase in chain length of the alkyl group attached to the imidazolium cation, the polarity is found to decrease. This is also true for other cation containing RTILs as well. From the outcome of the different studies on RTILs, it is found that polarity (i.e. $E_T(30)$) of almost all RTILs is more than that of acetonitrile but less than methanol. In fact, the polarity of most of the RTILs are observed to be very similar to that of the short chain alcohols.[48]

1.1.2. *Structural Informations and Heterogeneity of RTILs*

Structural information i.e. the organization of the chemical entities in the RTILs is extremely important since it affects the chemical reaction, solubility of different polar and nonpolar solute etc. Many experimental and theoretical investigations are carried out to understand the structural organization in solid and liquids state of RTILs. Structure of some RTILs which are solid at room temperature were determined by X-ray diffraction methods.[68] These study show that the solid consists of an extended network of cations and anions connected together by hydrogen bonding network among them. The hydrogen bond formation may be either through the aromatic hydrogen of the imidazolium ring or through the hydrogen atoms of the methyl or methylene groups, directly attached to the ring with each cation surrounded by at least three anions and each anion surrounded by at least three cations. Although the number of anions that surround the cation (and vice-versa) can change depending upon the anion size and the imidazolium alkyl substituent, the hydrogen bonding network of ions is a common feature of imidazolium crystals.[69] On a later stage, from the

neutron diffraction analysis,[70] it was found that dialkylimidazolium cation containing RTILs have a close relationship between solid and liquidus nature, emphasizing once again the importance of hydrogen bonding interaction between ionic constituents of RTILs. The existence of hydrogen-bonded clusters both in the solid and liquid phases are also confirmed by IR and Raman spectroscopy[71, 72], NMR[73], and mass spectrometry[74, 75].

Quite interestingly, many investigations have revealed that the neat ionic liquids are also heterogeneous in nature.[76-82] The multiscale coarse grained structure simulation by Wang and Voth[76] and atomistic simulations by Lopes and Padua[77] indicate towards a nanostructural organization in these media. Recently, optical heterodyne-detected Raman induced Kerr effect (OHD-RIKES)[78] studies provide further indication towards heterogeneous nature of RTILs. Samanta and coworkers[79] have also proved microheterogeneous nature of ionic liquids by exploiting excitation wavelength dependence fluorescence behaviour of several probes in RTILs. Later, Hu and Margulis[80] through molecular dynamics (MD) simulation studies have demonstrated that the red edge excitation wavelength dependent fluorescence behavior of molecules arises from probes trapped in quasi-static solvent cages that relax in time scale longer than the fluorescence lifetime of the probes. Very recently, Maroncelli[81] and Bhattacharyya[82] independently have studied the excitation wavelength dependent solvation dynamics in neat ionic liquid and ionic liquid microemulsion using time-resolved emission spectroscopy. From the outcome of these investigations, it is revealed that RTILs are heterogeneous in nature and different polar and nonpolar domain formation among ionic constituents are responsible for this behavior.[73, 74] However, the issue of heterogeneity of ILs is not yet fully resolved. More and more theoretical and experimental investigations are further necessary to understand this phenomenon.

1.1.3. *Applications of RTILs*

RTILs have a number of qualities which make them unique and interesting solvents in contrast to the conventional volatile organic solvents in chemical reactions and catalysis.[83-86] RTILs are of interest as stationary phases in gas-liquid chromatography or as mobile phases in liquid chromatography.[87] A series of RTILs can be tried as ionic matrices for use with matrix-assisted laser desorption/ionization mass spectrometry (MALDI-MS). Potential application have been found for the use RTILs with proteins, such as dissolving hydrophobic ligands to incorporate them it to crystal, improved solubility, monodispersity, as a precipitating agent and as an additive also.[88] A number of RTILs have been found which can act as biocatalysts.[89] RTILs are potentially very useful as ionic-conducting agents in electrochemical systems and as proton conducting agent in polymer membrane fuel cells (PEMFCs). Because of high proton conductivity, low reactivity, and wide electrochemical window provided by the ILs, these system serve as excellent electrolyte in electrochemical applications such as in lithium ion batteries, double-layer capacitors, fuel cells, and actuators.[90-92] The biphasic acid scavenging utilizing ionic liquids (BASIL) method has been widely used in industrial applications for example, alkoxyphenylphosphines based raw materials for the production of photoinitiators to cure coatings and printing inks by exposure to UV light have been synthesized by this method. [3, 85]

Out of these, RTILs have been recognized for different application such as propellants, lubricants.[93] In the last decades, various types of functionalized RTILs specifically categorized as being "task-specific" ionic liquids (TSILs) have been designed and synthesized for specific purposes such as catalysis[94], organic synthesis[4], and separation of specific materials[4] as well as for the construction of nanostructure materials[29] and ion conductive materials etc.

1.1.4. *Photophysical Studies in RTILs*

Utilization of new molecular solvent in practical applications requires not only the knowledge of bulk properties but also a molecular level understanding of the intermolecular interaction, structure, and dynamics of these substances. Scientific communities have immense interest to understand their structure-property relationship[76-82], molecular level picture through both simulation[76, 77, 95-100] and experimental studies[42, 79, 81, 82, 101-163]. Studies have also been carried out to control the photophysical[164-178] and photochemical[179] processes of various systems in RTILs. Many of these studies revealed that RTILs are not homogeneous like common conventional solvents.[76, 77, 79, 81, 82, 101-108, 146-148] Some of the important photophysical studies in RTILs relevant to the present thesis work are discussed in the following sections.

***Solvation dynamics*:** Dynamics of many chemical reactions in solution are strongly influenced by the dynamical behavior of the solvent molecules surrounding reacting species. Studies of solvent relaxation processes are thus fundamentally important to get a proper understanding on the reaction dynamics in solution, especially the processes like electron transfer, charge transfer, proton transfer, conformational relaxation, etc.[180] Besides other methods, the time-dependent fluorescence Stokes shift (TDFSS) measurements have been used extensively to understand solvent relaxation dynamics in large number of systems in last few decades.[109-149,181-186] In this study, the time dependent response of a polar solvent to a changing charge distribution of polar solute is investigated.[180] Chemical reactions usually involve charge transfer, redistribution of electron density, stabilizations of various intermediates and products, which are formed during chemical reaction, are intimately connected to the time scale at which the surrounding solvent molecules reorganize. Understanding the time scale of solvent reorganization in RTILs may therefore be important.

Outcome of these studies are expected to be helpful in designing a solvent for carrying out a specific reaction for a desired product.

The probes for studying TDFSS should posses some special characteristics. Firstly, they should undergo large change in the dipole moment upon optical excitation. Secondly, these molecules should exhibit fluorescence with a long lifetime. Thirdly, any excited state phenomena other than solvation process should be avoided for the study of solvation dynamics.[180] Molecular diagrams of some well know dipolar probes are shown in Chart 1.3.[119, 186]
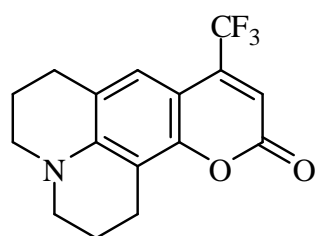
Coumarin153 (C153)
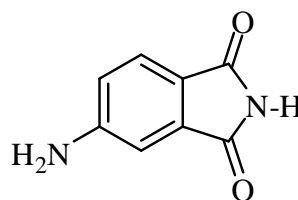
4-aminophthalimide (AP)
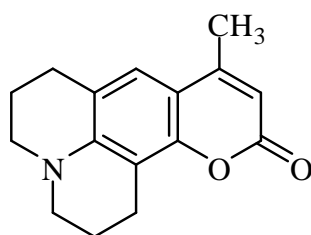
Coumarin480 (C480)
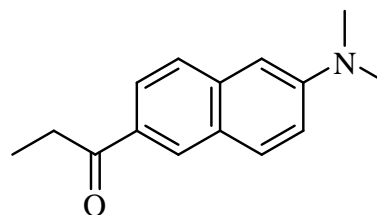
PRODAN

Chart 1.3. Some of the dipolar molecules used in the measurement solvation dynamics of the RTILs

The process of solvation can be described as follows. Let us consider that a solute molecule in its ground state is in equilibrium with the surrounding solvent molecules. Then, the equilibrium charge distribution of the solute is immediately altered through the optical excitation. This represents a non-equilibrium situation. Subsequent to the optical excitation, the surrounding solvent molecules start to reorient and rearrange themselves to stabilize the newly created charge distribution of the excited state of the probe. The time dependent

response of the solvent environment is manifested through the continuous red shift of the emission spectra of the probe with time.[180] The process of solvation is schematically illustrated in Scheme 1.1 for RTILs.
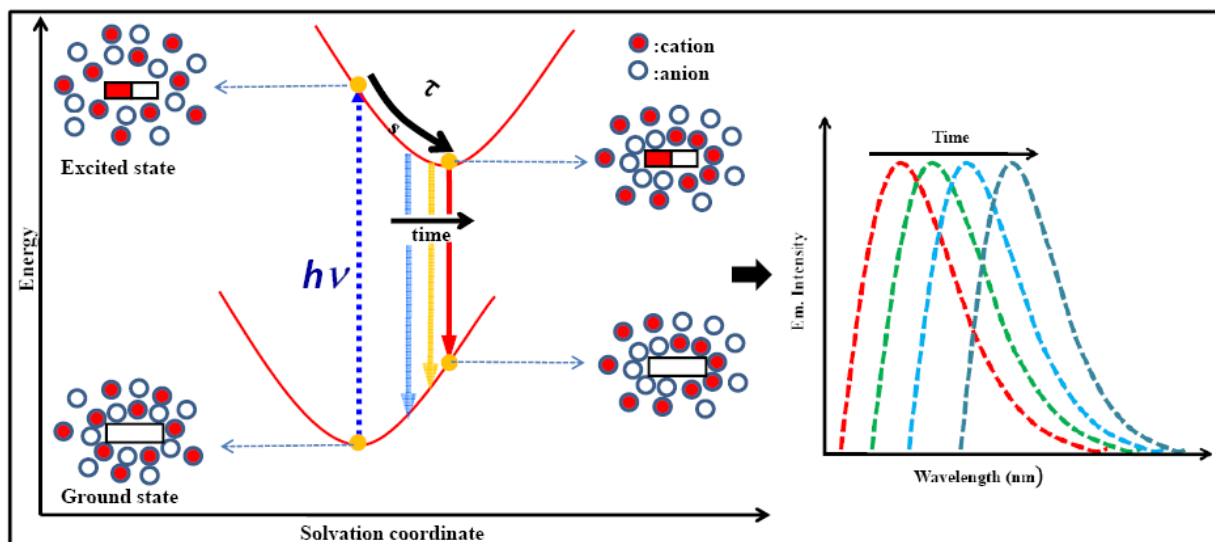
Scheme 1.1. Pictorial illustration of dynamic Stokes shift in RTILs.

Since RTILs are sufficiently polar[48, 49], time dependent fluorescence Stokes shift measurements on dipolar solute probe molecules can give valuable information on the time scale of the reorganization of the ionic constituents of the RTILs. To get an insight into the solute-solvent and solvent-solvent interactions, first Samanta and coworkers[109-117] have carried out the pioneering work on dynamics on solvation by monitoring this time-dependent fluorescence Stokes shift (TDFSS) of a dipolar solute in RTILs. Subsequently Maroncelli[118-128], Sarkar[129-135], Bhattacharyya[82], Petrich[136, 137] and Biswas[138-143] have also made significant contribution to this area. The main findings of these works are collected in the recent review articles.[112, 113, 116] These studies have revealed that solvation dynamics in RTILs is slow compared to that of the common molecular solvents such as acetonitrile, methanol, or water. The time-resolvable component of the dynamics is bi-exponential or non-exponential in nature, with the average solvation time dependent on the viscosity of the media. Almost 50% of the spectral relaxation dynamics is quite fast (<25 ps). Though, time scale and origin of

ultrafast component is under debate, recent studies based on femtosecond fluorescence upconversion technique show that only 10-20 % of the dynamics is ultrafast and occurs within 10 ps timescale.[187] The solvation dynamics in RTILs is found to be probe dependent.[111, 114, 119, 144] Recently, Solvation dynamics studies have also been carried out in mixtures of RTILs with conventional solvents[115, 129, 131, 135, 145, 149] and also in micellar[82] solutions of RTILs.

The mechanism of solvation process in RTILs is fundamentally different from that in polar conventional solvents.[113] Dipolar solvent molecules undergo reorientation around the photoexcited species without moving from their original positions i.e. reorientation of solvent molecule is primarily responsible for the stabilization of the photoexcited probe. However, because of their ionic charge, the ionic species of the RTILs experience a net force when the dipole moment of the solute changes on photoexcitation. As a result, the ions move from their initial position and, hence, the translational motion of the constituent ions mainly contributes significantly to solvation process in the case of RTILs.[113] This fundamental difference of the mechanism of solvation has been illustrated in the form of an oversimplified diagram in Scheme 1.2.
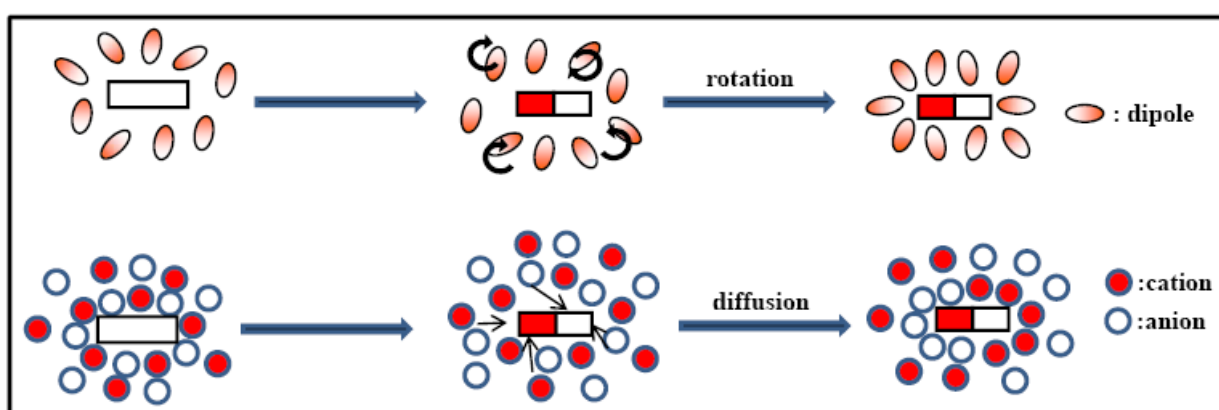
Scheme 1.2. Oversimplified diagram illustrating the fundamental difference in the mechanism of solvation of a dipolar molecule in conventional molecular solvents and in RTILs.

Simulation studies have also been carried out to have a better understanding of solvation dynamics in RTILs on these aspects. However, different pictures have emerged while assigning fast and slow component to molecular motion. For example, Shim et al. reported that the fast component is due to the translational motion of the anions[95], whereas Kobrak and Znamenskiy considered it because of collective cation-anion motion[96, 97]. Later on, Shim et al.[98] attributed the ultrafast dynamics to the local density of the ions near the solvation probe molecule. When the local density is high, few ions in close proximity to the probe molecule are responsible for the ultrafast component and when the local density is low, the ions from the region further away contribute significantly to the ultrafast component.

Excitation wavelength dependence fluorescence study: According to Kasha's rule, fluorescence generally originates from the lowest vibrational energy level of the lowest excited state of the same spin multiplicity. Hence, emission spectrum is expected to be independent of excitation wavelength.[188] However, under certain conditions fluorescence of some organic fluorophore are observed to shifts towards longer wavelength upon increasing the excitation wavelengths particularly at the red region of the absorption spectra.[189-195] This phenomenon is commonly known as "red-edge effect" (REE)[192, 193], although some other terminologies such as edge excitation shift (EES)[191], edge excitation red shift (EERS)[194], and red edge excitation shift (REES)[193] are also used to describe this unusual observation. Two conditions have to be satisfied by fluorescence organic molecules for observing this unusual phenomenon.[189, 190] There must be presence of ensemble of energetically different molecules in the ground state which may arise due to solute-solvent interaction energy which leads to inhomogeneous broadening of the absorption spectrum. Again, another necessary condition that needs to be fulfilled for the occurrence of REE phenomenon is that excited sate relaxation of the fluorescent solute molecule must be slower or comparable to the excited state lifetime of the molecule. Since each molecule in a condensed system does not

57

necessarily experience an equal environment, large numbers of different environments are indeed possible and one can expect a variation of interaction energies between the solute and the solvent leading to a broadening of the absorption. If the media is heterogeneous, this will also allow different ensemble of solvation sites and contribute to significant additional broadening of the absorption spectra. REES has been observed for some organic fluorescent dipolar molecules in RTILs.[79] Molecular basis of this phenomenon is illustrated pictorially by a schematic diagram which is shown in scheme 1.3.
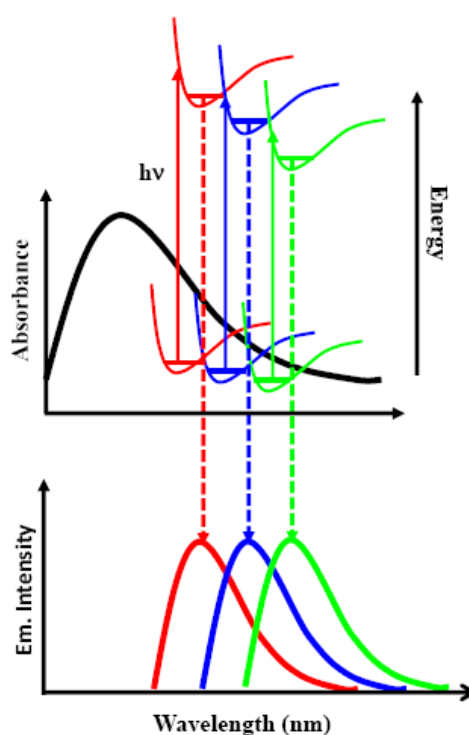
Scheme 1.3. Pictorial illustration of red-edge effect (REE).

Fluorescence anisotropy; rotational dynamics: Fluorescence anisotropy is a measure of emission depolarization of a fluorescent molecule that absorbs polarized light. Rotational motion in the excited state is the common cause of emission depolarization.[196] In a homogeneous solution, the ground-state fluorophores are all randomly oriented in the medium. When such an isotropic ensemble of chromophores is preferentially excited with a polarized light beam, an anisotropic distribution is generated in the excited state due to the selective excitation of the suitably oriented chromophoric molecules in the solution. This

58

preferential excitation of molecules creates anisotropy in excited electronic state. The anisotropy measurements reveal the average angular displacement of the fluorophore that occurs between the absorption and the subsequent emission of fluorophore. This angular displacement is dependent upon the rate and the extent of the rotational diffusion of the excited species during the lifetime of the excited state. Rotational diffusion of a molecule depends upon its size and shape as well as on the viscosity or the rigidity of its local microenvironment. In view of this, studies on the fluorescence anisotropy have been utilized extensively to explore the local environment of the fluorescence dyes as well as to investigate their interactions in host-guest assembly. Probing interactions of solvents with molecules through rotational dynamics study is also expected to be very useful in a sense that well-developed theoretical frameworks for the analysis of the experimental data are available in literature. Solute–solvent interactions play an important role in determining the physicochemical properties of liquids and solutions[197] proper understanding of which is highly desirable.

The Stokes-Einstein-Debye (SED) theory has been found to be suitable for explaining the rotational diffusion of medium sized solute molecules when the coupling between solute and solvent is purely hydrodynamic in nature. It has been observed that the SED theory correctly predicts the linear dependence of the rotational diffusion times of solutes on the solvent viscosity. According to this theory rotational time (τ_r^{SED}) of non-interacting solute in a solvent continuum of viscosity η is given by[196]

$$\tau_r^{SED} = \frac{V_h \eta}{k_B T}$$

(1.2)

where V_h is the hydrodynamic volume of the solute molecule, and V_h is the product of the van der Waals volume V of the molecule, its shape factor f and the boundary condition

59

parameter C. T is the absolute temperature and k_B is the Boltzmann constant. The shape factor f depends on the axial ratio of the semi axes. For a spherical solute f is unity, and is greater than 1 for an asymmetric ellipsoid. When the size of the rotating solute is much bigger than the solvent molecule, the boundary condition parameter, C, is unity, and is represented as the stick boundary condition. In the case of a solute of comparable size, C is less than unity and remains commonly within the range $0<C<1$. SED theory is helpful for the calculation of rotational coupling constants (C_{rot}) values which measure the departure from the normal hydrodynamic behavior.

It is also observed that the experimentally measured rotational reorientation times of a number of solutes could not be well described by the SED theory. Sometime, it is found that hydrodynamic behavior of rotating solute goes beyond slip boundary. This discrepancy arises due to the fact that SED theory takes in to account only the size of the solute molecule and not that of the solvent. In this regard, quasihydrodynamic theories[198, 199] were developed to take care of size of the solvent molecules.

An in-depth understanding of various interactions that exist between constituents of RTILs and also their interaction with added solute are important to improvise their application in new avenues. Recently, a number of studies have been carried by different groups including ourselves towards attaining this goal.[150-163] These studies indicate that apart from viscosity, solute–solvent hydrogen bonding interaction significantly hinders solute rotation.[114, 151, 152] It is also found that the solvent size controls the solute rotation in the absence of specific interactions.[151] As RTILs are composed of ions, and it is obvious to expect that it will influence the rotational dynamics of either cationic and/or anionic charged probe molecules. Interestingly, most of the rotational relaxation studies reveal that the rotational times of the charged species in RTILs depend on the viscosity of the medium and

the effect of ionic constituents of the RTILs on the rotational dynamics is found to be negligible.[150] However, as it is possible to design RTILs with proper choice of different ionic constituents, and tailor their physicochemical properties, it may be possible that the scenario of molecular rotation is changed with the modification of ionic constituents in RTILs.

Photoinduced electron transfer: Photoinduced electron transfer (PET) is the basis of the design and development of systems for solar energy conversion [200, 201] and making components of electronic devices[202]. Electron transfer reaction also plays important role in many applications of ionic liquids such as their use in photovoltaic cells.[203] Hence, it is important to understand electron transport and transfer in ionic liquids. In particular, it is important to learn the similarities and differences in rate of electron transfer between conventional solvents and RTILs. Study of Intermolecular PET reaction between pyrene and N, N-dimethylaniline (DMA) by Paul and Samanta[204] have revealed that the mechanism of electron transfer depends on the microscopic properties of the ionic liquids but not on their bulk properties. The rate constant of PET induced fluorescence quenching (k_q) is found to be higher than the diffusion controlled rate constant (k_{diff}) suggesting that the microviscosity around the donor-acceptor pair is different from the bulk viscosity of the RTILs. However, similar observation have also found by Maroncelli[205] and Vauthey[206] independently in conventional organic solvents having comparably high viscosities, indicating that this behavior is not unique to ionic liquids and rate of electron transfer is not faster in RTILs compared to conventional solvents.

Samanta[207, 208] and Manocelli[209] independently reported that intramolecular PET reactions are solvent controlled in RTILs. Recent report by Wu[210] and Lee[211] et al. have also shown that rate of intramolecular PET reactions in RTILs is hindered compare to conventional solvents and this is due to slow solvent relaxation of RTILs compared to common conventional solvents. These studies have also revealed that intramolecular electron

transfer reaction in RTILs should be treated using a solvent controlled electron-transfer model where solvent relaxation time has a significant role in controlling this process.

Apart from solvation dynamics and rotational diffusion studies, photophysical studies by employing fluorescence correlation spectroscopy (FCS) have also been carried out to understand structure-property relationship in RTILs and these studies have provided evidence in support of microheterogeneous nature of RTILs.[103, 108]

1.2. Objective behind the thesis

The main interest is to explore solvation dynamics and rotational diffusion studies in systematic way in a variety of RTILs such that a comprehensive and quantitative understanding of the relationship among structure, intermolecular interaction and dynamics in ionic liquids is obtained.

Solvation dynamics in RTILs depends on the choice of probe molecule.[128, 132,136] As solvation dynamics is a solvent property, solvent organization times is normally expected to be independent of the probe molecules used. However, it is observed that the value of average solvation time varies significantly with change in the probe molecules. To understand the probe dependency on solvation dynamics, we have investigated the fluorescence response of C153 and AP in a hydrophobic RTIL, 1-(2-methoxyethyl)-1-methylpyrrolidinium tris(pentafluorethyl)trifluorophosphate (MOEMPLFAP)(Chart 1.4). Again, although a large number of reports are available on solvation dynamics[109-149], very limited numbers of studies on solvation dynamics have been performed with the systematic variation of the ionic constituents. Keeping this fact in mind, we have carried out studies on solvation dynamics in 1-ethyl-3-methylimidazolium alkylsulfate to understand the effect of alkyl chain length on the dynamics of solvation in RTILs. (Chapter 3)

As discussed earlier, rotational diffusion studies provide a great deal of information about the solute-solvent interaction and microenvironment of the solute in these media; study

of the rotational dynamics by doing the systematic variations in the constituents of the ILs would be helpful to understand the nature of various forces that are responsible for solute-solvent interactions, also the interactions between the constituents of the ILs and microenvironment of the added solute. In view of this, we have undertaken the dynamics of rotational diffusion of two neutral organic solutes, AP and C153 in a series of 1-ethyl-3-methylimidazolium alkyl sulfate and 1-ethyl-3-methylimidazolium cation containing ILs to understand the effect of alkyl chain lengths and H-bond basicity of anions on the rotational diffusion behavior of C153 and AP. (Chapter 4)

RTILs are not easily available like common conventional solvents and are also expensive. Hence, the scale at which the neat RTILs should be used in the practical applications has not been reached till date. One of the possible approaches to expand the uses of RTILs would be to use various molecular solvent as cosolvents with RTILs.[212, 213] RTIL-cosolvent mixtures are also known to show interesting physicochemical properties. However, a deeper understanding of their physicochemical properties in terms of IL-cosolvent interactions and their response to the photoexcited probe are extremely important so that the systems can be used more efficiently. To understand the effect of nonpolar cosolvent, we have investigated the solvation and rotational relaxation behavior C153 in MOEMPLFAP and its toluene mixture. Again to understand the effect of polar cosolvents in these dynamical phenomena, the solute and solvation dynamics of C153 in 1-butyl-3-methylimidazolium trifluoroacetate (BMIMTFA) and also its mixture with water and methanol have also been carried out separately. (Chapter 5)

Since the RTILs are heterogeneous in nature, this factor may also contribute significantly towards the solvent reorganization in these media. Therefore, it is of paramount importance to study solvation dynamics in ionic liquids as a function of excitation wavelengths so that a clearer picture about the heterogeneous nature of this media comes out.

Keeping all this aspects in mind we have carried out the temperature as well as excitation wavelength dependence on solvation and rotational relaxation of C153 in 1-(2-methoxyethyl)-1-methylpyrrolidinium [MOEMPL], 1-(2-methoxyethyl)-1-methylmorpholinium [MOEMMO] cation containing RTILs with a fixed anionic moiety such as FAP. (Chapter 6)

R= C$_2$H$_5$(EMIMESU)
= C$_4$H$_9$(EMIMBSU)
= C$_6$H$_{13}$(EMIMHSU)
= C$_8$H$_{17}$(EMIMOSU)

EMIM   alkylsulfate

MOEMMO   MOEMPL   FAP

TFA   TFB   TCB
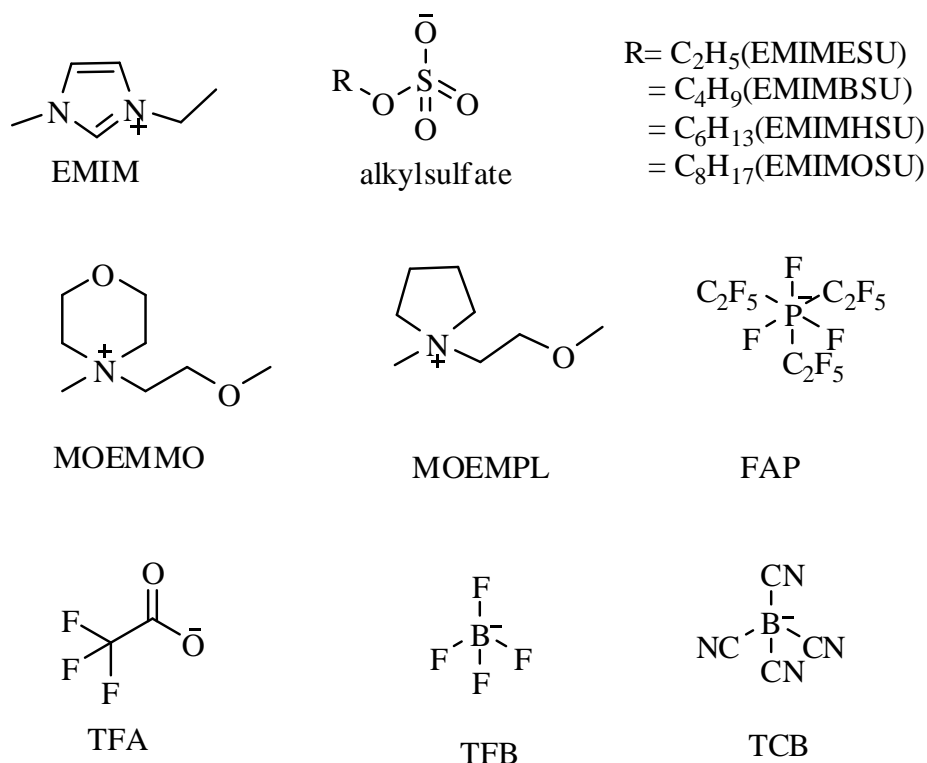
Chart 1.4. Molecular diagrams of RTILs under the present study. EMIM, 1-ethyl-3-methylimidazolium; ESU, ethylsulfate; BSU, butylsulfate; HSU, hexylsulfate, OSU, octylsulfate; MOEMPL, 1-(2-methoxyethyl)-1-methylpyrrolidinium; MOEMMOFAP, 1-(2-methoxyethyl)-1-methylmorpholinium;FAP, tris(pentafluoroethyl)trifluorophosphate.

Instrumentations and Methods

2.1. Introduction

This chapter presents descriptions of various experimental techniques that have been applied to carry out the research work pertaining to the present thesis. Various methodologies used in the present investigation have also been discussed. Theoretical studies for the determination of structural properties of various systems are described.

2.2. Experimental Techniques for the Purification of RTILs

RTILs used in the present studies were purchased from Merck, Germany. Optical purity of RTILs were checked by absorption spectroscopy. If any impurity was found, it was purified by activated charcoal treatment and subsequently characterized with different spectroscopic methods. Different thermophysical properties were also measured and compared with the literature values. RTILs were dried under high vacuum at 45°C overnight prior to each spectroscopic measurement.

2.3. Sample Preparation for Spectroscopic Measurements

RTILs were taken in different long-necked quartz cuvettes of 1 cm path length and requisite amount of solute was added to prepare the solution of the fluorescence probe at room temperature so that the optical density did not exceed 0.4 to avoid problems due to the inner filter affects. Proper precaution was taken to avoid moisture absorption by these RTILs during transferring it into the long necked quartz cuvette and it was sealed by septum and parafilm to avoid moisture adsorption by these green media.

2.4. Instrumentations

For characterization of the compounds, NMR spectra were recorded using Bruker biospin 400 MHz NMR spectrometer. The viscosities of the RTILs were measured by a LVDV-III Ultra Brookfield Cone and Plate viscometer (accuracy: 1% and repeatability:

0.2%). For temperature dependent viscosity measurements a Julabo water circulator bath was used. An Anton Paar (DMA 5000) density meter was used to measure the densities of the RTILs.

2.4.1. *Instrumental Techniques for Absorption and Steady State Emission Measurements*

2.4.1.1. *Absorption Measurements*

To get idea on the effect of light on chromophoric systems, it is very essential to know the complete absorption and emission signature of the system under investigation. Optical absorption (UV-vis) spectroscopy is a widely used technique to get information about the ground state absorption characteristics of choromophoric systems in terms of the energy, wavelengths of the absorption bands and the molar extinction coefficients at different wavelengths. UV-vis absorption spectroscopy, being dependent on the chemical structure and the surrounding environment of the absorbing molecules, allows the characterization or the identification of various chromophoric systems and their surrounding microenvironments.[214-216] Changes in the solvent polarity, polarizability and hydrogen bonding nature often induces significant shift in the absorption spectra. Hence, this simple spectrometric technique can provide more useful information regarding the nature of interactions between the ground state of a chromophoric molecule and its surrounding microenvironment.

According to Lambert Beer's law "absorbance (A_λ) of an absorbing species in a solution is directly proportional to the concentration (*C)* of the species and its molar extinction coefficient (ε_λ) at the measuring wavelength (λ)" and is given by the following relation[196, 214-216]

$$A_\lambda = log\ (I_0/I)\ = \varepsilon_\lambda Cl$$

where I_0 and *I* are the intensities of the incident and transmitted light, respectively, and *l* is the path length for the light beam passing through the sample. For absorbance measurement,

the sample was usually kept in a long neck quartz cuvette of 1 cm path length, sealed with septum and parafilm to further ensure dry condition.

Absorption spectra were recorded using either a Varian, UV1007M138 (Carry 100BIO) or a Perkin Elmer (Lambda 750) spectrophotometer. The minimum wavelength resolution for Perkin Elmer (Lambda 750) spectrophotometer is 0.15 nm and lowest absorbance measurable is ~0.005. For the Varian instrument the minimum wavelength resolution is ~0.2 nm and measureable lowest optical density is ~0.005.

2.4.1.2. *Steady State Fluorescence Measurements*

Fluorescence spectroscopy is a widely used and extremely powerful technique to investigate various photophysical and photochemical processes which occur in the excited state of the fluorescent molecules. It also provides informations about the surrounding media. The intensity, position of the emission maximum, as well as the shape of the emission spectrum are in general very sensitive to the microenvironments of the probe molecules.[196, 214-216] Thus, it provides a better idea about the surrounding region of the fluorescent molecule. During present investigation, steady state fluorescent measurements were performed using a Perkin Elmer (LS55) fluorescence spectrometer. The present system uses a 150 watt continuously powered high pressure xenon lamp as the excitation source and R-928F (Hamamatsu) photomultiplier tube (PMT) as the photodetector. Samples were excited in a 1 cm × 1 cm super sealed, degassed long neck quartz cuvette and the fluorescence is collected and measured in a perpendicular direction with respect to the direction of the excitation beam. Temperature of the sample holder was controlled by the Perkin Elmer, PTP1 peltier temperature programmer by the circulation of water through the sample holder.

2.4.2. *Instrumental Technique for Time-resolved Studies*

2.4.2.1. *Fluorescence Lifetime Measurements*

Time-resolved fluorescence measurements are very important as it provides information regarding the kinetics and dynamics of various photophysical and photochemical processes. Excitation of a fluorescent molecule with a very short pulse of light, results in an initial population (n_0) of fluorophore in the excited state. This excited state population decays with a rate (k_r+k_{nr}) according to following equation[196, 214-216, 217-220]

$$-\frac{dn(t)}{dt} = (k_r + k_{nr})n(t)$$

(2.1)

where $n(t)$ is the number of excited molecule at time t following the excitation of fluorophore molecule with the very short pulse light, k_r and k_{nr} are the radiative and nonradiative decay rate constant respectively. As emission is random event, and each excited fluorophore has the same probability of emitting in a given period of time. This results in an exponential decay of the excited state population which is given below

$$n(t) = n_0 \exp(-t/\tau)$$

(2.2)

It is often difficult to know the exact number of the excited molecules present in the sample. However, knowing the fact that the florescence intensity is directly proportional to the number of excited molecules present in the solution, Equation 2.2 simply can be expressed in terms of the time dependent intensity $I(t)$ and the integration of the resulting equation gives the expression for the fluorescence decay $I(t)$ as,

$$I(t) = I_0 \exp(-t/\tau_f)$$

(2.3)

where I_0 is the intensity at zero time and τ_f is the fluorescence lifetime of the sample which is related to the radiative and nonradiative decay rate constants as follows,

$$\tau_f = \frac{1}{k_r + k_{nr}}$$

(2.4)

Normally, fluorescence lifetime is estimated through time-correlated single photon counting (TCSPC) technique. It is important to mention in this context that since the excited fluorophore emit randomly, different molecules spend different scale of times in the excited states. Thus, for an ensemble of excited molecules in the system, some may emit at very short times following the excitation but others may emit at times much longer than the measured τ_f values of the sample. Accordingly, the time distribution of these emitted photons actually represents the measured fluorescence decay curve of the experimental sample. It is thus evident that, the estimated lifetime from the observed fluorescence decay is actually the statistical average of the times that the excited molecules spend in the excited state.

In the present study, TCSPC setup (Edinburgh OB920 Model) was used to measure the fluorescence lifetimes of the samples. The important aspects related to the present TCSPC spectrometer are described in the following sections.

2.4.2.2. *Basic Principle of TCSPC Technique*

The principle of TCSPC is somewhat unique. In this TCSPC technique, each single photon emitted by the sample is detected followed by its excitation by a short light pulse.[196, 218-221] The principle of TCSPC setup is based on the fact that the time dependent probability distribution of the single photon emission from an excited fluorophore following its excitation is equivalent to the time dependent changes in the fluorescence intensity of the sample following its excitation by the short light pulse.[217-220] The working principle of TCSPC technique, operated in forward mode is shown by a schematic diagram in scheme 2.1.

According to Scheme 2.1, an excitation pulse from the pulsed excitation source is split into two parts, one part is used to excite the sample which is kept in the sample chamber and the other part of the light pulse is directed to a start PMT. The optical signal at the start PMT generates an electrical START pulse, which is then passed through the Constant Fraction Discriminator (CFD) which accurately measures the arrival time of the pulse. This signal is

passed through START input to the Time to Amplitude Converter (TAC), which generates a voltage ramp which increases linearly with time. The part of the optical pulse, which excites the sample, effectively gives rise to the emission of photons. These photons are then detected one by one by the stop PMT to generate electrical STOP pulses for each of the individual photons received. The STOP pulses thus generated in the stop PMT are also routed through a CFD and a variable delay line to the STOP input of the same TAC unit. After detecting the first STOP pulse, the TAC unit stops the generation of voltage ramp. Now, the TAC contains a voltage which is proportional to the time delay (Δt) between the excitation and emission signals. The TAC output pulse is then fed to the input of a Multichannel Analyzer (MCA) through an Analog-to-Digital Converter (ADC). The ADC generates a numerical value proportional to the height of the TAC output pulse and thus selects the corresponding memory address (channel) in the MCA, where a single count is added up.
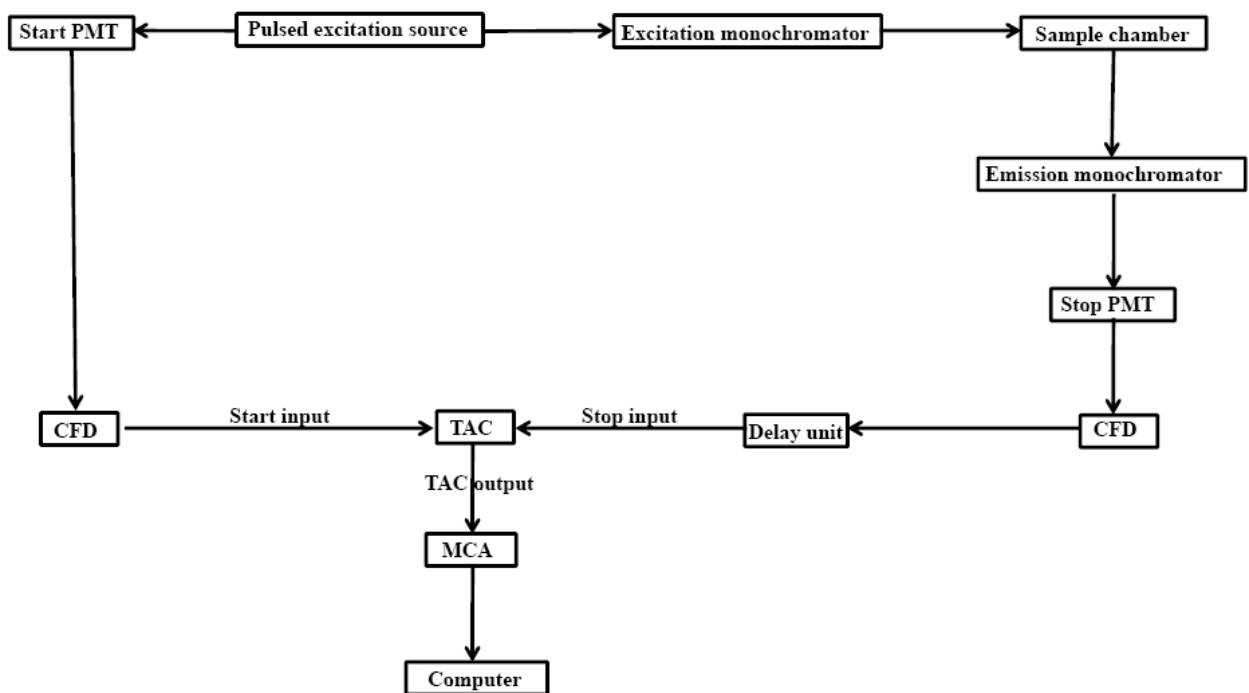
Scheme 2.1. A Schematic diagram for the working principle of TCSPC setup.

The above cycle (from the triggering of the pulsed excitation light source to the data storage in the MCA) is repeated again and again for a large number of times and thus a

histogram of counts is collected in the MCA channels. Scheme 2.1 has shown for a TCSPC technique which is operated in forward mode. However, presently almost all TCSPC measurements are performed in the "reverse mode"[196]. For the present work instrumental set up is used in "reverse mode". The process is almost same as described above except that the emission pulse is used to start the TAC and the excitation pulse is used to stop the TAC. This procedure is used because of the high repetition rate of modern pulsed-light sources. The TAC has to be reset and set to zero before each start pulse, which takes a finite amount of time. The TAC can be constantly in reset mode if the start signals arrive too rapidly. The emission signals occur about 1 per 100 excitation pulses, and thus much less frequently than the excitation pulses. These emission pulses are used to start the TAC, and the next laser pulse is used to stop the TAC. Present electronics for TCSPC setup only allow the detection of the first arrival photon. From the measured fluorescence decay curves, the fluorescence lifetimes of the samples are calculated following a suitable analysis procedure which is discussed later.

2.4.2.3. *Important Components of a TCSPC Setup*

The important components of the present TCSPC instrument are given below.

(i) Pulsed excitation source: Different diode lasers (EPL 375nm, 405nm, 445nm) had been used as the excitation sources to excite the fluorophore. The instrument response function (IRF) for this TCSPC setup is around 100 ps which has been measured from full width at half height maximum (FWHM) of IRF pulse and it is varied with the excitation source. The repetition rate for excitation pulses was usually kept at 1 MHz.

(ii)Constant Fraction Discriminator(CFD): In a typical TCSPC setup, signal from the two PMTs (START and STOP PMTs) are routed through two independent CFDs to achieve the following two goal: (i) to improve the signal to noise ratio (S/N) by discarding the signals below a threshold height such that the counts recorded by the instrument are actually due to

the photons detected by the PMTs and not due to spurious electrical noises.(ii) to provide the correct timing information for the START and STOP inputs to the TAC unit such that the timing jitter in the detection is minimized. As the leading edge discriminators are always associated with significant timing errors, the CFDs are recognized to be the best suited discriminators for the TCSPC measurements to obtain the accurate timing information for the START and STOP signal.

(iii)Delay line: A variable delay line is included in the path of STOP pulse which is situated between CFD and TAC. It delays the STOP pulse intentionally such that it reaches TAC only after the START pulse and thus fruitfully counts the photons by the TCSPC setup. Moreover, by adjusting the variable delay line it is possible to trigger the TAC and MCA combination effectively in such a way that the measured fluorescence is placed and stored within the suitable range of the MCA channels.

(iv)Time-to-Amplitude Converter (TAC): In TCSPC setup, time correlation between the START and STOP pulse is carried out by using the TAC unit which is considered as the heart of this setup. On receiving the START pulse, following the preset delay which is already set in the TAC itself, a timing capacitor in the TAC start charging linearly with time from a constant current source. When the charging is discontinued upon receiving a STOP pulse, the charging process is stopped and TAC unit generates an output pulse. The amplitude of charge accumulated on the TAC capacitor is proportional to the measure of time difference between the arrivals of START pulse and STOP pulse, because the charging process of the capacitor in the TAC is linear with time. In the present Edinburgh TCSPC setup, the TAC range can be varied from 2.5 ns to 50 μs. A suitable TAC range was judicially selected for a particular TCSPC measurement depending on the expected fluorescence lifetime of the sample used.

(v) Multichannel Analyzer (MCA): The MCA used in a TCSPC setup can be operated in two modes: (i) Pulse Height Analysis (PHA) mode for measuring fluorescence decays, (ii)

Multichannel Scaling (MCS) mode for measuring time-resolved emission spectra. The data stored in the MCA channels are transferred to a computer for further analysis and processing.

(vi) START and STOP PMTs: Though in a typical TCSPC instrument suitable start and stop PMTs are used to carry out the measurements, only a single PMT with very high gain and low transit time is used in the present Edinburgh OB920 instrument to detect the emission photons from the sample. Thus the only photodetector used in the present instrument is a special Hamamatsu (R3809U-50) PMT, used in combination with a Quantum, North West (TC 125) temperature controller. The detector is having a spectral response from ~300 to 800 nm. In this instrument the measurement is in fact made in a reverse mode, i.e., the signal from the special PMT is used as a start pulse for the TAC unit and an electrical signal synchronized with the pulsed diode laser is used as the stop pulse. This reverse mode is adopted especially for faster data collection using high repetition rate of the excitation pulses (0.5 or 1 MHz). This reverse mode of detection is essential to avoid unnecessary charging of the TAC unit by the high repetition rate excitation pulses. In this context, it should be mentioned that in Edinburgh OB920 model TCSPC set up a PC based TCC card is used which incorporates both TAC and MCA directly and has been used for the data collection. PC monitor is used to display the measured decay curve. Suitable analysis software is used to fit the measured decay curves and obtain the fluorescence lifetimes of the samples.

2.5. Methods

2.5.1. *Analysis of the Fluorescence Decay Curves Measured by TCSPC Technique*

2.5.1.1. *Data Analysis*

To estimate fluorescence lifetimes from the fluorescence decay curves reconvolution least squares method was employed.[221] When the measure decay time is longer than the pulse-width of the excitation source, the excitation pulse can be expressed as a δ-function. However, when the excited state lifetime is short, distortion of the experimental data occurs by several factors such as the finite decay time of the source pulse, response time of the

photomultiplier tube and related electronics. As a result, instrument response function depends on decay time of the lamp pulse and response time of the photomultiplier and associated electronics. Since the measured decay function is convolution of the true fluorescence decay and instrument response function, it is necessary to analyze the data by deconvolution of instrument response function so as to get the fluorescence lifetime. The mathematical form of the procedure can be described by the following relation[214-216, 222-224]

$$I_m(t) = \int_0^t I_R(t - t')R(t')dt'$$

(2.5)

where, $I_m(t)$ is the fluorescence intensity at time t, $R(t')$ is the intensity of the exciting pulse at time t' and $I_R(t-t')$ is the response function of the experimental system. Instrument response function was measured using a dilute Ludox solution and deconvolution was performed with iterative reconvolution method.

A nonlinear least squares (NLLS) data processing method is then applied to fit the ideal decay following some assumed functional form. The objective of a least square analysis is to fit all data points and test whether the chosen mathematical method is consistent with the real data points or not. The least square analysis is only applicable if the data points satisfy certain assumptions. The main assumptions are that there should be a sufficient number of independent experimental data points, the uncertainties in the experimental data points are Gaussian distributed and there should be no systematic error in the experimental data points. Experimentally, one can obtain both $I_m(t)$ and $R(t')$ from the TCSPC setup. During analysis, a decay function $G(t)$ is first assumed for the sample and this function is deconvoluted with the observed $R(t')$ according to equation 2.5 to obtain a calculated curve Y(t), which is then compared with the experimentally observed decay curve $I_m(t)$.[214-216, 222, 224] The variables in the function $G(t)$ is iteratively changed until a good comparison (best fit) between the $Y(t)$ and $I_m(t)$ is obtained. The function G(t) is usually assumed to be a sum of exponentials in such a way that,

$$G(t) = \sum_i B_i \exp(-t/\tau_i)$$
(2.6)

where B_i is the pre-exponential factor for the ith component and τ_i is the corresponding fluorescence lifetime constant. The success of an analysis and accordingly the acceptance of a fit to the observed decay curve are determined from the judicial judgments of the following statistical parameters.

2.5.1.2. *Reduced Chi-square (χ^2) Values*

Reduced χ^2 values are used to judge the goodness of fit and if the model does fit the data, it is expected to be close to unity. It is defined as

$$\chi^2 = \frac{\sum_i W_i \{Y_i - I_i\}^2}{n - p}$$
(2.7)

where Y_i is the count of ith channel of the calculated curve, I_i is the count at the ith channel of the experimentally measured curve. W_i [$W_i = I/I_i$], is the weighting factor of the counts in the ith channel, n is the number of channels used for the decay to be analyzed and p is the number of degrees of freedom in the decay function consider for the analysis which is equal to the number of variables in the function G *(t)*. For a very good fit, the χ^2 values should be very close to unity. Normally a χ^2 values between 1.00 to 1.20 is considered to represent a good fit of the data points.

2.5.1.3. *Distribution of Weighted Residuals*

The weighted residuals are the differences between the measured data and the fitted function. It is one of the most important parameters for the judgments of the success of an analysis of TCSPC data set and defined by the following relation

$$r_i = \sqrt{W_i} \{Y_i - I_i\}$$
(2.8)

where W_i, Y_i and I_i are as defined earlier. For a good fit, the weighted residuals should be randomly distributed about the zero line for the whole range of the data channels used in the

decay analysis and the quality of the fit will be judged by visual inspection of this residuals. For deconvoluting the instrument response function, each decay curve is fitted by using a suitable mathematical function with an iterative deconvolution program F900 maintaining the χ^2 values between 1 and 1.2.

2.5.2. Construction and Fitting of Time-resolved Emission Spectra (TRES)

The time-resolved decay profiles were collected at magic angle (54.7°) and measured at 5/10 nm intervals across the entire steady state emission spectra.[196] The total number of measurements was 25-30 in each case. After deconvolution of instrument response function, each emission intensity decay curve for a specific wavelength was fitted by using a multiexponential decay function which is given in equation 2.9 with the iterative deconvolution program F900 maintaining the χ^2 values between 1 and 1.2 and with the visual inspection of random distribution of weighted residuals throughout the time.

$$I(\lambda, t) = I_o \sum_i a_i(\lambda) \exp[-\frac{t}{\tau_i(\lambda)}], \quad \sum_i a_i(\lambda) = 1 \tag{2.9}$$

To get the time-integrated intensity at each wavelength equal to the steady state intensity at that wavelength, a set of $H(\lambda)$ values is calculated by the following relation[225]

$$H(\lambda) = \frac{I_{ss}(\lambda)}{\sum_i \alpha_i(\lambda)\tau_i(\lambda)} \tag{2.10}$$

where $I_{ss}(\lambda)$ is the steady state intensity, $\alpha_i(\lambda)$ is the preexponential coefficient, and $\tau_i(\lambda)$ is the decay time at that wavelength with $\sum \alpha_i(\lambda)=1$. The time-resolved emission spectra (TRES) at different times are calculated from the appropriately normalized decay function $I'(\lambda, t)$ for different wavelengths and at different times where $I'(\lambda, t) = H(\lambda) \times I(\lambda, t)$. Each wavelength dependent emission spectra are then converted to frequency based spectra. Then, emission peak frequency at each time, $\nu(t)$ is obtained by fitting the spectrum to a log-normal line-shape function which is given below[225]

$$I^{'}(\lambda,t) = h\exp[-\ln 2\left\{\frac{\ln(1+\alpha)}{\gamma}\right\}^2] \text{ for } \alpha > \text{-1}, \alpha = \frac{2\gamma(\nu - \nu_p)}{\Delta}$$

$$= 0 \quad \text{for } \alpha \leq \text{-1} \tag{2.11}$$

Where h, γ, ν_p and Δ are the peak height, asymmetry parameter, peak frequency and width parameters of the spectra respectively.

2.5.3. *Solvation Dynamics and Missing Component Calculation (MC)*

The solvation dynamics described by the normalized Stokes shift correlation function *C (t) is* defined as[225]

$$C(t) = \frac{\nu(t) - \nu(\infty)}{\nu(0) - \nu(\infty)} \tag{2.12}$$

where $\nu(0)$ is the peak frequency at time $t = 0$, just after the electronic excitation and $\nu(t)$ is the peak frequency at time $t = t$. Again, $\nu(\infty)$ is the peak frequencies at $t = \infty$ when solvent molecules are in the equilibrium position around the photoexcited probe molecule. The time dependence of the calculated *C(t)* was fitted by a bi-exponential function of the form[109-117, 129-135, 138-149]

$$C(t) = a_1 e^{-t/\tau_1} + a_2 e^{-t/\tau_2} \tag{2.13}$$

where τ_1 and τ_2 are the solvent relaxation time and a_1 and a_2 are normalized pre-exponential factors. After having the value of τ_1, τ_2, a_1 and a_2 the average solvation time ($<\tau_s>$) was calculated by using the following relation.

$$\langle \tau_s \rangle = a_1 \tau_1 + a_2 \tau_2 \tag{2.14}$$

Again, one can fit *C(t)* by the stretched exponential function which given below[118-128]

$$C(t) = exp(-(t/\tau_{solv})^{\beta}) \qquad \text{where } 0 < \beta \leq 1 \tag{2.15}$$

After having the value of τ_{solv} and β, the average solvation time was calculated by using the following relation.

$$\langle \tau_{st} \rangle = \frac{\tau_{solv}}{\beta} \Gamma(\beta^{-1})$$

(2.16)

where, Γ is the gamma function and τ_{st} is solvation time considering *C(t)* is stretched exponential function.

The accuracy of the experimentally measured time-zero spectra depend strongly on the time resolution of the experimental TCSPC setup. Fee and Maroncelli[226] have discussed the unreliability of time-zero spectra derived by the extrapolating observed spectra back to zero time and described a method for estimating the time-zero spectrum based on steady state absorption and emission spectra. The basic idea of this method is the assumption that prior to solvent relaxation the Stokes shift of a given fluorophore in a polar solvent should be the same as its Stokes shift in a nonpolar solvent. An approximate time zero frequency, $\nu(0)$ can be calculated by the following relation

$$\nu_p(0) \cong \nu_p(abs) - \{\nu_{np}(abs) - \nu_{np}(emi)\}$$

(2.17)

where the subscripts "p" and "np" represent the polar solvent of interest and a reference nonpolar solvent, respectively. The chosen nonpolar solvent depends on the peak position of absorption of probe molecule in the polar solvent of interest. Then, the percentage of missing component in dynamics of solvation can be calculated by the following relation[226]

Percentage of missing component (MC) = $[\{\nu_{cal}(0) - \nu_{obs}(0)\} / \{\nu_{cal}(0) - \nu_{obs}(\infty)\}] \times 100$ (2.18)

2.5.4. *Time-resolved Fluorescence Anisotropy Measurements*

The decay of the fluorescence anisotropy reveals the average angular displacement of fluorophore that occurs between absorption and subsequent emission.[196] Scheme 2.2[196] illustrates the pictorial representation of the typical fluorescence anisotropy measurement. The orientation of the emission polarization is defined by the electric vector of the excitation

pulse. I_{vv} represents the emission intensity observed with parallel polarization (excitation and emission polarizer are in vertical position) and I_{VH} indicates the intensity of perpendicularly polarized emission (excitation and emission polarizer are in vertical and horizontal position respectively). The ideal anisotropy, r(t), is then defined as,

$$r(t) = \frac{I_{vv}(t) - I_{VH}(t)}{I_{VV}(t) + 2I_{VH}(t)}$$

(2.19)

The difference between parallel and perpendicular emission is normalized by the total emission intensity, so the anisotropy is a dimensionless quantity and independent of the fluorophore concentration as well as the total emission intensity.
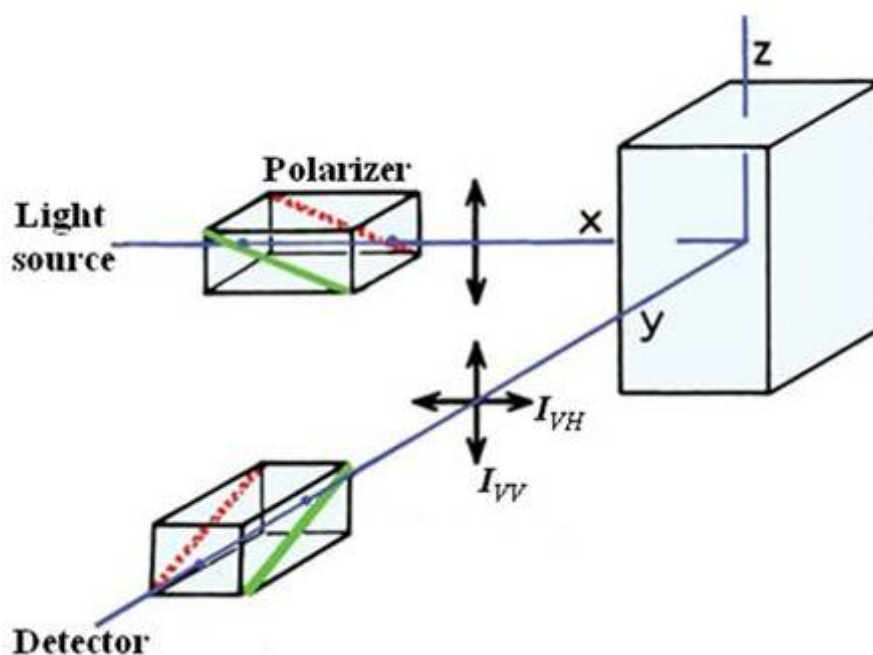
Scheme 2.2. A pictorial representation of fluorescence anisotropy measurement with the help of time-resolved fluorescence anisotropy.

In TCSPC technique, experimental setup and electronics influence the detector sensitivity, so it influences the real intensity ratio between the parallel and perpendicular emission. So, it is mandatory to correct the measured intensity by a factor G, the relative sensitivity of the detection system to these different polarizations. G varies with the emission wavelength and the band pass of the monochromator. It can be determined by

$$G = \frac{I_{HH}}{I_{HV}}$$

(2.20)

where I_{HH} and I_{HV} are the emission intensities when the excitation and emission polarizers are in horizontal-horizontal, horizontal-vertical position respectively. For the present study, the G factor is calculated based on the ratio between I_{HH} and I_{HV} at the emission maxima. G factor also can be calculated by the experimental tail matching of the measured anisotropy decay curve of a standard sample in a known standard solution. The measured anisotropy is then calculated by the following equation

$$r(t) = \frac{GI_{vv}(t) - I_{VH}(t)}{GI_{VV}(t) + 2I_{VH}(t)}$$

(2.21)

For the time-resolved fluorescence anisotropy decay, Edinburgh OB920 TCSPC set up was used and measurements had been done using two polarizers by placing one of them in the excitation beam path and the other one in front of the detector. An alternate collection of the fluorescence intensity in parallel and perpendicular polarization (with respect to the vertically polarized excitation laser beam) for an equal interval of time had been carried out until the count difference between the two polarizations (at t = 0) is $\sim$5000. For G-factor calculation, the same procedure was adopted but with 5 cycles and horizontal polarization of the exciting laser beam. The time-resolved fluorescence anisotropy, r(t) can be fitted by various functions. Generally, we preferred to fit it by single or bi-exponential function which is varied from sample to sample and the functional form is given below.

$$r(t) = r_0 \exp(-\frac{t_i}{\tau_i})$$

(2.22)

The variation in fitting function would be explained with the proper reason in different circumstances in the present thesis. It is worth mentioning that the initial anisotropy value, r_0 should be within the range -0.20 to 0.40 for any single-photon excitation.[190]

2.6. Theoretical Calculations

To get better idea about the solute-solvent, solvent-solvent interaction different theoretical methods were employed in conjunction with different experimental techniques. For most of the systems, structural parameters were calculated with the help of density functional theory (DFT), which is a more improvement method of calculations than the Hartree-Fock theory in a sense that it includes both exchange energy and electron correlation.[227, 228] Instead of pure DFT method, a hybrid method in which exchange functional is a linear combination of the Hartree-Fock exchange and a functional integral was employed in the calculations. Structural parameters and interaction energy were calculated using hybrid DFT functional B3LYP[228, 229] at the 6-311++G (d, p) level. Charge density analysis was performed using natural bond orbital (NBO)[230] approach based on B3LYP/6-311++G (d, p) wave function. All the calculations were carried out using the GAUSSIAN 03[231] software program.

2.6. Standard Error Limits

Standard error limits involved in the experimental results were

Viscosity (η)	$\pm 2\%$
Density (ρ)	$\pm 2\%$
λ_{max} (abs./flu.)	± 1 nm
τ_f (> 1ns)	$\pm 5\%$
Solvent relaxation time	$\pm 5\%$
Rotational relaxation time	$\pm 5\text{-}10\%$

Fluorescence Response of Coumarin 153 and 4-Aminophthalimide in Room Temperature Ionic Liquids: A Probe and Alkyl Chain Length Dependence Study

3.1. Introduction

In recent era, room-temperature ionic liquids (RTILs) have gathered considerable attention primarily because of their diverse applications towards chemical, material and biological sciences.[1-12] The emergence of RTILs as specialty media or material for several advance processes has been possible owing to their physicochemical properties such as wide liquidous range, negligible vapour pressure and high viscosity etc. The interionic interactions in these RTILs are believed to be responsible for their high boiling point, high viscosity and low vapor pressure.[12, 13] Since the properties of the RTILs can be tuned by appropriate choice of cations and anions, they are also termed as 'designer solvent'.[3]

Many experimental and theoretical studies on RTILs have been carried out to understand structure-property relationship of this media.[76-149] To get an insight into the solute-solvent and solvent-solvent interactions, Karmakar and Samanta[109] have carried out the pioneering work on dynamics of solvation by monitoring the time-dependent fluorescence Stokes shift (TDFSS) of a dipolar solute in RTILs.[109-117] Subsequently, Maroncelli [118-128], Sarkar [129-137] and Biswas[138-143] have also independently made significant contribution to this area.[129-137] The main findings of these work are collected in recent review articles.[113, 116] These studies have revealed three major outcomes. (i) Solvation dynamics in ionic liquids (ILs) is slow when compared to that of the common molecular solvents such as acetonitrile, methanol, or water. (ii) The time-resolvable component of the dynamics is bi-exponential or non-exponential in nature, with the average solvation time dependent on the viscosity of the media. (iii) Nearly 50% of the spectral relaxation dynamics is quite fast (<25 ps). Quite

interestingly, many recent studies have also revealed that the neat ionic liquids are heterogeneous in nature. [76-82]

One important aspect that needs attention is the probe dependency of solvation dynamics.[111, 114, 119] These studies have revealed that the average solvation times vary significantly with the choice of probe molecules. However, the solvation times measured by different groups are found to be varying rather irregularly. It can be seen that the average solvation time for 1-ethyl-3-metylimidazolium bis(trifluoromethyl)sulfonylimide (EMIMTf$_2$N), as measured by Samanta and coworkers, is the lowest with 6-propionyl-2-dimethylaminonaphthalene (PRODAN) and highest with 4-aminophthalimide (AP).[110] However, for 1-butyl-3-metylimidazolium bis(trifluoromethyl)sulfonylimide (BMIMTf$_2$N), the trend is exactly opposite.[110] Maroncelli and coworkers[119] found that the average solvation time for 1-butyl-3-metylimidazolium hexafluorophosphate (BMIMPF$_6$) is the lowest with Coumarin153 (C153) and highest for PRODAN, similar to the trend observed in the case of 1-butyl-1-methylpyrrolidinium bis(trifluoromethyl)sulfonylimide (BMPYTf$_2$N).[111] The reason behind the probe dependent solvation dynamics is not clearly understood. However, sometime strong hydrogen bonding interaction between probe and RTIL has been attributed to the observed variation of average solvation and rotational times.[114]

As stated earlier that constituents of ILs play important role in governing the physicochemical properties and consequently the structural variations of the constituents of ILs may give rise to nontrivial behavior of ILs.[77, 108, 232-234] Of late, many studies have been carried out to find out how the structural variations on constituents of ILs can influence the properties of the ILs. Many interesting observations have emerged from these studies. Variation of alkyl chain length on ionic moieties changes many properties of ILs such as heterogeneity[108], surface properties[232] etc. ILs are also known to exhibit nanoscale organization depending on the length of the alkyl chain.[77, 233] On the contrary, Bowron and

coworkers reported that there is little or no long-range correlated nanostructure in case of 1-alkyl-3-methylimidazolium hexafluorophosphate.[234]

Recently Shirota and coworkers[235] have investigated the microscopic aspects of ILs-water system by Raman and IR spectroscopy. They have shown that the magnitude of the frequency shifts of the anions' vibrational modes in presence of water becomes smaller as length of alkyl chains of 1-alkyl-3-methylimidazolium cation is increased. Subsequently, Tsuzuki et al.[236] showed that the conformational flexibility of the alkyl chains in cations is one of the important factors determining the diffusion of ions. Recent studies on orientation dynamics by Fayer[151] and Dutt[153] demonstrated that length of the alkyl side chain in the cationic moiety of ILs has noticeable influence on the rotational behavior of the organic solute in the ILs.

It is evident from the above discussions that majority of the studies carried out to investigate the structure-property correlation of ILs are focused only on the structural variations in the cationic moiety of ILs. However, studies that focus on the structural variation in the anionic moiety of ILs are elusive. Moreover, no study on dynamics of solvation on this aspect has been carried out. Studies on solvation dynamics by employing systematic variations in the ionic constituents would be helpful in providing the comprehensive and quantitative picture which will entail a significant step forward in our understanding the subtleties of mechanism of dynamics of solvation in ILs.

Keeping these facts in mind, in the present study, we have investigated the solvation and rotational relaxation of both C153 and AP in a hydrophobic RTIL, 1-(2-methoxyethyl)-1-methylpyrrolidinium tris(pentafluorethyl)trifluorophosphate (MOEMPLFAP) (Chart 3.1), to understand the probe dependency on solvation dynamics. The solvation probes used for the present study are depicted in Chart 3.1 are well-known solvatochromic probes suitable for dynamic Stokes shift measurements.[225] Out of these probes, C153 is found not to be sensitive

to specific interaction with solvents[225, 237] whereas, AP is found to be more sensitive to hydrogen-bonding interactions.[114] The choice of the present IL, MOEMPLFAP, is primarily governed by the fact that this is ultra hydrophobic due to the presence of bulky tris(pentafluoroethyl)trifluorophosphate moiety.[238] It has been shown that moisture content of the present type of IL is less than that of ILs containing the bis(trifluoromethyl)sulfonylimide (NTf_2^-) and is more than 10 times less than that of ILs containing PF_6^- anion.[239-241] Moreover, the present IL is non aromatic and is expected to be more optically transparent than its imidazolium analogues.[242]
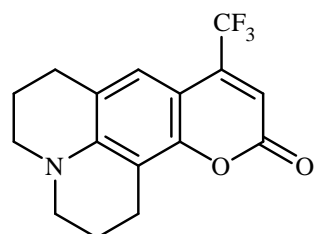
(A) coumarin153 (C153)   (B) 4-aminophthalimide (AP)
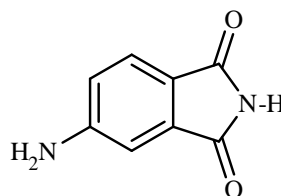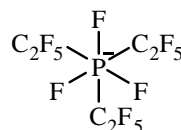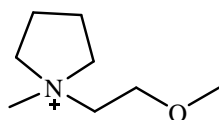
(C) 1-(2-methoxyethyl)-1-methylpyrrolidinium tris(pentafluoroethyl)trifluorophosphate
(MOEMPLFAP)
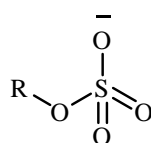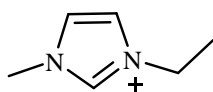
R = C_4H_9 (EMIMBSU)
= C_6H_{13} (EMIMHSU)
= C_8H_{17} (EMIMOSU)

(D) 1-ethyl-3-methylimidazolium (EMIM)   alkylsulfate

Chart 3.1. Molecular diagrams of (A) Coumarin153, (B) 4-aminophthalimde, (C) 1-(2-methoxyethyl)-1-methylpyrrolidinium   tris(pentafluorethyl)trifluorophosphate (MOEMPLFAP) and (D) 1-ethyl-3-methylimidazolium alkylsulfates.

To understand the role of alkyl chain lengths on the solvation dynamics, we have investigated the steady state and time-resolved fluorescence response of C153 in a series of 1-ethyl-3-methylimidazolium alkyl sulfate ILs, viz 1-ethyl-3-methylimidazolium butylsulfate (EMIMBSU), 1-ethyl-3-methylimidazolium hexylsulfate (EMIMHSU), and 1-ethyl-3-methyl

imidazolium octylsulfate (EMIMOSU) (Chart 3.1). These ILs are purposefully chosen to maintain a systematic variation of alkyl group in their anionic moiety.

3.2. Experiments and Methods

C153 (laser grade, Excition) and AP (TCI, Japan) were used as received. RTILs were obtained from Merck Germany (>99% purity). The water content of the present RTILs were less than 100 ppm. The present RTILs had less than 100 ppm free halide content. Details procedure of sample preparation for steady state and time-resolved measurements are described in details in Chapter 2. Details of instrumental techniques for steady state absorption and emission, time-resolved fluorescence, viscosity measurements are also discussed in Chapter 2.

3.3. Results and Discussion

3.3.1. *Fluorescence Response of C153 and AP in MOEMPLFAP*

3.3.1.1. *Steady State Behavior*

The absorption spectrum of the MOEMPLFAP is shown in Figure 3.1.The optical density of the present RTIL is measured to be very less (0.009 in a 1 cm cell) at 375 nm. The representative absorption and emission spectra of the probe molecules, AP and C153, in MOEMPLFAP are shown in Figure 3.1. The emission maxima are measured to be 463 nm for AP and 514 nm for C153. We have not seen any significant changes in peak position in the steady state absorption and emission behavior of C153 while changing the temperature from 293 K to 303 K. We have also not observed any significant emission from these media.
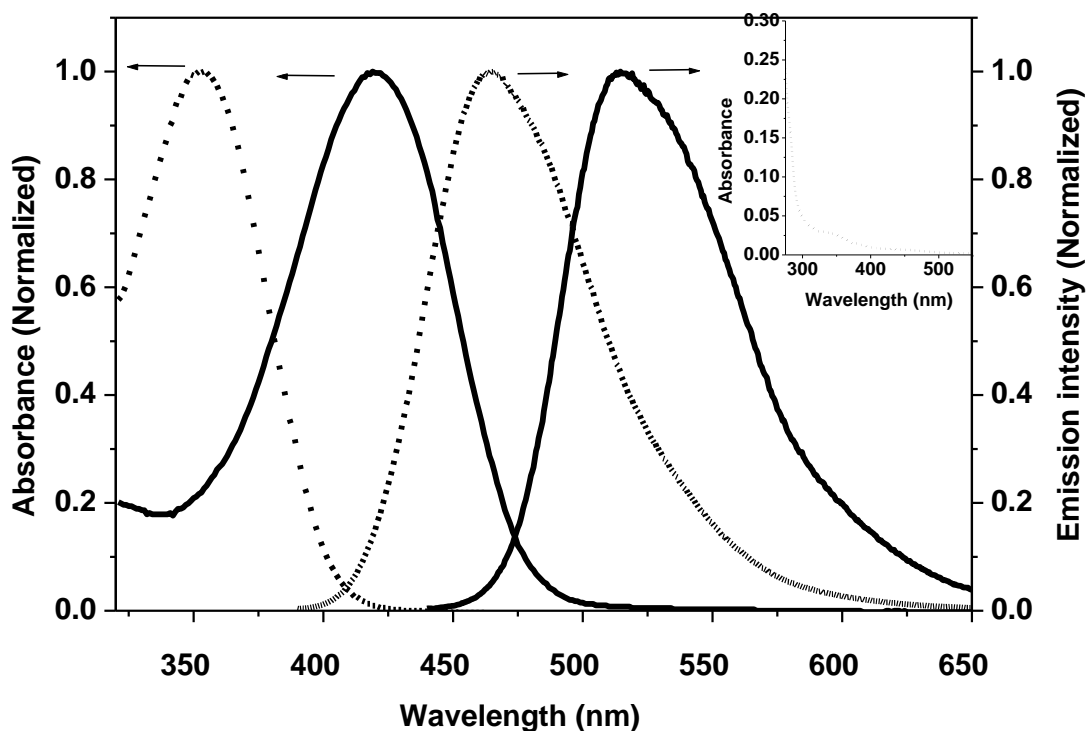
Figure 3.1. Steady state absorption and fluorescence spectra of AP (dotted lines) and C153 (solid lines) in neat MOEMPLFAP at 298 K. $\lambda_{exc.}$ = 375 nm. All spectra are normalized at their corresponding peak maximum. Inset shows the absorption spectrum of neat MOEMPLFAP.

3.3.1.2. *Time-resolved Studies*

3.3.1.2.1. *Solvation Dynamics*

The emission decay profile of AP and C153 in the present ionic liquid have been measured at several wavelengths (5-10 nm intervals) across the entire emission spectra by exciting the sample at 375 nm and also at three different temperatures 293K, 298K and 303K respectively. The decay profiles are found to be strongly dependent on the monitoring wavelength. In all cases, when decay is monitored at the shorter wavelength, a faster decay is observed, and at the longer wavelength, we have observed a decay profile that consists of a clear rise with usual decay. Representative wavelengths dependent decay profiles of AP in present ionic liquid are shown in Figure 3.2.
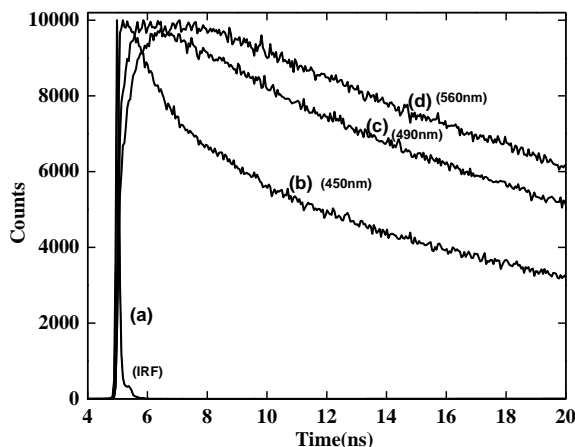
Figure 3.2. Time-resolved fluorescence decay behavior of AP in neat MOEMPLFAP at 298K. $\lambda_{exc.}$ = 375 nm. The IRF and decay profiles at different monitoring wavelength are shown in the same figure.
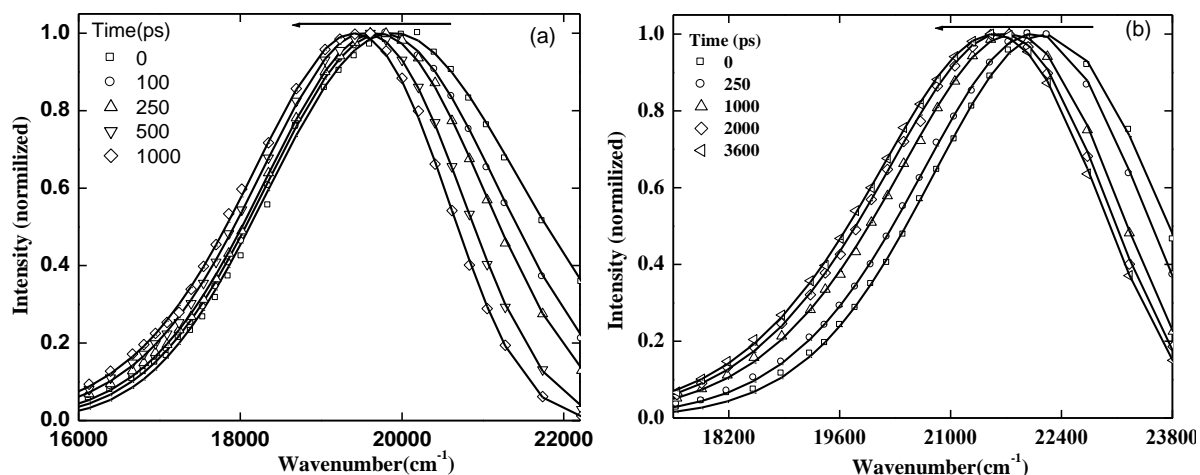
Figure 3.3. Time-resolved emission spectra (TRES) of (a) C153 and (b) AP in neat MOEMPLFAP at 303K. $\lambda_{exc.}$ = 375 nm.

Time-resolved emission spectra (TRES) have been constructed following the procedure of Fleming and Maroncelli.[243] TRES exhibits progressive red shift of the fluorescence maximum with time. Representative TRES of AP and C153 at $\lambda_{exc.}$ = 375 nm are shown in Figure 3.3. The total Stokes shift of the fluorescence maximum observed for the systems between $t = 0$ to $t = \infty$ are collected in Table 3.1. The time constants of the observable dynamics have been obtained from the plot of the spectral shift correlation function, *C(t)* versus time. Average solvation time has been calculated by exploiting both a bi-exponential function as well as by stretched exponential function. However, we resort to the bi-

88

exponential fitting as it gives the better fit. Decay of solvation correlation function, *C(t)*, of

AP and C153 in neat RTIL at different temperatures are shown in the Figure 3.4. The

relaxation parameters of solvation of C153 at different temperatures are collected in Table

3.1.
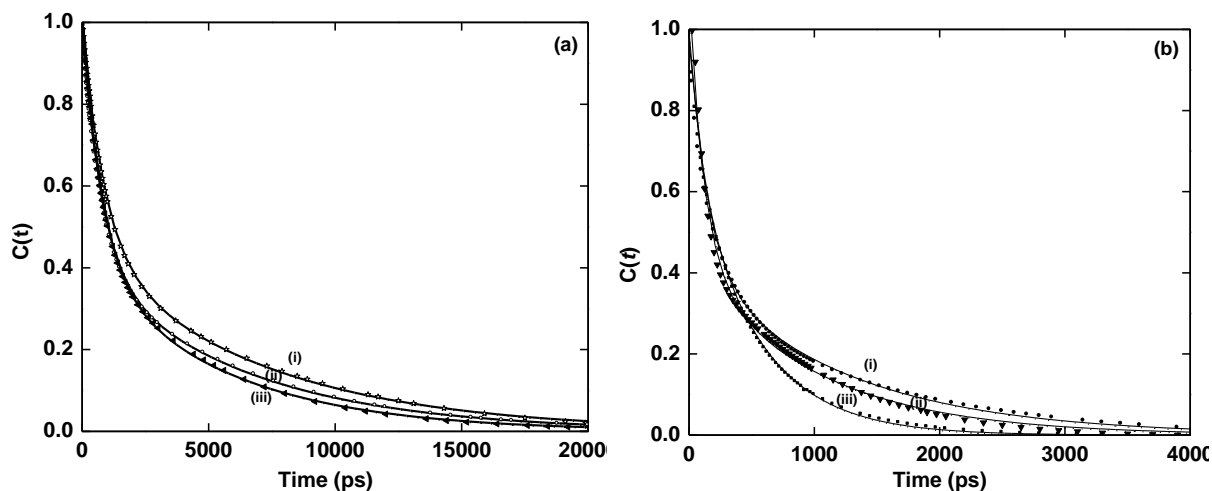
Figure 3.4. Decay of the spectral shift correlation function, *C(t),* of (a) AP and (b) C153 in MOEMPLFAP at (i) 293 K (ii) 298 K and (iii) 303 K. $\lambda_{exc.}$ = 375 nm. In both cases, solid lines denote the bi-exponential fit to the data points.

Table 3.1. Relaxation parameters of solvation and observed shift for AP and C153 in MOEMPLFAP

			bi-exponential fit					stretched exp. fit			obs. shift[†]
Temp.(K)	Vis.(cP)	probes	a_1	$\tau_1(ns)$	a_2	$\tau_2(ns)$	$\tau_{av.}(ns)$	β	$\tau_{solv.}(ns)$	$\tau_{st\,(ns)}$	(cm^{-1})
293	128	AP	0.55	0.85	045	6.89	3.57	0.68	2.56	3.33	1028
		C153	0.56	0.15	0.44	1.19	0.61	0.59	0.39	0.60	808
298	98	AP	0.59	0.74	0.41	6.02	2.90	0.68	1.96	2.90	952
		C153	0.58	0.12	0.42	0.99	0.48	0.67	0.36	0.52	744
303	75	AP	0.59	0.77	0.41	5.38	2.66	0.73	1.87	2.28	837
		C153	0.29	0.10	0.71	0.51	0.39	0.78	0.34	0.39	648

[†]Observed shift has been calculated from [$\bar{v}(0) - \bar{v}(\infty)$]; experimental error is ± 5%.

Interestingly, the average solvation times are measured to be different for C153 and AP

in all three temperatures (Table 3.1). In fact, the average solvation time of AP is found to be

~6 times higher than that of C153 in all temperature. In this regard, we would like to point out that solvation dynamics being a solvent property should not depend on the probe molecules. We have also calculated the missing component in the solvation dynamics according to the procedure described by Fee and Maroncelli.[226] For example; at 298 K missing components are calculated to be 65% and 45% for AP and C153 respectively. This implies that the significant amount of solvation occurs in a time scale faster than the effective time-resolution of the instrument.
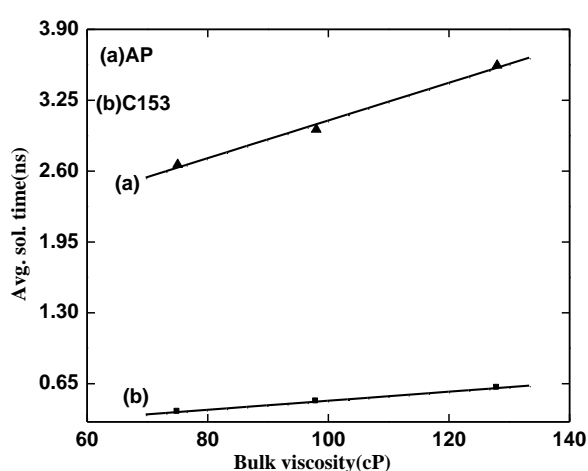
Figure 3.5. Plot of average solvation time vs. bulk viscosity of MOEMPLFAP at $\lambda_{exc.}$ = 375 nm

The temperature variation study reveals that the average solvation time of both AP and C153 decreases with increase in temperature (Table 3.1). This correlates well with the decrease in the bulk viscosity of the RTIL with increase in the temperature (Table 3.1). The plot of average solvation time versus the viscosity of the RTIL is shown in Figure 3.5. As can be seen from the Figure 3.5, average solvation times are linearly correlated with the bulk viscosity of the present RTIL. We have also compared our data with the existing literature by plotting the average solvation time of AP and C153 versus viscosity of different ionic liquids (Figure 3.6). While average solvation time corresponding to C153 correlates linearly with the bulk viscosity of the RTILs, the average solvation time corresponding to AP in the present

RTIL deviates considerably from the linearity (Figure 3.6). This observation indicates the possible role of specific interaction between probe and IL towards the solvation dynamics.
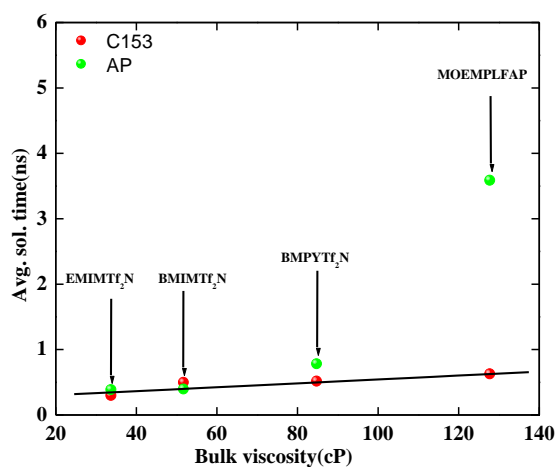
Figure 3.6. Viscosity dependence of average solvation time of C153 and AP in different room temperature ionic liquids. The data points shown in the plot are collected from the reference 113 and the present study. The solid line represents the linear fit to all the data points except that for AP in MOEMPLFAP.

3.1.2.2.2. *Rotational Dynamics*

Time-resolved fluorescence anisotropy (r(t)) is estimated using Equation 2.21 and details procedure for the estimation of rotational relaxation time is described in Chapter 2 in section 2.4.4. The representative anisotropy decay profile of AP in the neat RTIL at various temperatures is shown in Figure 3.7. A bi-exponential fit to rotational anisotropy decay profiles is used to calculate average rotational relaxation times (Table 3.2).

As can be seen from Table 3.2, the average rotational time at any given temperature for C153 is higher than that of AP. In this regard, it should be noted that in the absence of any specific interaction, the solute rotation is mainly governed by the volume of the solute and the viscosity of the medium. In the present scenario, the larger size of C153 as compared to AP is primarily responsible for the higher average rotational time of C153. We have also observed that with increase in the temperature from 293K to 298K, the average rotational relaxation times of both AP and C153 decreases in the present RTIL. This can be rationalized by the fact that according to the hydrodynamic theory, the rotational relaxation time of the probe is

91

proportional to the viscosity and inversely proportional to the temperature. We have also calculated the rotational coupling constants (C_{rot}) using Equation 1.2, which are the measure of the extent of departure from normal hydrodynamic behavior of a solute due to specific interaction. We have used the probe properties that are available in literatures. [119]
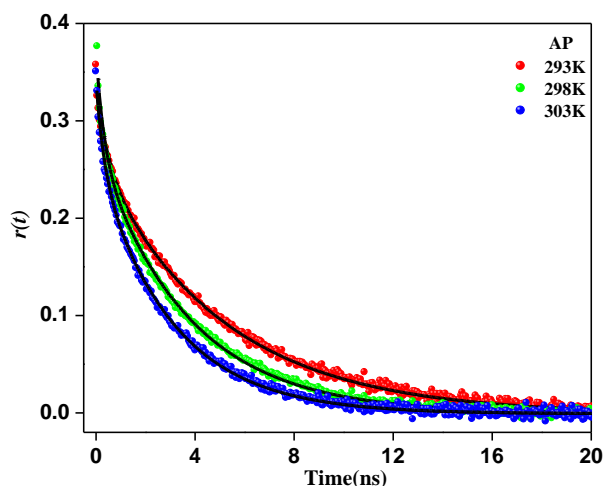
Figure 3.7. Decay of time-resolved anisotropy (r(t)) of AP in neat MOEMPLFAP] at $\lambda_{exc.}$ = 375 nm at different temperatures.

TABLE 3.2. Rotational relaxation parameters for AP and C153 in neat MOEMPLFAP at different temperature at $\lambda_{exc.}$ = 375 nm

Temp.(K)	Vis.(cP)	Probe	[t]r_0	a_1	τ_1(ns)	a_2	τ_2(ns)	$<\tau_r>$ (ns)	[†]C_{rot}
293	128	AP	0.36	0.24	0.48	0.76	5.03	3.94	0.68
		C153	0.37	0.28	0.93	0.72	6.58	5.00	0.44
298	98	AP	0.38	0.24	0.30	0.76	3.63	2.83	0.65
		C153	0.36	0.26	0.75	0.74	5.30	4.12	0.57
303	75	AP	0.35	0.25	0.30	0.75	3.02	2.34	0.61
		C153	0.37	0.27	0.61	0.73	3.97	3.06	0.57

[t] r_0 is the initial anisotropy. The C_{rot} values have been calculated by following the procedure from ref. 119.

The C_{rot} values of AP are found to be greater than that of C153. This observation supports the interplay of specific interaction between AP and MOEMPLFAP. In this context, it may also be mentioned that a small-step angular displacement of a flexible hydrogen bond

during its lifetime will not cause any solvent to be dragged and thus there will be negligible effect on molecular rotation.[244, 245]

3.3.1.3. *Theoretical Calculations*

To get further insight into the solute-solvent interaction, in particular, to find out whether the F atoms in the IL are participating in the H-bonding interaction with the probe molecules, we have optimized the structure of AP and C153 in presence of MOEMPLFAP. We have carried out the calculation by incorporating a solvation shell around the solute molecules. The solvation shell is created by doing a classical molecular dynamics simulation studies by using HyperChem package (Release 5.0) for Windows obtained from Hypercube, Inc. In particular, single ion pair of the present IL is replicated around the probe molecules in three dimensions to obtain a simulation box. The temperature, time and the step size for the simulation are 298 K, 1 ns and 1 fs respectively. Figure 3.8 represent the structures of the two solute molecules in the ambience of RTIL. From the simulation profile, closest pair of IL-solute are chosen and the structures have been optimized with B97-D functional [246], def2-SVP basis set[247, 248] using Turbomole V6.2 program[249]. Optimized structure of MOEMPLFAP-AP and MOEMPLFAP–C153 are also shown in the Figure 3.9. The selected structural parameters as obtained from the optimized structures are collected in Table 3.3.

The van der Waals criterion for hydrogen bonding is that for the formation of A-H….B bonds, the distance A…..B should be less than the sum of the A-H covalent bond distance and the van der Waals radii of H and that of the B.[250] The optimized structure of the present RTIL reveals C-H…F interactions between cationic and anionic fragment of the RTIL (Table 3.3).
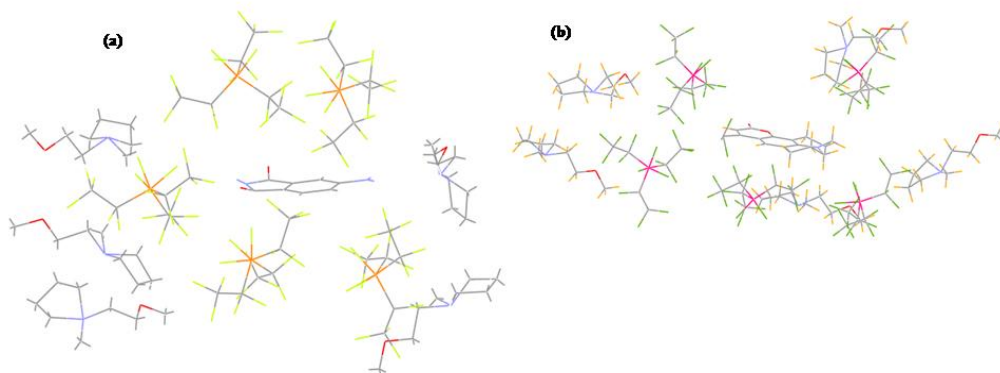
Figure 3.8. Structures of solute molecules and the solvent shell; (a) AP and RTIL and (b) C153 and RTIL.
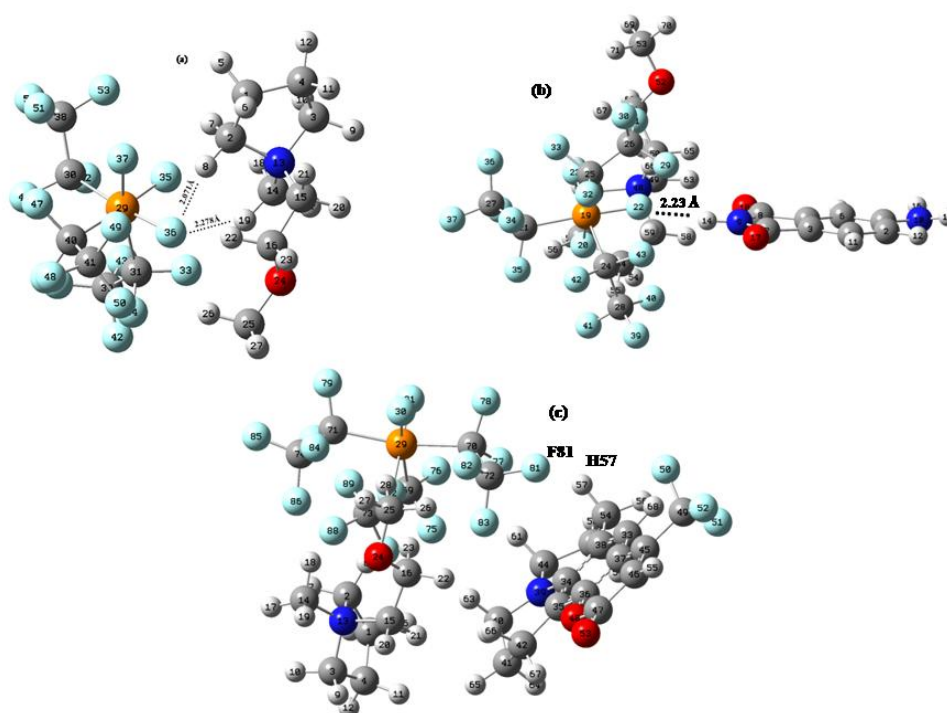
Figure 3.9. Optimized Structures of (a) neat MOEMPLFAP, (b) MOEMPLFAP-AP and (c) MOEMPLFAP-C153.

Interestingly, in the optimized structure of the MOEMPLFAP-AP complex, N9-F22 distance is measured to be 3.224 Å, which is shorter than the sum of N9-H14 covalent bond distance (1.023 Å) and the van der Waals radii of H (1.20 Å) and that of the F (1.47 Å), supporting the hydrogen bonding (N-H…F) between F22 of the ionic liquid and H14 of the probe, AP. Interestingly, we have not observed any such type of short contacts between C153 and the present RTIL.

Table 3.3: Structural parameters obtained from the B97-D functional. Def-SVP level optimized structures of neat MOEMPLFAP, MOEMPLFAP-AP and MOEMPLFAP-C153

systems	distance	(Å)	angle	(°)
Neat MOEMPLFAP	F36-H8	2.071	C14-H19-F36	139
	F36-H19	2.278	C2-H8-F36	128
	C2-F36	2.961		
	C14-F36	3.181		
	C2-H8	1.094		
	C14-H19	1.094		
MOEMPLFAP-AP	F22-H14	2.234	N9-H22-F22	162
	P19-F22	1.724		
	N9-H14	1.023		
	N9-F22	3.224		
MOEMPLFAP-C153	F81-H57	2.745	F81-H57-C54	120

To quantify these interactions, we have calculated the interaction energy between RTIL and AP. The ground state energies of the concerned species are calculated in vacuo using hybrid DFT functional B3LYP[228, 229] at 6-31+G (d, p) level using Gaussian 03 Program[231]. The initial optimization of the structures has been carried out by using the B97-D functional, def2-SVP basis set using Turbomole V6.2 program. By using the ground state energy of the corresponding constituents, interaction energy (ΔE_{int}) of the MOEMPLFAP-AP complex is computed by the following equation which is the difference between the energy of the MOEMPLFAP-AP complex and the total energy of the MOEMPLFAP and AP system.

$$\Delta E_{int} = E_{MOEMPLFAP-AP} - (E_{MOEMPLFAP} + E_{AP}) \qquad (3.4)$$

The interaction energy, predominantly N-H…F interaction energy, is calculated to be -3.04 k cal/mole. In this context, we would like to mention that the O-H…O and the N-H…O hydrogen the bond energy values lie in the range of 4-7 kcal/mol[251-253].

Theoretical calculations reveal the existence of N–H. . .F interaction between the fluorine atom of FAP anion and the imide hydrogen of AP, while no such specific interaction for C153 could be found. Here, it may be mentioned that the ability of the FAP anions to form hydrogen bond with a hydrogen bond donor (Rhodamine 110) has also been reported by Dutt[153]. Now, considering the observation in the present study, we can assume that there is a specific interaction between AP and the RTIL which is not strong enough to make any significant impact on the normal hydrodynamic behavior of the probe molecules but can play a vital role in the dynamics of solvation in this medium.

3.3.2. *Fluorescence Response of C153 in 1-Ethyl-3-Methylimidazolim Alkylsulfates*

3.3.2.1. *Steady State Behavior*

The representative absorption and emission spectra of C153 in the 1-ethyl-3-methylimidazolium alkylsulfates are shown in Figure 3.10. Emission spectra for all neat ILs are also shown in the same figure. The emission maxima for C153 in butyl, hexyl and octyl systems are measured to be 535 nm, 529 nm and 524 nm respectively. The absorption and emission maxima of C153 in neat ILs are collected in Table 3.4. The blue shift in the absorption and emission maxima of C153 from butyl to octyl system clearly indicates that there is an appreciable increase in the nonpolar character of the ILs with increase in the alkyl chain length. No significant changes in the steady state absorption and emission behavior of C153 have been observed upon changing the experimental temperature.

Table 3.4. Absorption and emission maxima, Stokes shift of C153 in different RTILs

RTILs	Abs. max.λ_{max}(nm)	Em.max. λ_{max}(nm)	Steady state stokes shift$\Delta\gamma$(cm^{-1})
EMIMBSU	426	534	4748
EMIMHSU	425	529	4571
EMIMOSU	424	524	4501

Experimental error $\pm$ 1nm
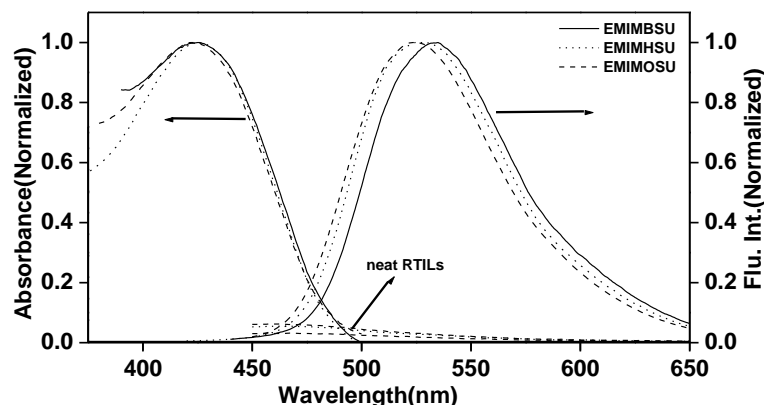
Figure 3.10. Steady state absorption and emission spectra of C153 in neat RTILs at 298 K. All spectra are normalized at the corresponding peak maximum. Emission spectra for different ILs are also shown at the bottom at $\lambda_{exc.} = 405$ nm.

3.3.2.2 *Time-resolved Studies*

3.3.2.2.1. *Solvation Dynamics*

A representative TRES for C153 in EMIMBSU at different time intervals at 293K is shown in Figure 3.11. In all cases, time dependent shift of the emission maximum towards the lower energy has been observed indicates solvent induced stabilization of excited state of the dipolar molecule. The time dependent stokes shift due to solvent relaxation, measured from the differences between the wavenumbers corresponding to the emission maxima at zero time ($\bar{\nu}(0)$) and infinite ($\bar{\nu}(\infty)$), is observed to be 718 cm^{-1}, 830 cm^{-1}, 910 cm^{-1} for C153 in butyl, hexyl and octyl analogue respectively (Table 3.5). It is evident from these data that the observed shift gradually increases upon increasing the length of alkyl side chain.

Table 3.5. Observed shift ($\Delta\bar{\nu}$) and missing component (MC) in solvent relaxation for C153 in different RTILs at 293K.

RTILs	$\bar{\nu}(0)$ (cm^{-1})	$\bar{\nu}(\infty)$ (cm^{-1})	$\Delta\bar{\nu}$ (cm^{-1})	MC (%)
EMIMBSU	19440	18722	718	51
EMIMHSU	19699	18869	830	38
EMIMOSU	19836	18926	910	33

3.2.2.1.1. *Time-zero Spectra*

Since the emission maximum at zero time, that is, time-zero spectrum, is useful in interpreting the microenvironment around the probe molecule[115], we have carefully monitored the location of the maximum of the time-zero emission spectrum of C153 in all three ionic liquids. Interestingly, steady and noticeable blue shift of the measured time-zero spectrum of C153 has been observed with increasing alkyl chain lengths (Table 3.5).
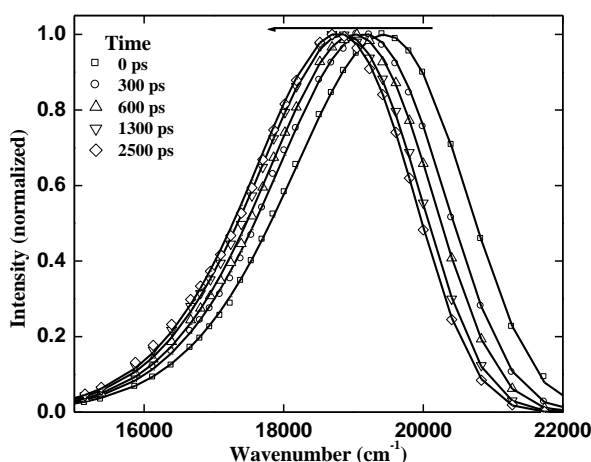
Figure 3.11. TRES of C153 in EMIMBSU at different time span at 293K. The time intervals are indicated by the corresponding symbols. All spectra are normalized at their corresponding peak maximum.

The observed blue shift of the emission maximum of the time zero spectrum with increasing alkyl chain length of ILs indicates that the probe molecule is experiencing less polar environment in the early part of the dynamics as we go from butyl to octyl analogue. The full width at half maximum (FWHM) of the time-resolved spectra gradually decreases with increasing time, as shown for C153 in EMIMBSU in Figure 3.12. This indicates solvent mediated stabilization of photoexcited probe. The present observations clearly show that the length of alkyl side chain plays an important role in controlling the dynamics of solvation in these media.

3.2.2.1.2. *Observed Shift and Missing Component*

While the total blue shift of the time-zero spectrum ($\bar{\nu}(0)$) of C153 on going from butyl to octyl system is found to be 396 cm^{-1} (Table 3. 5), the corresponding shift of ($\bar{\nu}(\infty)$) is

much less, i.e. ~204 cm^{-1} (Table 3. 5). Larger blue shift of ($\overline{v}(0)$) compared to ($\overline{v}(\infty)$) with increase in the alkyl chain length indicates that the increase in the chain length induces more nonpolar character of the microenvironment of the probe molecule at the early stage of dynamics as compared to the final stage.
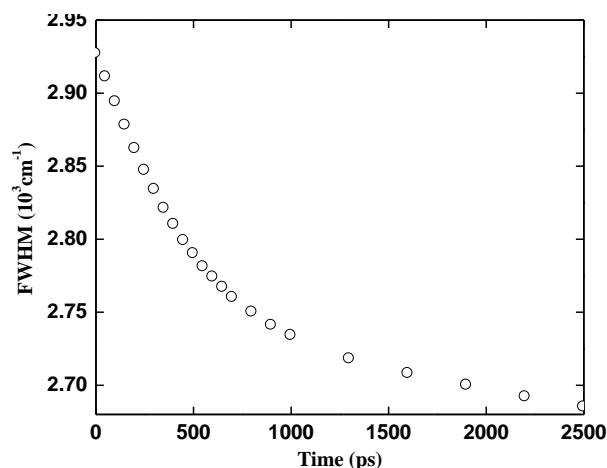
Figure 3.12. Plot of FWHM, obtained from several time-resolved emission spectra of C153 in EMIMBSU, at different time span at 293K.

As can be seen from Table 3.5, the measured Stokes shift ($\Delta\overline{v}$) due to the solvent relaxation increases with increasing alkyl chain length. Interestingly, the difference between the emission maxima of the time-resolved spectra to that of steady state spectra (Tables 3.4 and 3.5) is found to increase gradually with an increase in the alkyl chain length of the ILs (4 cm^{-1}, 34 cm^{-1}, 157 cm^{-1} for EMIMBSU, EMIMHSU and EMIMOSU respectively). This reflects the incomplete relaxation of the solvent molecules due to larger size; the larger the solvent molecules, weaker the relaxation. Since at lower temperature and high viscous condition of the medium, the non-relaxation dynamics are known to contribute to the observed relaxation of solvation energy[254, 255], at lower temperature such non-relaxation dynamics cannot be entirely ruled out for larger system like EMIMOSU. Total expected Stokes shift, estimated by the procedure described by Fee and Maroncelli [226] is 1462 cm^{-1} for EMIMBSU. This suggests that more than 50 % of the dynamics is missed due to the limited-time-resolution of our TCSPC set up.

3.2.2.1.3. *Observable Dynamics*

Plots of Spectral correlation function, *C(t)*, versus time plots for all three ILs along with the bi-exponential and stretched exponential fits are shown in Figure 3.13. In the present case, both biphasic and nonexponential treatment of observable dynamics yields very similar average solvation times (Table 3.6). However, considering the quality of the fit, bi-exponential fitting is found to be more relevant than the stretched exponential fitting (Figure 3.13). The average solvation times of C153 in butyl, hexyl and octyl analogues are estimated to be 0.85 ns, 1.3 ns and to 1.6 ns respectively at 293K.

Table 3.6. Relaxation parameters of solvation for C153 in different RTILs at different temperatures

RTILs	Temp.(K)	Vis.(cP)	a_1	τ_1(ns)	a_2	τ_2(ns)	$\langle\tau_s\rangle^c$(ns)	β	τ_{solv}	$\langle\tau_{st}\rangle$(ns)
				from bi-exponential fit[a]					stretched exp. fit[b]	
EMIMBSU	293	191	0.67	0.42	0.33	1.73	0.85	0.81	0.686	0.770
	298	141	0.70	0.42	0.30	1.39	0.71	0.86	0.609	0.665
	303	106	0.86	0.42	0.14	1.49	0.57	0.92	0.500	0.520
EMIMHSU	293	389	0.62	0.45	0.38	2.70	1.30	0.69	0.928	1.191
	298	284	0.65	0.43	0.35	2.48	1.15	0.71	0.808	1.010
	303	211	0.70	0.42	0.30	2.25	0.97	0.74	0.687	0.827
EMIMOSU	293	646	0.56	0.46	0.44	3.05	1.60	0.70	1.208	1.529
	298	453	0.61	0.42	0.39	2.98	1.42	0.68	1.005	1.309
	303	329	0.64	0.41	0.36	2.76	1.26	0.70	0.894	1.132

[a]using equation 2.13, [b]using equation 2.15 and [c]experimental error is 5%

The increase in average solvation times with increase in alkyl chain length is in tune with the increase in the bulk viscosity of the ILs with increasing chain length. The variation of average solvation times with the bulk viscosity of the present ILs are shown in Figure 3.14(i). From Figure 3.14(ii) we also notice that the weighted short component ($a_1\tau_1$) is not so sensitive to the change in viscosity, whereas longer component ($a_2\tau_2$) is quite sensitive to

viscosity change, and follows similar trend like average solvation time. In all temperature, average solvation time decreases due to the lowering of the bulk viscosity of the media (Table 3.6).
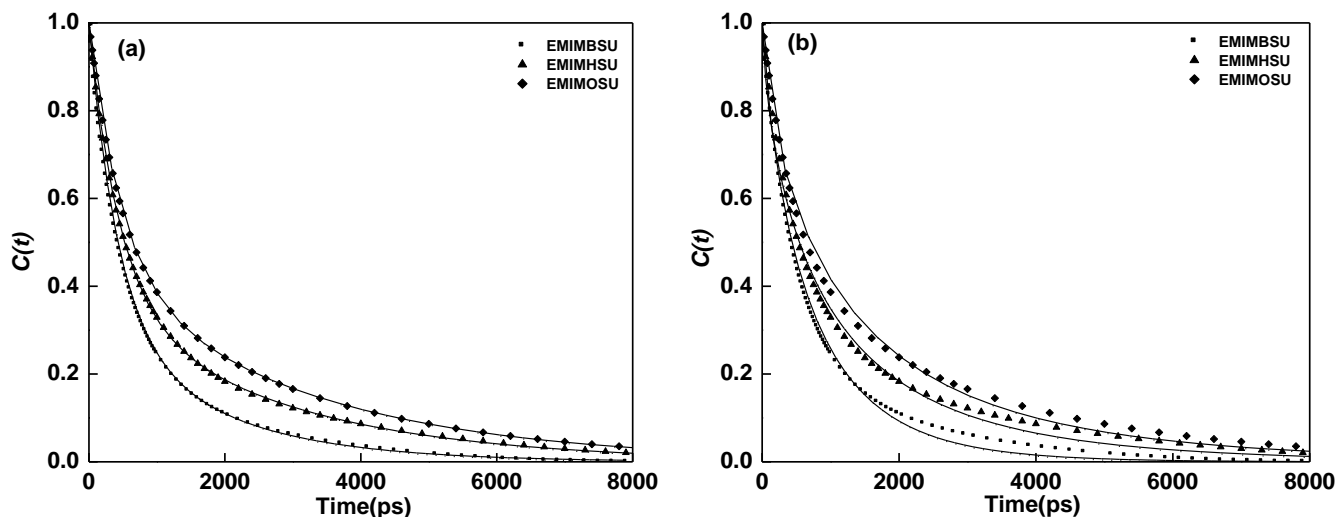
Figure. 3.13. (a) Bi-exponential fits of the spectral correlation function, *C(t)*, of C153 in different RTILs at 293 K. (b) stretched exponential fits of *C (t)* of C153 in different ILs at 293 K.
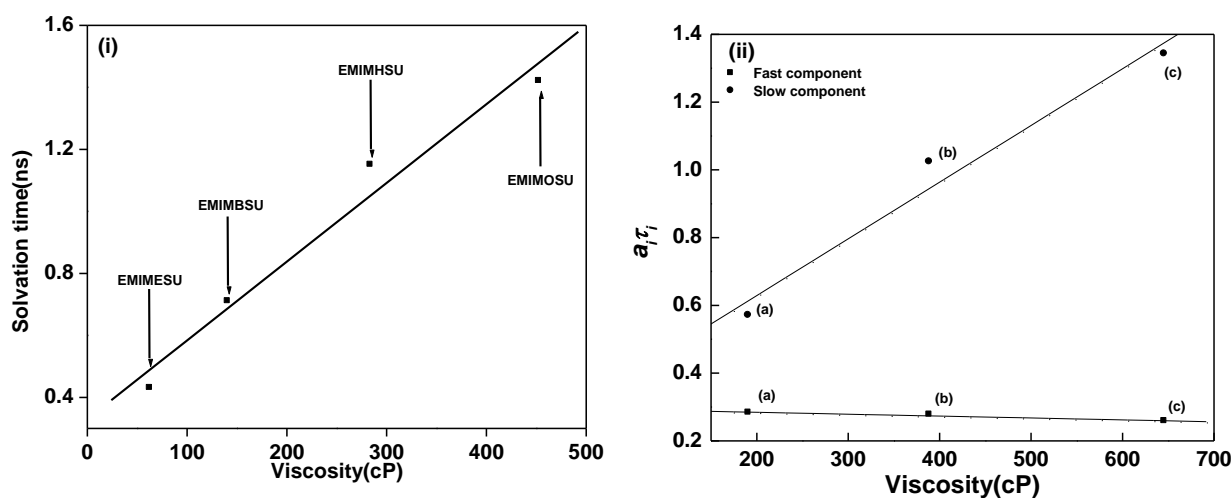
Figure 3.14. (i)Variation of average solvation times with respect to the viscosity of different RTILs at 298 K. The solid line represents linear fit to the data. Data for 1-ethyl-3-methylimidazolium ethylsulfate (EMIMESU) is taken from reference 135. (ii) Plot of weighted solvation time-components vs. bulk viscosity of ILs at 293 K. The symbol represents data points and solid line represents linear fit to the data. (a) EMIMBSU, (b) EMIMHSU and (c) EMIMOSU.

3.4. Conclusion

This chapter examines the effect of probe molecules and ionic constituents of RTILs on solvation dynamics. In the first case, we have studied the steady state and time-resolved fluorescence behavior of two dipolar molecules namely AP and C153 in a hydrophobic MOEMPLFAP in order to determine the dynamics of solvation in general and to investigate probe dependency in solvation dynamics in particular. The present RTIL is well suited to study dynamics of solvation for its low moisture content. The average solvation time for AP is found to be six times larger than that of C153. Rotational coupling constants obtained from the time-resolved anisotropy data also show a higher value for AP as compared to C153. The present observation possibly indicates that the solute–solvent specific interaction even though weak in nature may play important role towards dynamics of solvation. However, we would like to emphasize that more experimental and theoretical studies are needed to provide further insight into the mechanism of probe dependent solvation dynamics in ILs. In the second case, steady state and time-resolved fluorescence behavior of C153 has been investigated in a series of 1-ethyl-3-methylimidazolium alkylsulfate ILs to understand the role of alkyl side chains on solvation dynamics of C153 in these media. A steady blue shift of the time-zero maximum of the fluorescence spectrum with increasing alkyl chain length indicates that the probe molecule experiences a less polar microenvironment in the early part of the dynamics on going from butyl to octyl analogue. The average solvation time increases with increasing length of the alkyl side chain, and this is attributed to the increase in bulk viscosity of ILs with increasing alkyl chain lengths.

Effect of Anions and Alkyl Chain Length on the Rotational Relaxation of Coumarin153 and 4-Aminophthalimide in Room Temperature Ionic Liquids

4.1. Introduction

Solute–solvent interactions play an important role in determining the physicochemical properties of liquids and solutions.[197] As a consequence, understanding these interactions has been one of the long-standing goal in physical chemistry. Since inter-ionic interactions in room temperature ionic liquids (RTILs) are believed to be an important factor for their interesting physicochemical properties.[12, 13] a closer investigation on the intermolecular interactions is desirable. Dielectric relaxation[63, 256], solvation dynamics[109-149], rotational diffusion[150-163], intramolecular electron/charge transfer[164-169, 177, 178], are some of the studies, which have been carried out in recent times to address these issues. It may be mentioned that studies on orientational dynamics are often helpful to find out specific solute-solvent interactions.[197] Even though available literature on the rotational dynamics of various solutes in conventional solvents is quite extensive, similar information on ionic liquids (ILs) is rather limited.

Earlier, Ingram et al.[118] have studied the rotational dynamics of N, N′-bis(2,5-di-tert-butylphenyl)-3,4,9,10-perylenecarboximide (BTBP) and 4-aminophthalimide (AP) in 1-butyl-3-methylimidazolium hexafluorophasphate (BMIMPF$_6$) as a function of temperature. Ito et al.[119] have also studied the rotational dynamics of neutral and charged solutes in the same IL. These studies have revealed that rotational dynamics of organic solutes are mainly governed by the viscosity of the medium. However, no evidence of electrostatic and/or specific hydrogen bonding interactions has been found.

Later on, Mali et al.[152, 257] have shown that solute-solvent (IL) hydrogen bonding interaction in the RTILs significantly hinders solute rotation. Effect of specific solute-solvent

hydrogen bonding interaction on the rotational dynamics of a neutral organic solute has also been observed by Paul et al.[114] in an alcohol-functionalized IL. In recent times, rotational dynamics of ionic solutes have also been carried out in different ILs to throw more light on solute-solvent interaction.[150-163] Fruchey and Fayer[151] have studied the rotational diffusion of a charged solute, sodium 8-methoxypyrene-1,3,6-sulfonate (MPTS) and a neutral solute, perylene, in a series of 1-alkyl-3-methylimidazolium bis(trifluoromethanesulfonyl)imide RTILs. Anionic MPTS is found to exhibit superstick behavior due to its strong interaction with the imidazolium cation of the ILs. However, rotational motion of perylene becomes increasingly subslip with increasing alkyl chain length of the cationic moiety. A similar rotational dynamics study of ionic solutes in 1-butyl-3-methylimidazolium tetrafluoroborate (BMIMBF$_4$) and glycerol by Samanta and coworkers[150] reveals that there is no observable effect of electrostatic interaction between these ionic solutes and ILs. However, hydrogen bonding interaction is found to play an important role towards the rotational motion of the solutes. Dutt and coworkers[153] have also studied the rotational behavior of rhodamine 110 (R110) and 2, 5-dimethyl-1, 4-dioxo-3, 6-diphenylpyrrolo [3,4-*c*] pyrrole (DMDPP) in a series of 1-alkyl-3-methylimidazolium ILs containing fluoroalkylphosphate(FAP) anions. They have observed that the rotational behavior of R110 is closer to stick boundary condition due to the specific solute-solvent interaction, whereas DMDPP follows slip hydrodynamics. Interestingly, rotational behavior of DMDPP is found not to be influenced by the alkyl chain lengths. It is evident from the earlier reports that although the experimentally measured reorientation times generally lie between the broad limits of slip and stick hydrodynamic boundary conditions, a perfect match has not often been achieved and significant deviations from normal hydrodynamic conditions have also been observed. It is, therefore, evident from the above discussions that the exact nature of solute-solvent interactions in ILs is still not clear. Study of rotational dynamics by doing the systematic variations in the constituents of

the ILs would be helpful to understand the nature of various forces that are responsible for solute-solvent interactions and also the interactions between the constituents of the ILs. While the effect of alkyl chain length on the cationic part of ILs towards the rotational dynamics of organic solutes in the ILs have been demonstrated by Fayer[151] and Dutt[153] coworkers independently, no studies on this aspect by varying alkyl chain length in the anionic part of the ILs have been carried out. In this regard, it would also be interesting to study rotational relaxation dynamics study in ionic liquids having different anions with different H-bond basicity values such that a correlation between average rotational relaxation time and H-bond basicity is obtained.

Keeping these facts in mind, studies on rotational relaxation dynamics study of organic solutes in two sets of RTILs have been carried out independently. In one study 4-aminophthalimide (AP) and coumarin153 (C153) have been investigated in a series of 1-ethyl-3-methylimidazolium alkyl sulfate RTILs, viz. 1-ethyl-3-methylimidazolium ethylsulfate (EMIMESU), 1-ethyl-3-methylimidazolium butylsulfate (EMIMBSU), 1-ethyl-3-methylimidazolium hexylsulfate (EMIMHSU), and 1-ethyl-3-methyl imidazolium octylsulfate (EMIMOSU), as a function of temperature. This particular study has been undertaken to examine the role of alkyl side chains on the rotational dynamics of these two solutes. In other study, rotational diffusion of same solutes in three different RTILs, viz. 1-ethyl-3-methylimidazolium trifluoroacetate (EMIMTFA), 1-ethyl-3-methylimidazolium tetrafluoroborate (EMIMTFB) and 1-ethyl-3-methylimidazolium tetracyanoborate (EMIMTCB) have been carried out. These ILs are purposefully chosen so that an appreciable variation of the hydrogen bond basicity of anions in these ILs is achieved. In all ILs under present study, a fixed cationic moiety is used so that the effect of anions and alkyl chain length on sulfate anion on the rotational dynamics is exclusively monitored. Out of the probes, only AP has the hydrogen-bond donating ability by virtue of its acidic nature of imide

proton. Molecular diagrams of solutes and RTILs are provided in Chart 4.1 and Chart 4.2 respectively.
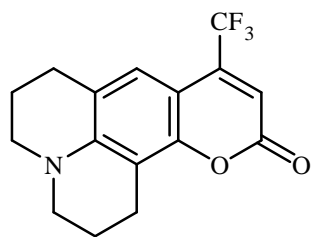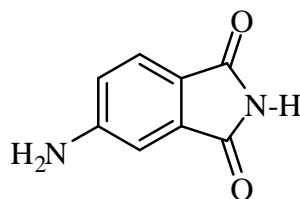
Coumarin153 (C153)   4-aminophthalimide (AP)

Chart 4.1: Molecular diagrams of (A) Coumarin153, (B) 4-Aminophthalimde.
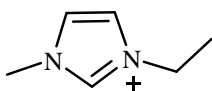
1-ethyl-3-methylimidazolium (EMIM)   alkylsulfate
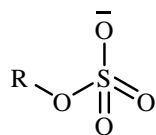
$R = C_2H_5$ (EMIMESU)
$= C_4H_9$ (EMIMBSU)
$= C_6H_{13}$ (EMIMHSU)
$= C_8H_{17}$ (EMIMOSU)
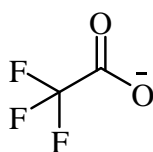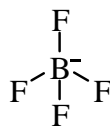
trifluoroacetate (TFA)   tetrafluoroborate (TFB)   tetracyanoborate (TCB)
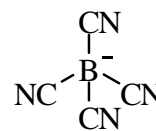
Chart 4.2: Molecular diagrams of RTILs under present study.

4.2. Materials and Experimental Techniques

C153 (laser grade, Exciton) and AP (TCI, Japan) were used as solute probes. RTILs weree obtained from Merck Germany (>99% purity) with water and halide contents less than 100 ppm. Deuterated dimethyl sulfoxide (DMSO-d_6) was obtained from sigma Aldrich and used for NMR experiments. Procedure of sample preparation for steady state and time-resolved measurements are discussed in details in Chapter 2. The Details of viscometer, density meter, TCSPC technique, experimental procedures and methods are described in Chapter 2.

106

4.3. Results and Discussion

4.3.1. *Time-resolved Fluorescence Anisotropy Study of C153 in 1-Ethyl-3-Methylimidazolium Alkylsulfates*

The time-resolved fluorescence anisotropy, r*(t)*, is measured using Equation 2.21. The details of procedure for the determination rotational diffusion times are described in Chapter 2 in great detail. Representative time-resolved fluorescence anisotropy decay profiles of C153 in neat RTILs at various temperatures are shown in Figure 4.1. Figure 4.2, which shows the plot of *ln(η)* versus *1/T* for these four ILs, reveals that there is gradual increase in the viscosity with an increase in the alkyl chain length on the sulfate anion. The rotational relaxation parameters for C153 in these ILs at different temperatures are collected in the Table 4.1. Both bi-exponential and single exponential fit to the anisotropy decay profiles of C153 in the ILs are acceptable. The bi-exponential fits are found to be slightly better than the single exponential fits. However, the average rotational times, $<\tau_{rot}>$, obtained from bi-exponential fits are found to be very similar to those obtained from single exponential fits.
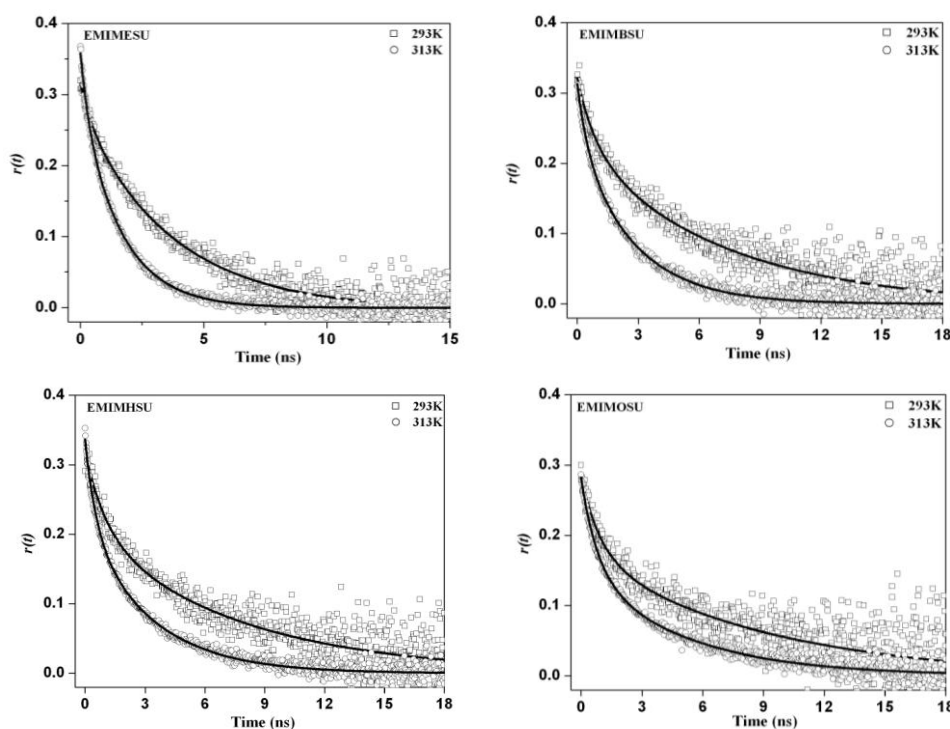
Figure 4.1. Time-resolved fluorescence anisotropy decay profiles of C153 in 1-ethyl-3-methylimidazolium alkylsulfates. Long and short decay profiles are at 293K and 313K respectively. Solid lines represent the bi-exponential fit to the data points.
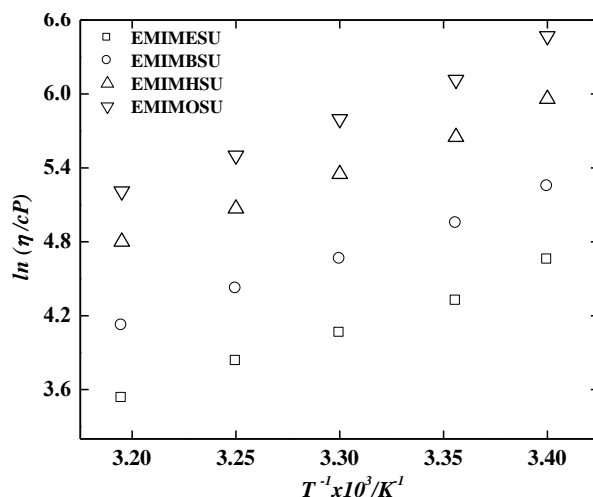
Figure 4.2. Plots for *ln(η)* versus *1/T* for all four 1-ethyl-3-methlimidazolium alkylsulfates. The line passing to the data points are drawn as visual aid.

Table 4.1. Summary of the rotational relaxation parameters of C153 in 1-ethyl-3-methlimidazolium alkylsulfates at different temperatures

RTILs	Temp.(K)	Vis.[a](cP)	r_0[b]	a_1	τ_1(ns)	a_2	τ_2(ns)	$\langle\tau_{rot}\rangle$ (ns)[c]	C_{rot}[d]
EMIMESU	293	105	0.34	0.12	0.46	0.88	3.66	3.28	0.35
	298	75	0.36	0.19	0.90	0.81	3.34	2.88	0.43
	303	58	0.36	0.29	1.00	0.71	2.73	2.23	0.44
	308	46	0.33	0.21	0.71	0.79	2.10	1.81	0.46
	313	34	0.38	0.19	0.36	0.81	1.63	1.39	0.48
EMIMBSU	293	191	0.31	0.30	0.92	0.70	6.87	5.08	0.29
	298	141	0.34	0.29	0.77	0.71	5.16	3.88	0.31
	303	106	0.37	0.25	0.60	0.75	3.95	3.11	0.34
	308	82	0.36	0.30	0.66	0.70	3.30	2.51	0.35
	313	63	0.33	0.26	0.54	0.74	2.77	2.19	0.40
EMIMHSU	293	389	0.30	0.37	1.08	0.63	7.67	5.23	0.15
	298	284	0.31	0.34	0.89	0.66	5.77	4.11	0.16
	303	211	0.31	0.34	0.64	0.66	4.62	3.27	0.18
	308	160	0.30	0.35	0.67	0.65	4.20	2.96	0.21
	313	122	0.35	0.36	0.62	0.64	3.36	2.37	0.23
EMIMOSU	293	646	0.28	0.39	0.95	0.61	8.86	5.77	0.10
	298	453	0.28	0.42	0.93	0.58	7.28	4.61	0.11
	303	329	0.28	0.40	0.80	0.60	6.00	3.92	0.14
	308	245	0.28	0.41	0.75	0.59	5.51	3.56	0.17
	313	183	0.28	0.47	0.81	0.53	5.03	3.04	0.20

[a] ± 5%. [b] initial anisotropy .[c] rotational relaxation time (error limit 5%). [d] rotational coupling constant.

It is evident both from the anisotropy decay profiles shown in Figure 4.1 and the data presented in Table 4.1 that with increase in temperature, the rotational diffusion becomes faster due to the lowering of the viscosity of the media. More interestingly, the data that are

collected in Table 4.1 also reveals that the average rotational times of C153 increase with increase in alkyl chain length of ILs. However, the decay does not become as slow as it is expected from the increase in the bulk viscosity values with concomitant increase in the alkyl chain length. For example, at 293K, on going from ethyl to butyl analogue, the average rotational time increases by 54% with a change in the viscosity value from 105 cP to 191 cP. However, on going from butyl to octyl analogue, the average rotational time changes by only 13%, whereas the viscosity value changes by 455 units. The observation indicates that rotational diffusion of C153 actually becomes faster as we increase the alkyl chain length in the anionic moiety.

In an attempt to have a comprehensive understanding on the rotational dynamics of C153, we have analyzed our experimental data by the most commonly used Stokes-Einstein-Debye (SED) hydrodynamic model of rotational diffusion which is described in detail in Chapter 1. For the calculation of the rotational diffusion time (τ_r^{SED}) with the help of SED theory for the corresponding probes, we have used the probe properties that are available in the literatures.[119] The values for the probe molecules are collected in Table 4.2. Since all three axial radii are different, each solute molecule is treated as an asymmetric ellipsoid. The friction coefficients (ξ_i) with stick and slip boundary conditions along the three principle axes of rotation are estimated from the literature available numerical tabulations.[258, 259] From the calculated friction coefficients, the diffusion coefficients along the three axes (D_i) are obtained by using the following Einstein relation [260]

$$D_i = \frac{k_B T}{\xi_i}$$

(4.1)

109

Considering that the direction of the transition dipole coincides with the long axis of the molecule, the rotational times are calculated from the diffusion coefficients by the following equation.[261]

$$\tau_r = \frac{1}{12}(\frac{4D_a + D_b + D_c}{D_aD_b + D_bD_c + D_cD_a})$$
(4.2)

where, D_a, D_b and D_c are the diffusion coefficients along a, b and c axis, respectively. The boundary condition (C_{slip}) are estimated from the calculated rotational times.

Table 4.2. Solute dimensions and van der Waals volumes together with shape factors and boundary condition parameters calculated using the SED hydrodynamic theory

Solute	Axial radii/Å^3	van der Waals volume/Å^3	Shape factor(f)	Boundary conditions(C_{slip})
C153	$6.0 \times 3.9 \times 2.5$	243	1.5	0.18
AP	$5.0 \times 3.5 \times 1.8$	134	1.6	0.16

Figure 4.3 shows log-log plots of experimentally measured reorientation times of C153 vs. η/T in four 1-ethyl-3-methylimidazolium alkylsulfate ILs along with the calculated stick and slip lines. As can be seen from Figure 4.3, the rotational dynamics of C153 in EMIMESU lie between the stick and slip boundary conditions. Interestingly, Figure 4.3 also reveals that with an increase in the alkyl chain length on the sulfate moiety, the rotational dynamics of C153 changes to slip and finally reaches to subslip condition as in case of the highest member (EMIMOSU) of the series. The faster rotation of C153 with an increase in the alkyl chain length on the anionic constituent of the ILs is also evident when we fit the τ_r and η/T data for C153 to the function, $\tau_r = A(\eta/T)^p$, a procedure described by Mali et al.[152, 257]

C153 in EMIMESU, $\tau_r = (7.042 \pm 0.760) (\eta/T)^{0.70\pm0.074}$ (N = 5, R = 0.9857) (4.3)

C153 in EMIMBSU, $\tau_r = (6.966 \pm 0.180) (\eta/T)^{0.76\pm0.029}$ (N = 5, R = 0.9980) (4.4)

C153 in EMIMHSU, $\tau_r = (4.301 \pm 0.067) (\eta/T)^{0.64\pm0.037}$ (N = 5, R = 0.9953) (4.5)

C153 in EMIMOSU, $\tau_r = (3.871 \pm 0.063)\,(\eta/T)^{0.48\pm0.030}$ $\qquad$ (N = 5, R = 0.9944) $\qquad$ (4.6)

In these expressions, N and R are the number of data points and regression coefficients, respectively.
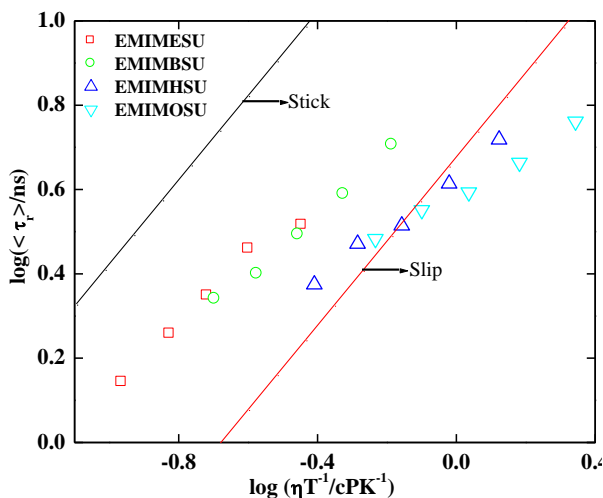
Figure 4.3. log-log plots of average rotational relaxation time of C153 vs. η/T in different 1-ethyl-3-methlimidazolium alkylsulfates with slip and stick boundary condition parameters. Symbols denote the experimental data points.

We have also calculated the rotational coupling constants (C_{rot}) with the help of Equation 1.2. Interestingly, C_{rot} values (Table 4.1) indicate the faster rotation of C153 with an increase in alkyl chain length. It is pertinent to mention here that the study by Fruchey et al.[151] shows that the rotational behavior of perylene becomes increasingly subslip as alkyl chain length on the cation moiety is increased. As mentioned earlier, no alkyl chain length dependence on the rotational dynamics of DMDPP in FAP containing ILs has been observed.[153] In view of this, the rotational behavior of C153 in different ionic liquids used in this work is quite interesting.

In this context, we note that quasihydrodynamic theories of Gierer-Wirtz (GW)[198] and Dote-Kivelson-Schwartz (DKS)[199] tells that the size of the solvent molecules has profound effect on the solute rotation in the sense that larger solvent molecules provide lower friction to rotating solutes. Consequently, boundary condition parameter (C), obtained from SED theory, is modified by both the GW and DKS theories. Since SED theory is not successful in explaining the rotational behavior of C153 in the ILs (EMIMHSU and EMIMOSU), we resort

to both the DKS[198] and GW[199] models to explain the faster rotation of C153 with increasing length of alkyl side chains.

According to GW theory, the solvent is made up of concentric shells of spherical particles surrounding the spherical solute molecule at the center. The boundary condition parameter (C_{GW}) is determined by considering the decrease in the angular velocity of the solvent molecules in successive shells surrounding the solute as a function of distance away from it. The boundary condition parameter is expressed by the following relation[198]

$$C_{GW} = \sigma \, C_0 \tag{4.7}$$

where σ is the sticking factor, which is given by the relation

$$\sigma = \left[1 + 6 \left(\frac{V_S}{V_P} \right)^{\frac{1}{3}} C_0 \right]^{-1} \tag{4.8}$$

and C_0 is given by the following expression

$$C_0 = \left[\frac{6 \left(\frac{V_S}{V_p} \right)^{\frac{1}{3}}}{\left[1 + 2 \left(\frac{V_S}{V_P} \right)^{\frac{1}{3}} \right]^4} + \frac{1}{\left[1 + 4 \left(\frac{V_s}{V_P} \right)^{\frac{1}{3}} \right]^3} \right]^{-1} \tag{4.9}$$

In the above relation V_S and V_P are van der Waals volume of solvent and solute respectively. The van der Waals volumes of the ILs are estimated using the Edward increment method.[262] Figure 4.4 depicts the log-log plots of average rotational relaxation time of C153 vs. η/T in different ILs with boundary condition parameters obtained from GW model. As can be seen from Figure 4.4, GW model is quite successful in explaining the

rotational dynamics of C153 in EMIMHSU. However, in larger system (EMIMOSU) the same model is found not to be successful (Figure 4.4).
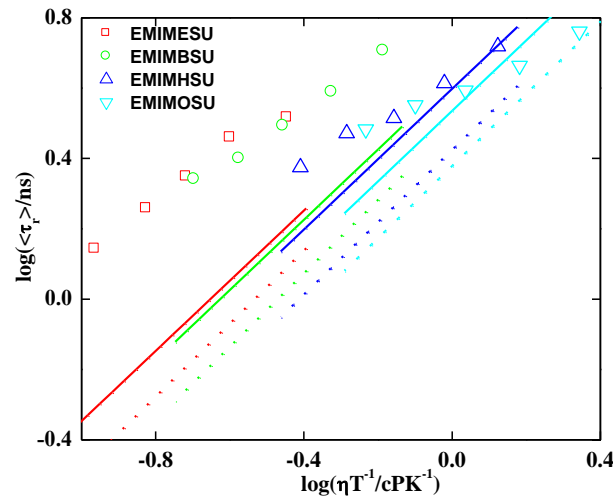
Figure 4.4. log-log plots of average rotational relaxation time of C153 vs. η/T in different 1-ethyl-3-methlimidazolium alkylsulfates with boundary condition parameters obtained from DKS and GW model. Symbols denote the experimental data points. Solid and dotted lines represents the boundary condition for GW and DKS model respectively (red=EMIMESU, green = EMIMBSU, blue=EMIMHSU, cyan=EMIMOSU).

We have also analyzed our data by employing DKS model. DKS theory takes into account the free volume of the solvent along with solvent-to-solute volume ratio while calculating the boundary condition parameter. The boundary condition parameter for DKS model, is given by the following relation[199]

$$C_{DKS} = (1 + \gamma/\phi)^{-1} \tag{4.10}$$

$$\text{where } \gamma = \frac{\Delta V}{V_P} \left[\left(\frac{V_P}{V_S} \right)^{\frac{2}{3}} + 1 \right] \tag{4.11}$$

and $\phi = f\, C_{\text{slip}}$, where C_{slip} is the solute-solvent coupling parameter under slip boundary condition.[263] In Equation 4.11, ΔV is the smallest volume of free space per solvent molecule which is empirically related to viscosity, Hilderbrand-Batschinski parameter, and isothermal compressibility of the solvent.[196] Anderton and Kauffman[264] have shown that in the case of associative solvents, the measure of free volume can be represented by the following relation

$$\Delta V = V_m - V_s \tag{4.12}$$

where V_m is the solvent molar volume divided by the Avogadro number. Molar volumes of all the ILs have been calculated by estimating the density of the ILs. There is a 4% decrease in C_{DKS} values obtained for C153/EMIMOSU solute-solvent combination from 293 K to 313 K due to decrease in density of the media. Figure 4.4 depicts log-log plots of average rotational relaxation time of C153 vs. η/T in different ILs with boundary condition parameters obtained from DKS model. The DKS model is successful in explaining the faster rotation of C153 in EMIMOSU (Figure 4.4). The observation shows that rotational behavior of C153 is mainly governed by the size of the alkyl chains. Since the larger solvent molecules offer lower friction to the rotating solutes, the rotation of C153 becomes faster with increasing length of alkyl side chains.

It may be mentioned in this context that rotational dynamics in the subslip domain are sometimes attributed to the complex solvation structure near the probe molecule.[265, 266] This structuring sometimes creates void spaces, which reduce the rotational friction below slip. When the rotational diffusion data is more carefully analyzed we have seen that, in the case of hexyl analogue, the rotational dynamics of C153 follows the GW theory at higher viscosity, but at lower viscosity it follows the slip boundary condition (Figure 4.4). In the case of the octyl analogue, at lower temperature and higher viscosity, rotational dynamics of C153 follows the DKS model, but at lower viscosity it follows the GW prediction (Figure 4.4). The results seem to suggest that none of the hydrodynamic descriptions are appropriate for solute rotation in these systems. Only one description for a given IL comes close to the measured values, while another prediction holds for another IL. The hydrodynamic theories were developed for isotropic (spherical) bodies, and their failure of these theories indicates failed assimilation of a nonspherical volume into a spherical volume.

This observation is quite interesting in the sense that the results obtained by studying the rotational dynamics of organic solutes in other RTILs by Fayer[151] and Dutt[153] are quite different. Interestingly, they did not reveal that probe molecules in a particular medium can follow different boundary conditions relating to different descriptions of hydrodynamics, as is observed in the present case. The inapplicability of hydrodynamic models to describe the rotation of C153 in these ILs possibly indicates diffusion–viscosity decoupling during the rotation of probe molecule. In this context, the rotational relaxation data in Table 4.1 reveal that solute rotation is decoupled from medium viscosity. Generally diffusion-viscosity is analyzed through fractional viscosity dependence of the measured rotational times $\langle\tau_r\rangle$: $\langle\tau_r\rangle \propto (\eta/T)^p$ (p is the exponent, and T is the temperature). As can be seen from Equation 4.3 to 4.6, in the present case, fractional viscosity dependency increases (p values decreases from 0.76 to 0.48) with an increase in alkyl chain length from butyl to octyl analogue in the anionic moiety. It may be mentioned that solute rotational relaxation dynamics have been found to be decoupled from the medium viscosity in deep eutectic melts due to its microheterogeneous behavior.[267, 268] It is also found that fractional viscosity dependence arises in highly organized medium during solute rotational relaxation dynamics.[117, 161] In view of this, it can be concluded that structural organization and heterogeneity increases with increase in alkyl chain length on the anionic moiety of these RTILs.

4.3.2. *Time-resolved Fluorescence Anisotropy Study of AP in 1-Ethyl-3-Methylimidazolium Alkyl sulfates*

Representative time-resolved fluorescence anisotropy decay profiles of AP in the neat 1-ethyl-3-methylimidazolim alkylsulfate ILs at various temperatures are shown in Figure 4.5. We resort to single exponential fitting for the anisotropy data of AP because a bi-exponential fit to the anisotropy data does not improve the quality of the fitting and also, the average rotational time estimated from the bi-exponential fit is found to be very similar with that

obtained from the single exponential fit. The rotational relaxation parameters for AP in ILs at different temperatures are collected in the Table 4.3.
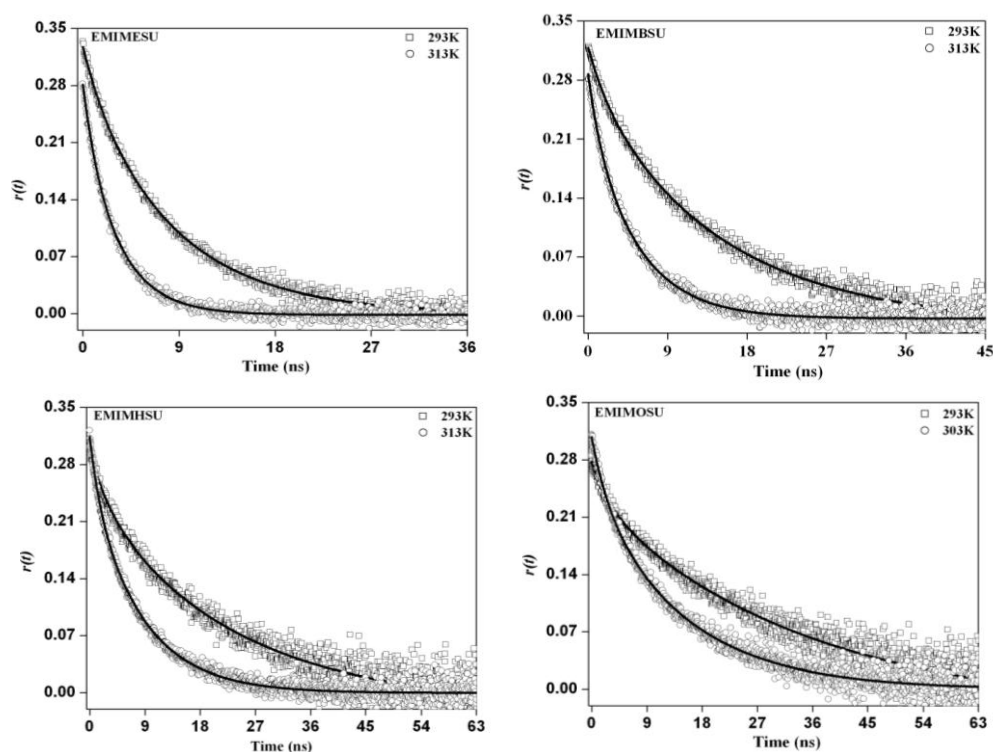
Figure 4.5. Anisotropy decay profiles of AP in the four 1-ethyl-3-methylimidazolium alkylsulfates. Long and short decay profiles are at 293 K and 313 K respectively. Solid lines represent the single exponential fit to data points.

As can be seen from Table 4.3, with an increase in the temperature, the rotational diffusion of AP becomes faster due to the lowering of the viscosity of the media. We have also analyzed the rotational behavior of AP by the most commonly used Stokes-Einstein-Debye (SED) hydrodynamic model. In case of AP, Figure 4.6 represents the log-log plots of experimentally measured reorientation times of AP vs. η/T in four ILs along with the calculated stick and slip lines. As can be seen from Figure 4.6, the rotational time of the AP is significantly higher than that predicted by the stick boundary condition in EMIMESU. This kind of behavior is known as "superstick" behavior, which indicates the strong association of the probe molecule with the solvent.[118] Here, we note that a recent study by Samanta and coworkers[150] shows that ethidium bromide (EB) follows superstick behavior in BMIMBF$_4$ by virtue of solute-solvent hydrogen bonding. Again, Kurnikova et al.[269] has also pointed the role

116

of hydrogen bonding interaction in explaining the superstick behavior of thionine in dimethylsulfoxide (DMSO). Hence, the present superstick behavior of AP in the present ILs can be attributed to the hydrogen bonding interaction between AP and ILs.

Table 4.3. Summary of the rotational relaxation parameters of AP in different 1-ethyl-3-methlimidazolium alkylsulfates at different temperature

System	Temp.(K)	Vis. (cP)[a]	r_0[b]	τ_{rot} (ns)[c]	C_{rot}[d]
EMIMESU	293	105	0.34	7.67	1.4
	298	75	0.36	5.84	1.5
	303	58	0.36	4.63	1.6
	308	46	0.33	3.76	1.6
	313	34	0.38	3.02	1.8
EMIMBSU	293	191	0.31	12.39	1.2
	298	141	0.34	9.63	1.3
	303	106	0.37	7.57	1.4
	308	82	0.36	6.00	1.4
	313	63	0.33	4.78	1.5
EMIMHSU	293	389	0.30	19.56	0.9
	298	284	0.31	15.80	1.1
	303	211	0.31	12.16	1.1
	308	160	0.30	9.26	1.1
	313	122	0.35	7.08	1.2
EMIMOSU	293	646	0.28	30.00	0.9
	298	453	0.28	23.28	1.0
	303	329	0.28	19.50	1.2
	308	245	0.28	15.60	1.3
	313	183	0.28	12.30	1.3

[a] $\pm$ 5%. [b] initial anisotropy .[c] rotational relaxation time(error limit 5%).[d] rotational coupling constant.
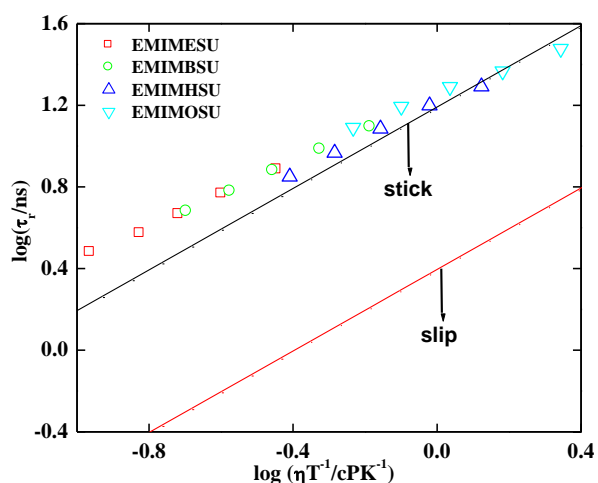
Figure 4.6. log-log plots of average rotational relaxation time of AP vs. η/T in different 1-ethyl-3-methlimidazolium alkylsulfates with slip and stick boundary condition parameters. Symbols denote the experimental data points.

In this context, it is to be mentioned that the mere presence of solute-solvent hydrogen bond may not slow down solute rotation. It should be strong enough such that the hydrogen bonding dynamics takes place on a time scale that is comparable to or slower than solute rotational dynamics.[244, 245] To confirm the hydrogen bonding interaction, we have also carried out the ^{1}H NMR investigation. A representative NMR spectrum showing the effect of solvent on the solute is shown in Figure 4.7. As can be seen, the N-H proton signal of AP which appears at 10.71 ppm becomes very broad in presence of the IL. The present NMR results confirm the hydrogen bonding interaction between the N-H fragment of AP and the sulfate moiety of the ionic liquid. Other ILs also broaden the N-H proton signal. However, the extent of broadening is found to be so large that it has not been possible for us to differentiate the NMR line width with respect to the variation of chain length of ILs. To find out the potential of AP as H-bond donor, we have carried the charge density analysis by optimizing the structure of AP at B3LYP[228, 229]/6-31++G (d,p) level, and using Gaussian 03 program.[231] Considerable charge density on the hydrogen atoms of amine (0.290) and imide (0.320) indicate the acidic nature of N-H hydrogens. Moreover, the ability of AP to act as H-bond donor is also demonstrated by Dobek and coworkers.[270] They have demonstrated that AP can form hydrogen bond (N-H•••O-S) with hydrogen bond acceptors like dimethyl sulfoxide (DMSO) and sodium dodecyl sulfate (SDS). Interestingly, Figure 4.6 also reveals the influence of alkyl chain length on the rotational behavior of AP. Figure 4.6 clearly shows that the hydrodynamics of AP changes from superstick to stick with increase in the alkyl chain length. The following relationship has been obtained when we fit the τ_r and η/T data for AP in to the function, $\tau_r = A(\eta/T)^p$.

AP in EMIMESU, $\tau_r = (17.392 \pm 0.324) (\eta/T)^{0.79 \pm 0.013}$ (N = 5, R = 0.9996)   (4.13)

AP in EMIMBSU, $\tau_r = (17.632 \pm 0.163) (\eta/T)^{0.81 \pm 0.011}$ (N = 5, R = 0.9998)   (4.14)

AP in EMIMHSU, $\tau_r = (15.795 \pm 0.244) (\eta/T)^{0.79 \pm 0.044}$ (N = 5, R = 0.9960)   (4.15)

AP in EMIMOSU, $\tau_r = (17.919 \pm 0.176) (\eta/T)^{0.65\pm0.017}$ $\qquad$ (N = 5, R = 0.9990) $\qquad$ (4.16)

In these expressions, N and R are the number of data points and regression coefficient, respectively.

We have also measured C_{rot} for AP in all four ILs (Table 4.3). At a particular temperature, C_{rot} values (Table 4.3) for AP are found to be considerably larger in the present ILs than those[119] found in conventional non-hydrogen-bonding solvents. Since C_{rot} represents the measure of the extent of departure from normal hydrodynamic behavior of a solute due to specific interaction, the present observation is a clear reflection of hydrogen bonding interaction between the AP and the ionic liquids.
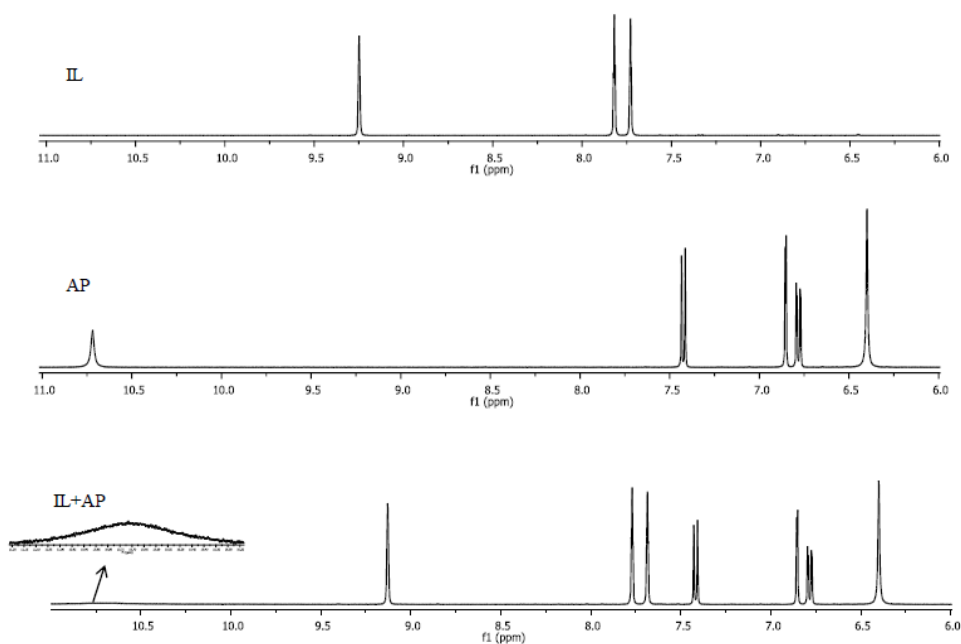
Figure 4.7. Proton NMR spectra for IL (EMIMESU), AP and AP with IL in DMSO-d_6.

Upon careful observation, we find that the value of C_{rot} decreases as we go from ethyl to hexyl and levels-up at octyl substituent. The average C_{rot} values are estimated to be 1.58, 1.36, 1.08 and 1.14 for ethyl, butyl, hexyl and octyl substituent respectively (Table 4.3). To explain the present observation, we have calculated the charge density on the oxygen atoms of the sulfate group by optimizing (at B3LYP/6-31++G (d,p) level) the structures of all four anions independently. The decrease in C_{rot} values with increase in alkyl chain length is in

tune with the decrease in total charge density [-2.766 (ethyl), -2.747(butyl), -2.727 (hexyl) and – 2.729 (octyl)] on four oxygen atoms of the sulfate group (H-bond acceptor) of alkyl sulfates. It has been reported in case of substituted salicylates by Shan et al.[271] that hydrogen bond strength increases with increase in negative charge density on hydrogen bond acceptor. The present observation is interesting in a sense that the previous two literature reports, which depict the alkyl chain length dependence on the rotational dynamics of MPTS [151] and R110[153], show that the values of rotational coupling constants increases with an increase in the alkyl chain length on the cationic moiety.

4.3.3. *Time-resolved Fluorescence Anisotropy Study of C153 in 1-Ethyl-3-Methylimidazolium Cation Containing ILs*

Time-resolved fluorescence anisotropy decay profiles of C153 in different 1-ethyl-3-methyl cation containing ILs at various temperatures are shown in Figure 4.8. The anisotropy decay profiles are fitted to both bi- and single exponential functions of time. The bi-exponential fits are found to be slightly better than the single exponential fits. It may be mentioned in this context that Maroncelli and coworkers used a bi-exponential function to fit the anisotropy decays of C153 in polar solvents, and have explained the observed behavior as a result of non-Markovian nature of the friction.[272] The average reorientation times of C153 in four ionic liquids estimated from bi-exponential fits at different temperatures are listed in Table 4.4. The plots of log (η) versus 1/T for four ILs are also shown in Figure 4.9. As can be seen from Figure 4.9, these anions play an important role in determining the viscosities of the ILs, and bulk viscosities of the ILs vary in the order TCB< TFB $\cong$ TFA < ESU.

Interestingly, anisotropy decay profiles reveal that anisotropy decays of C153 is the slowest in EMIMESU and fastest in EMIMTCB. However, the average rotational times are found to be same in case of EMIMTFA and EMIMTFB, and it is varied in-between aforementioned ILs. Consequently, the average rotational time of C153 in these ILs also follow similar trend (Table 4.4). For example, at 293K, the average rotational time of C153 in

EMIMESU and EMIMTCB are found to be 3.28 ns and 1.17 ns respectively which is found almost same in case of EMIMTFB and EMIMTFA is ~2.05 ns (Table 4.4). The observation shows that the average rotational times of the probe molecule vary with the bulk viscosities of the ILs. It is also evident both from the anisotropy decay profiles shown in Figure 4.8 and the data presented in Table 4.4 that with an increase in the temperature, the rotational diffusion becomes faster due to the lowering of the viscosity of the media.
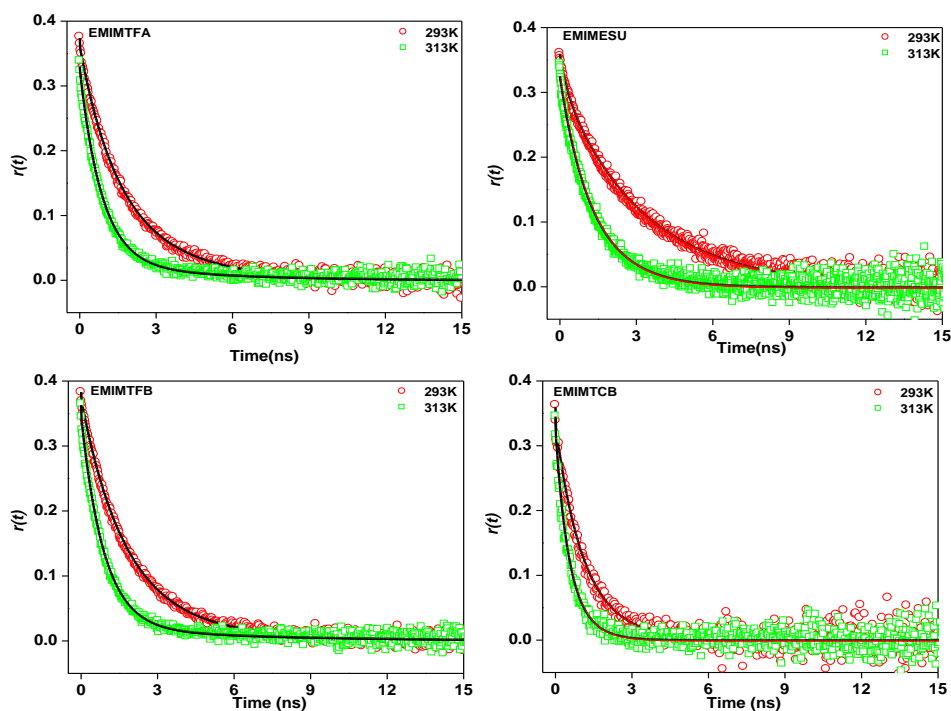
Figure 4.8. Time-resolved fluorescence anisotropy decay profiles of C153 in different 1-ethyl-3-methylimidazolium cation containing RTILs at different temperatures. Symbols denote experimental data points and solid lines passing to the experimental data points represent the bi-exponential fit to the data points.

Figure 4.10 shows the plots of experimentally measured reorientation times of C153 in four ILs along with the calculated stick and slip lines. As can be seen from Figure 4.10, the rotational dynamics of C153 in different ILs lie between the stick and slip boundary conditions. We fit the τ_r and η/T data for C153 to the function, $\tau_r = A(\eta/T)^p$, a procedure described by Mali et al.[152, 257], following relationship are obtained

C153 in EMIMESU, $\tau_r = (7.042 \pm 0.76) (\eta/T)^{0.70 \pm 0.074}$ (N = 5, R = 0.9857) (4.17)

C153 in EMIMTFA, $\tau_r = (8.300 \pm 0.320) (\eta/T)^{0.68 \pm 0.016}$ (N = 5, R = 0.9992) (4.18)

C153 in EMIMTCB, $\tau_r = (11.250 \pm 0.820) \, (\eta/T)^{0.85\pm0.024}$ (N = 5, R = 0.9988)   (4.19)

C153 in EMIMTFB, $\tau_r = (7.550 \pm 0.440) \, (\eta/T)^{0.64\pm0.025}$ (N = 5, R = 0.9978)   (4.20)

In these expressions, N and R are the number of data points and regression coefficient, respectively.

Table 4.4. Rotational relaxation parameters for C153 in 1-ethyl-3-methylimidazolim cation containing RTILs at different temperatures

ILs	Temp.(K)	Vis.[a] (cP)	[b]r_0	a_1	$\tau_1(ns)$	a_2	$\tau_2(ns)$	$<\tau_{rot}>(ns)^c$
EMIMESU	293	105	0.36	0.88	3.66	0.12	0.46	3.28
	298	75	0.36	0.81	3.34	0.19	0.90	2.88
	303	58	0.36	0.71	2.73	0.29	1.00	2.23
	308	46	0.34	0.79	2.10	0.21	0.71	1.81
	313	34	0.34	0.81	1.63	0.19	0.36	1.39
EMIMTFA	293	38	0.37	0.18	4.19	0.82	1.57	2.04
	298	31	0.37	0.17	4.12	0.83	1.30	1.78
	303	26	0.36	0.10	4.82	0.90	1.17	1.53
	308	22	0.36	0.08	4.89	0.92	1.04	1.35
	313	18	0.36	0.09	4.46	0.91	0.86	1.18
EMIMTCB	293	21	0.36	0.76	1.00	0.24	1.70	1.17
	298	17	0.36	0.74	0.95	0.26	1.03	0.97
	303	14	0.36	0.77	0.71	0.23	1.20	0.82
	308	12	0.36	0.72	0.78	0.28	0.43	0.68
	313	10	0.32	0.45	0.79	0.55	0.43	0.59
EMIMTFB	293	39	0.38	0.15	4.36	0.85	1.65	2.06
	298	32	0.36	0.07	6.58	0.93	1.47	1.83
	303	26	0.35	0.08	4.84	0.92	1.24	1.53
	308	22	0.36	0.06	6.14	0.94	1.08	1.38
	313	18	0.36	0.06	6.35	0.94	0.89	1.22

[a] $\pm$ 5%, [b] initial anisotropy and [c] average rotational relaxation time ($\pm$ 5%). τ_1, τ_2 are rotational relaxation time and a_1, a_2 are the normalized preexponential factors.
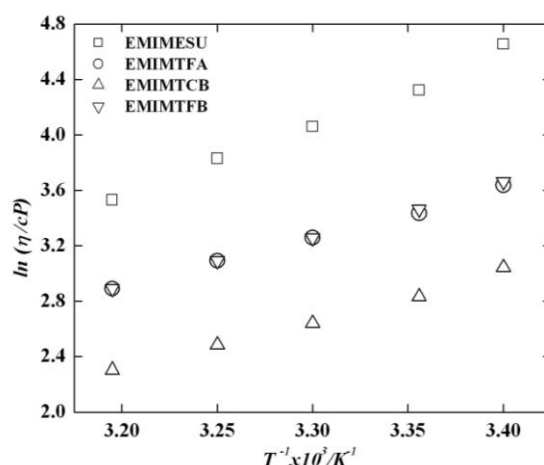
Figure 4.9. Plots of $ln(\eta)$ versus $1/T$ for all four 1-ethyl-3-methylimidazolium cation containing RTILs.
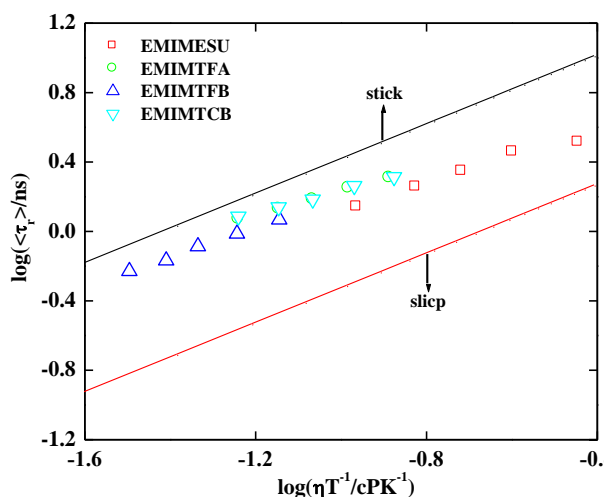
Figure 4.10. Plots for τ_r vs. η/T for C153 in 1-ethyl-3-methylimidazolium cation containing RTILs. Computed data are with slip, stick boundary conditions and experimentally measured data are shown by symbol.

The calculated average C_{rot} values obtained for C153 in ESU, TFA, TCB and TBF systems are 0.43, 0.68, 0.66 and 0.68 respectively. C_{rot} values vary from 0.4-0.7 which is comparable to the values that obtained in conventional solvents.[272] The observed C_{rot} values also indicate that there is no specific interaction between C153 and the ILs. Moreover, the differences in C_{rot} values that has been observed in the present case on going from one ionic liquid to another indicates the possible role of nonspecific interaction (long-range dipole-dipole interaction) and solute/solvent size in addition to the viscosity of the medium.

4.3.4. *Time-resolved Fluorescence Anisotropy Study of AP in 1-Ethyl-3-Methylimidazolium Cation Containing ILs*

Representative time-resolved fluorescence anisotropy decay profiles of AP in neat 1-ethyl-3-methylimidazolium cation containing ILs at various temperatures are shown in Figure 4.11. We resort to single exponential fitting of the anisotropy data of AP as bi-exponential fit does not improve the quality of data fitting and also the average rotational relaxation time calculated from bi-exponential fit is found to be very similar with that obtained from single exponential fit. The rotational relaxation parameters for AP in ILs at different temperatures are collected in the Table 4.5.

From the anisotropy decay profile, it can be noticed that the rotational motion of AP is the fastest in EMIMTCB and slowest in EMIMESU. Interestingly, the rotational motion of AP is found to be slower in EMIMTFA than in EMIMTFB despite the similar viscosity of two ILs (Figure 4.11). This observation indicates that in addition to the viscosity effect other factor like solute-solvent interaction may play a definite role in controlling the rotational motion of AP in these media. The variation of the average rotational times of AP (i.e. 7.6 ns, 3.7 ns, 1.95 ns and 1.13 ns for EMIMESU, EMIMTFA, EMIMTFB and EMIMTCB respectively at 293 K) bear this fact (Table 4.5). It is also noticeable from Table 4.5 that with an increase in the temperature, the rotational diffusion of AP becomes faster due to the lowering of the viscosity of a medium. At a particular temperature, the rotational times of AP in EMIMTFA are found to be significantly higher than for C153 although the size of AP is smaller than that of C153.[119]
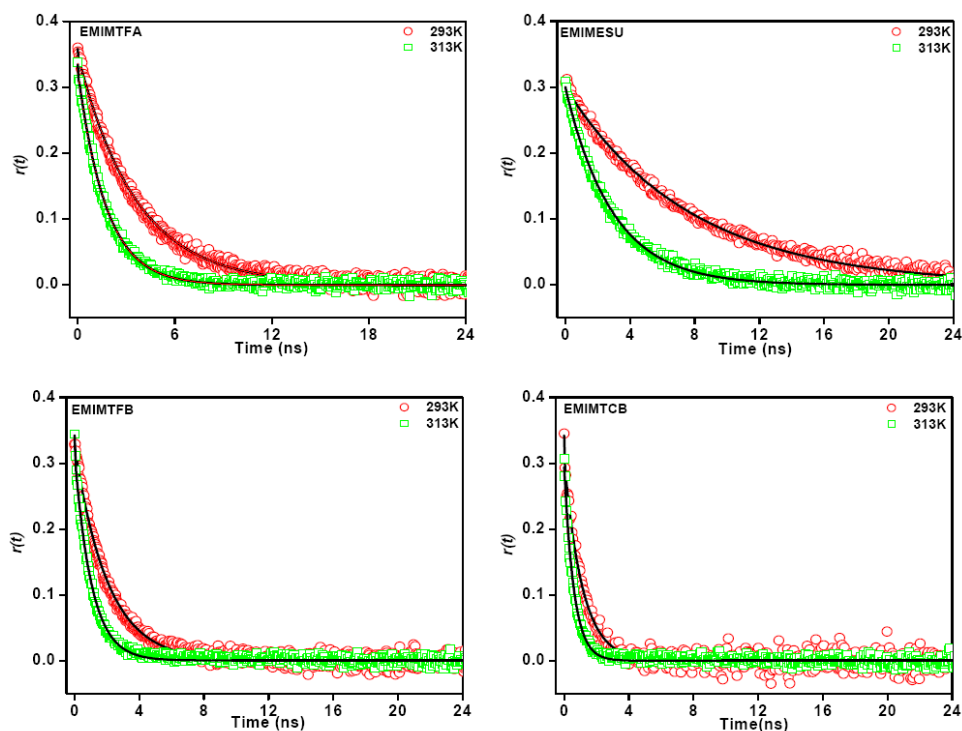
Figure 4.11. Time-resolved fluorescence anisotropy decays of AP in different 1-ethyl-3-methylimidazolium cation containing RTILs at different temperatures. The smooth lines passing to the experimental data points are fitted ones.

Table 4.5. Rotational relaxation parameters for AP in different 1-alkyl-3-methylimidazolium cation containing RTILs at different temperatures

RTILs	temp.(K)	vis.[a](cP)	r_0^b	τ_{rot} (ns)[c]
EMIMESU	293	105	0.33	7.60
	298	75	0.32	5.77
	303	58	0.30	4.67
	308	46	0.29	3.74
	313	34	0.29	3.00
EMIMTFA	293	38	0.36	3.70
	298	31	0.34	3.00
	303	26	0.35	2.50
	308	22	0.35	2.10
	313	18	0.33	1.80
EMIMTCB	293	21	0.34	1.13
	298	17	0.31	0.96
	303	14	0.31	0.82
	308	12	0.31	0.70
	313	10	0.31	0.60
EMIMTFB	293	39	0.36	1.95
	298	32	0.34	1.65
	303	26	0.33	1.40
	308	22	0.34	1.13
	313	18	0.32	0.95

[a] ± 5%, [b] initial anisotropy and [c] rotational relaxation time (± 5%).

This observation indicates that the solute-solvent interaction is stronger for AP than for C153 in these media. To get a better understanding of the rotational behavior of AP in ILs, we have also analyzed the data by employing Stokes-Einstein-Debye (SED) hydrodynamic model. In case of AP, Figure 4.12 represents the plots of experimentally measured reorientation times of AP in four ionic liquids along with the calculated stick and slip lines. As can be seen from Figure 4.12, the rotational time of the AP is significantly higher than that predicted by the stick boundary condition in EMIMESU and EMIMTFA. This kind of behavior is known as "superstick" behavior, which indicates the strong association of the probe molecule with the solvent.[118] The super stick behavior of AP in the present ionic liquids can be attributed to the hydrogen bonding interaction between AP and the ionic liquid. It is pertinent to mention in this context that as the C2-H proton of the EMIM cation is acidic in nature and hence there is a possibility that it may form hydrogen bond with the carbonyl

group of AP. However, we could not find any appreciable change in the NMR proton signal of C2-H of EMIM cation upon the addition of AP. This observation rules out the possibility of the involvement of C2-H proton in the hydrogen bonding interaction with AP. Figure 4.12 also reveals that AP follows the stick hydrodynamics in EMIMTCB and EMIMTFB. The relationship that has been obtained when we fit τ_r and η/T for AP to the function $\tau_r = A(\eta/T)^p$ are given below

AP in EMIMESU, $\tau_r = (17.10 \pm 0.28)\,(\eta/T)^{0.79\pm0.011}$ $\qquad$ (N = 5, R = 0.9997) $\qquad$ (4.21)

AP in EMIMTFA, $\tau_r = (23.87 \pm 1.37)\,(\eta/T)^{0.91\pm0.025}$ $\qquad$ (N = 5, R = 0.9995) $\qquad$ (4.22)

AP in EMIMTCB, $\tau_r = (8.88 \pm 0.54)\,(\eta/T)^{0.78\pm0.021}$ $\qquad$ (N = 5, R = 0.9992) $\qquad$ (4.23)

AP in EMIMTFB, $\tau_r = (10.95 \pm 0.97)\,(\eta/T)^{0.85\pm0.038}$ $\qquad$ (N = 5, R = 0.9970) $\qquad$ (4.24)

In these expressions, *N* and *R* are the number of data points and regression coefficient, respectively
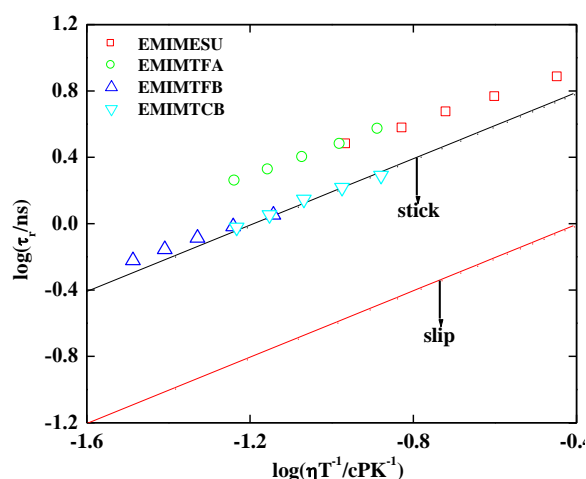
Figure 4.12. log-log plots for τ_r vs. η/T for AP in different 1-ethyl-3-methylimidazolium cation containing RTILs. Computed data are with slip, stick boundary conditions and experimentally measured data are shown by symbol.

To get an insight into the AP-ILs interaction, we have estimated the rotational coupling constants for AP in all four ILs used in this study (Table 4.6). At a particular temperature, C_{rot} values for AP are found to be considerably larger than the ones for non-hydrogen-bonding solvents.[119] Since the rotational coupling constant (C_{rot}) represents the measure of the extent of departure from normal hydrodynamic behavior of a solute due to specific interaction, the present observation is a clear manifestation of hydrogen bonding interaction between AP and

anionic components of the ionic liquids. Upon careful observation, one can see that C_{rot} values are different for different ILs. The variation of C_{rot} value can be explained by considering hydrogen bond basicity of the corresponding anions of the ILs. The hydrogen bond basicity corresponding to the anions of the concerned ILs are obtained from the literature report[273]. The hydrogen bond basicity of the anions is calculated based on COSMO-RS computation.[273]

Table 4.6. Rotational coupling constant(C_{rot}) of AP, obtained from the measured rotation times in four ILs and hydrogen bond basicity parameters for the anions of corresponding ILs

RTILs	C_{rot} for AP	HB_acc3[a] for anion
EMIMESU	1.56	19.2952
EMIMTFA	1.90	20.3944
EMIMTCB	1.12	3.4554
EMIMTFB	1.01	2.4740

[a]COSMO-RS descriptor of HB_acc3 (hydrogen bonding acceptors moment indicates hydrogen bond basicity)[273]

As described by Klamt[274], COSMO-RS is a statistical thermodynamic approach based on the results of quantum chemical-COSMO calculations. COSMO sigma-moments are molecular descriptors obtained from COSMO-RS calculation, among which the hydrogen bond moments (HB_acc3) chemically corresponds to the measures of H-bonding basicity.[273] As can be seen from Table 4.6 that observed C_{rot} values for AP (TFA> ESU> TCB> TFB) follows as similar trend as that of hydrogen bond basicity values (TFA> ESU> TCB> TFB) of the corresponding ILs. In this context we would like to note that very recently, Karve and Dutt[156] have studied the rotational diffusion of neutral and charged solutes in the series of ionic ILs that are different from the present study. They have found that the rhodamine110 follows stick hydrodynamics, and the variation in the boundary condition parameter can be correlated with the hydrogen bond basicities of the anions of the ILs. Considering all these, one can now conclude that the strength of specific solute-solvent interaction, which in turn is governed by the hydrogen bond basicity of the concerned anions, plays a key role in controlling the dynamics of rotation of the organic solutes in ILs.

4.4. Conclusion

Rotational dynamics of two neutral organic solutes, C153 and AP has been investigated in a series of 1-ethyl-3-methylimidazolium alkyl sulfate ionic liquids (alkyl = ethyl, butyl, hexyl and octyl) and 1-ethyl-3-methylimidazolium cation containing ILs with an aim to find out the effect of alkyl side chains and anions on the rotational dynamics of these organic solutes in these ILs. The results obtained while studying the alkyl chain length dependency on rotational dynamics indicate two distinct rotational environments for C153 and AP. Rotational dynamics of C153 lie between stick and slip boundary condition in ethyl analogue and finally reaches to subslip condition in case of the octyl substituent. Rotational dynamics of C153 becomes faster with an increase in the alkyl chain length primarily because of the fact that the larger solvent molecules offer lower friction to rotating solute. In case of AP, hydrodynamic behavior changes from superstick to stick with increase in the alkyl chain length. Superstick behavior has been attributed to the strong solute-solvent hydrogen bonding interaction between AP and ILs. Rotational coupling constant values have been found to decrease with increasing length of alkyl side chains. The observed rotational behavior of AP has been attributed to the decrease in the solute-solvent specific interaction with an increase in the alkyl side chain length on the sulfate moiety.

In the second study where rotational diffusion of C153 and AP have been investigated in ILs having different H-bond basicity values, it has been observed that the reorientation times of C153 depends on the viscosity of the ILs and follows normal hydrodynamics. The variation in rotational coupling constants (C_{rot}) values that has been observed for C153 in ILs also indicates the role of nonspecific interaction (long-range dipole-dipole interaction) and solute/solvent size towards the rotational motion of the probe. However, rotational diffusion of AP has been found to be significantly influenced by the nature of anions. AP shows superstick behavior in EMIMESU and EMIMTFA and follows stick hydrodynamics in

EMIMTFB and EMIMTCB. The super stick behavior is attributed to the strong specific solute solvent interaction. Rotational coupling constant values for AP are found to decrease in the order TFA> ESU> TCB> TFB. The variation in the rotational coupling constants, the measure of extent of departure from the normal hydrodynamics behavior due to specific solute-solvent interaction, is explained by considering the hydrogen bond basicity of the anionic moiety of the corresponding ILs.

Effect of Nonpolar and Polar Cosolvents on the Solute Rotation and Solvation Dynamics in Room Temperature Ionic Liquids

5.1. Introduction

Room temperature ionic liquids (RTILs) are not easily available like common solvents and are also expensive. Hence, the scale at which the neat RTILs should be used in the practical applications has not been reached till date. One of the possible approaches to expand the uses of RTILs would be to use binary and ternary mixtures of RTILs with various cosolvents. RTIL-cosolvent mixtures are also known to exhibit interesting physicochemical properties.[212, 213] However, a deeper understanding of their physicochemical properties in terms of RTIL-cosolvent interactions is extremely important so that the systems be used in more effective manner.

Recently, several studies have been carried out to understand the physicochemical properties of the mixtures of RTILs and conventional solvents. These studies have revealed that the solvent property can be fine-tuned by addition of conventional solvents which will eventually enhance the scope of applications of RTILs. It has been observed that the addition of a cosolvent into RTILs has profound influence in changing the physicochemical properties of RTILs such as viscosity, polarity, conductivity etc.[234, 275-279] Few studies have also been carried out to find the effect of cosolvent on solute and solvent dynamics.[115, 129, 130, 134, 135, 142] Quite interestingly, these studies reveal that presence of trace amount of organic cosolvents is capable of changing the local microenvironment of the probe molecule. Recent work by Sarkar and coworkers[135] have shown that the addition of water/organic solvent to 1-ethyl-3-methylimidazolium ethylsulfate (EMIMESU), decreases average rotational and solvation time of coumarin153 (C153) due to reduction of viscosity of media. However, these studies focus on moderate-to-high polarity solvents, and therefore, it is difficult to comment on the effect of nonpolar solvents on the dynamical behavior of ionic liquids (ILs). There is only one

report by Paul et al.[115], where they have investigated the effect of nonpolar solvents on the solute rotation and solvation dynamics in 1-butyl-3-methylimidazolium hexafluorophosphate (BMIMPF$_6$). It would be interesting to see the effect of a nonpolar cosolvent on the solvation and rotational relaxation behavior of a dipolar probe in an IL which is more hydrophobic than BMIMPF$_6$. Since the physicochemical properties of ILs depend on the constituents of ILs, different polar/nonploar cosolvents are expected to interact differently with the constituent of ILs. Thus it is of paramount importance to study the effect of cosolvents by taking ILs having different constituents. We would also like to point out that apart from lowering of average rotational and solvation time of probe solute due to reduction of viscosity of the media, not much physical insight has been obtained in earlier studies.

Keeping these facts in mind, we have investigated solvation and rotational dynamics of C153 in a ultra hydrophobic RTIL, 1-(2-methoxyethyl)-1-methylpyrrolidinium tris(pentafluorethyl)trifluorophosphate (MOEMPLFAP) and RTIL-toluene mixture to understand the effect of nonpolar cosolvent in these phenomena. The toluene has been chosen for the present study primarily because of the fact that it is extremely nonpolar, and has an appreciable solubility in the present RTIL. The present RTIL is ultra hydrophobic due to the presence of tris(pentafluoroethyl)trifluorophosphate moiety.[238] In the present RTIL, water and halide content are found to be less than 100 ppm.[155] To investigate the effect of polar solvent in solute and solvation dynamics, we have carried out separately solute and solvent relaxation of C153 in 1-butyl-3-methylimidazolium trifluoroacetate (BMIMTFA) and also its mixture with water and methanol. The choice of this ionic liquid in this particular study is governed by the fact that ionic liquid bearing the trifluoroacetate moiety has the high potential to be used in several industrial applications.[280, 281] Due to presence of the carboxylate moiety, it is also expected that it would participate in hydrogen bonding interaction with protic solvents[282] and thereby control the physiochemical property of the

131

medium. It is pertinent to mention in this context that ILs having TFA moieties are hygroscopic in nature, and TFA anion is primarily responsible for the water miscibility.[277] Considering the favorable interaction between TFA and polar protic solvents, we have chosen water and methanol as cosolvents for this study. Theoretical calculations have been carried out to understand the molecular origin of IL-cosolvent interaction. Molecular diagrams of MOEMPLFAP, BMIMTFA and C153 are provided in Chart 5.1.

1-(2-methoxyethyl)-1-methylpyrrolidinium tris(pentafluoroethyl)trifluorophosphate (MOEMPLFAP)

1-butyl-3-methylimidazolium trifluoroacetate (BMIMTFA)

coumarin153 (C153)
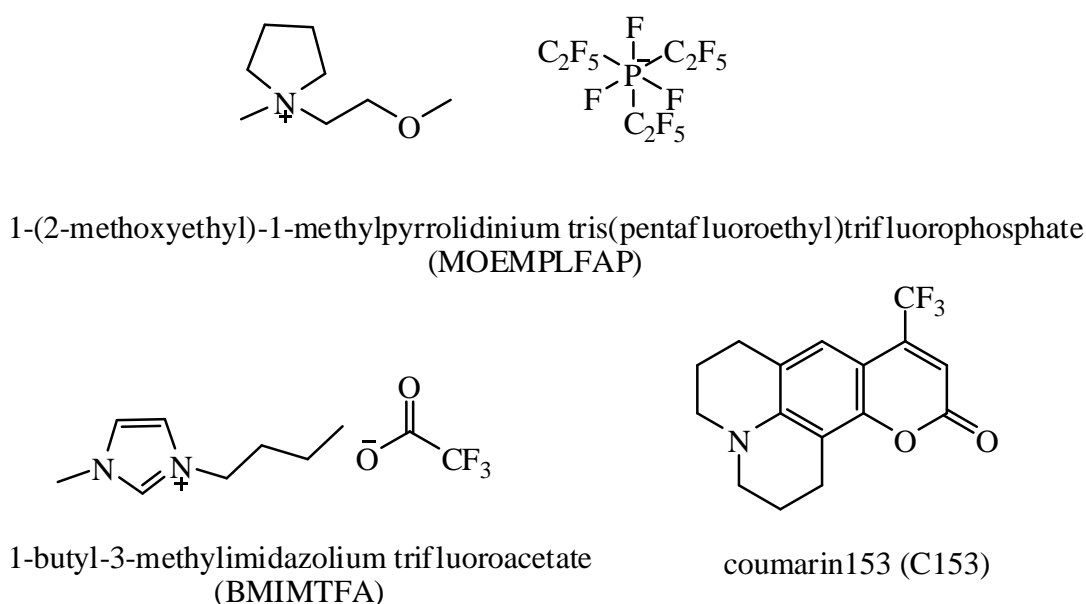
Chart 5.1. Molecular diagrams of BMIMTFA, MOEMPLFAP and probe C153.

5.2. Experiments and Methods

Laser grade C153 was used as received from Exciton, USA. RTILs (Chart5.1) were obtained from Merck, Germany (>99% purity) and used as received. The water and halide contents of these RTILs were <100 ppm. 2-Amino-7-nitrofluorene (ANF) was prepared following the method suggested by Sislak and Hamilton[283] and characterized by different spectroscopic method. Millipore water was used as received which was purified in Merck, Mili-Q. HPLC grade methanol and toluene were obtained from Merck, Germany and used without further purification. Water and methanol were added as cosolvents in BMIMTFA such that their mole fractions were maintained at 0.4. The probability of dye aggregation in BMIMTFA was ruled out and it was confirmed from the spectroscopic study. Toluene was

added as a nonpolar cosolvent in MOEMPLFAP such that their weight percentage was maintained at 3%. Details of instrumental techniques, procedure of data analysis and methods for estimation of solvent organization time are described in Chapter 2.

5.3. Results and Discussion

5.3.1. *Effect of Nonpolar Cosolvents*

5.3.1.1. *Optimized Structure of MOEMPLFAP*

Before describing the results and discussion of solvent and rotational relaxation of C153 in this RTIL and RTIL-toluene mixture, we have made an attempt to know the structural features of this media by optimizing the structure of this RTIL in the ground state. The geometry has been optimized in the gas phase with B97-D functional[246], def2-SVP basis set[247, 248] using Turbo mole V6.2 program[249]. The optimized structure of MOEMPLFAP is shown in the Figure 5.1.
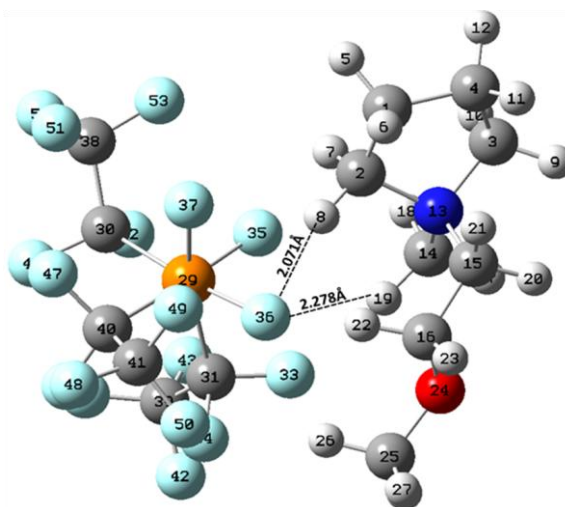
Figure 5.1. Optimized geometry of neat MOEMPLFAP.

In the optimized structure, the distance between F36-H8 and F36-H19 are 2.071 Å, 2.278 Å respectively. Again, distance among C2-F36, C14-F36, C2-H8 and C14-H19 are found to be 2.961 Å, 3.181 Å, 1.094 Å and 1.094 Å respectively. The van der Waals criterion for hydrogen bond formation is that for the formation of B-H···C bonds, the distance between B···C should be less than the sum of the B-H covalent bond and the van der Waals radii of H

133

and that of C.[250] The van der Waals radii of F and H are 1.47 Å and 1.2 Å respectively. The C14-H19-F36, C2-H8-F36 angle are 139°, 128° respectively. Measurement of both distance and angle suggest the presence of C-H···F interactions between the cationic and the anionic fragment of RTIL.

5.3.1.2. *Steady State Behavior*

The absorption spectra of C153 in present RTIL and RTIL-toluene mixture are shown in Figure 5.2(a). The absorption spectrum of neat ionic liquid is also shown in the same figure. The optical density of the present RTIL is measured to be very less (0.009 in a 1 cm cell) at 405 nm. The absorption maximum of C153 in the present RTIL is measured to be 419 nm. We have not observed appreciable changes in absorption behavior of C153 with addition of toluene to RTIL. The emission spectra for solute molecule in neat RTIL and RTIL-toluene mixture are also shown in Figure 5.2(b). The emission maximum is measured to be 514 nm for C153 in ionic liquid. With addition of toluene in ionic liquid, intensities of absorption and emission spectra are decreased as a result of dilution but no appreciable shift has been observed. The present steady state behavior indicates that the solvation shell of C153 is not much affected by the addition of toluene. We have not seen any significant emission from neat ionic liquid at $\lambda_{exc.}$ = 405 nm.
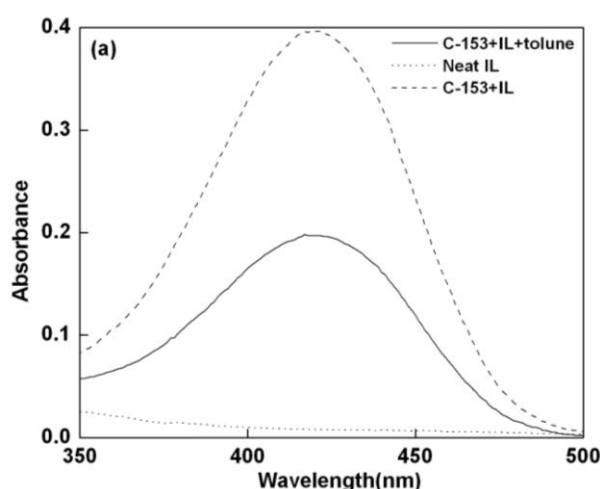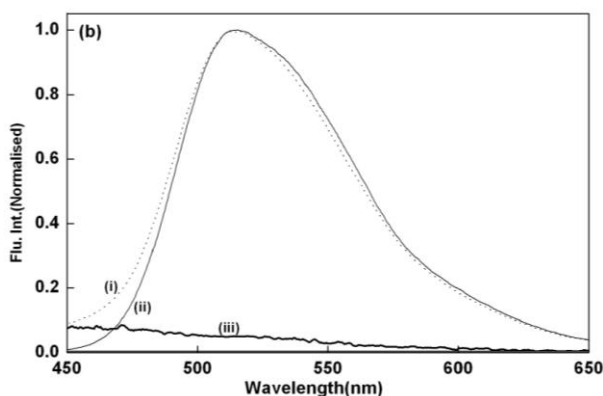
Figure 5.2. (a) Absorption spectra of neat MOEMPLFAP, C153 in neat RTIL, RTIL-toluene mixture and (b) steady state fluorescence spectra of (i) C153 in RTIL- toluene mixture, (ii) C153 in RTIL and (iii) neat RTIL.

5.3.1.3. *Time-resolved Studies*

5.3.1.3.1. *Solvation Dynamics*

The emission decay profile of C153 in the RTIL and RTIL-toluene mixture have been measured at several wavelengths (5-10 nm intervals) across the emission spectra by exciting the sample at 405 nm. TRES have been constructed following the procedure of Fleming and Maroncelli.[243] Representative TRES of C153 in RTIL-toluene mixture is shown in Figure 5.3. The time constants of the observable dynamics have been obtained from the plot of the spectral shift correlation function, *C(t)* versus time. A bi-exponential function of the form $C(t) = a_1 e^{-t/\tau_1} + a_2 e^{-t/\tau_2}$, where τ_1 and τ_2 are solvent relaxation time constants and a_1 and a_2 are normalized pre-exponential factors, are found to describe the time dependence of *C(t)*. Decay of solvation correlation function, *C(t)*, of C153 in neat RTIL and RTIL-toluene mixture are shown in Figure 5.4(a). The relaxation parameters of solvation of C-153 in RTIL and RTIL-toluene mixture are collected in Table 5.1.

135
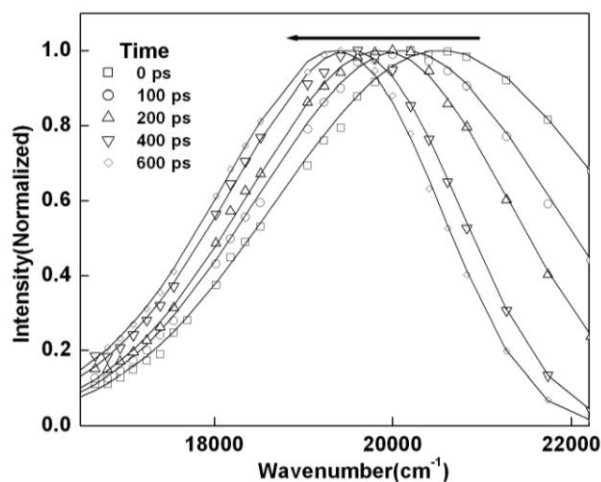
Figure 5.3. Time-resolved emission spectra (TRES) of C153 in RTIL-toluene mixture at different time intervals at 293 K. $\lambda_{exc.}$ = 405 nm.
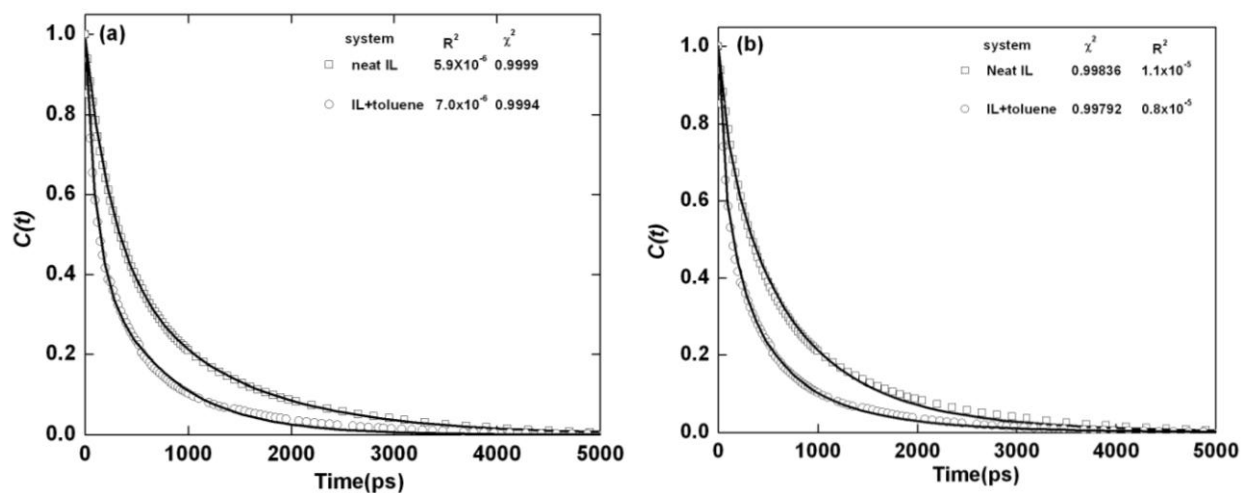
Figure 5.4. Decay of solvent correlation function *C(t)* of C153 in RTIL and RTIL-toluene mixture at 293K. In each case solid lines represent the (a) bi-exponential and (b) stretched exponential fit to the experimental data points, where χ^2 represents the goodness of fit and R^2 are the correlation coefficient values. $\lambda_{exc.}$ = 405 nm.

Table 5.1. Solvation relaxation parameters and observed shift for C153 in neat RTIL and RTIL-toluene mixture

System	vis. (cp)	a_1	τ_1 (ns)	a_2	τ_2 (ns)	τ_{av} (ns)	β	$\tau_{solv.}$ (ns)	τ_s (ns)	Obs. shift[†] (cm^{-1})
		from bi-exponential fit					From stretched exp. fit			
Neat RTIL	128	0.54	0.27	0.46	1.18	0.69	0.76	0.56	0.66	924
RTIL-toluene mixture	81	0.53	0.10	0.47	0.69	0.38	0.63	0.27	0.38	1308

[†]Observed shift has been calculated from [$\bar{v}(0) - \bar{v}(\infty)$]; experimental error is $\pm$ 5%.

136

Interestingly, a comparison of TRES in neat RTIL and RTIL-toluene mixture reveals that the time-zero spectrum of C153 in RTIL-toluene mixture is shifted to higher energy (20541 cm^{-1}) than that of neat IL (20107 cm^{-1}). The hypsochromic shift, measured from the difference in the $\bar{v}(0)$ values for neat RTIL and RTIL-toluene (3% w/w of toluene) mixture, is 434 cm^{-1}. However, the corresponding shift of the $\bar{v}(\infty)$ is only 50 cm^{-1}. The difference in the shift of $\bar{v}(0)$ and $\bar{v}(\infty)$ values is primarily responsible for larger observed Stokes shift (Table 5.1) with addition of toluene to the neat RTIL. It is pertinent to mention here that the similar blue shift has also been observed by Samanta and coworkers[115] while estimating the time-zero spectrum of C153 upon addition of toluene (4.7% w/w of toluene) to BMIMPF$_6$. However, the observed blue shift (260 cm^{-1}) as measured by Samanta and coworkers[115], is found to be significantly lower than the present study. The blue shift of the time-zero spectrum in the presence of toluene indicates the involvement of nonpolar cosolvent in the early part of the dynamics. It is also evident that toluene is infused in to the cybotactic region of the probe molecules. For a given concentration of toluene, the higher blue shift of the time-zero spectrum in the present RTIL than that of BMIMPF$_6$ can be rationalized by considering hydrophobicity of the two RTILs. Since the present RTIL, MOEMPLFAP is more hydrophobic[238] than BMIMPF$_6$, the penetration of toluene into the RTIL-rich cybotactic region of the probe will be higher for the former case due to more favorable hydrophobic interactions with nonpolar toluene. In this context, we note that FAP based ILs are capable of extracting polycyclic aromatic hydrocarbons owing to appreciable hydrophobic interactions between IL and the aromatic hydrocarbon.[238]

We have calculated average solvation times of C153 in RTIL and RTIL-toluene mixture from both bi-exponential (Figure 5.4(a)) and stretched exponential fit (Figure 5.4(b)). However, we resort to bi-exponential fit as it gives the better fit. The average solvation times for C153 in neat RTIL and RTIL-toluene binary mixtures are measured to be 0.69 ns and 0.38

ns respectively (Table 5.1). The addition of toluene to RTIL decreases the average solvation time due to lowering of viscosity of the medium. Since the extent of missing component cannot be accurately determined for the mixed systems[115], we have not calculated the missing component of dynamics of solvation for the present study.

5.3.1.3.2. *Rotational Dynamics*

The time-resolved fluorescence anisotropy, r(t), is calculated by Equation 2.21. The details of method for determination of rotational relaxation times are described in Chapter 2 in more details. The rotational relaxation parameters of C153 in neat RTIL and RTIL-toluene mixture are shown in Table 5.2.

The average rotational time for C153 in neat RTIL is 5.16 ns and RTIL-toluene mixture is 4.41 ns respectively. In this regard, it is to be noted that in the absence of any specific interaction, the solute rotation is mainly governed by the volume of the solute and viscosity of the medium. The rotational dynamics of the probe becomes faster in the presence of toluene due to lowering of viscosity of the medium. We have also calculated the rotational coupling constants (C_{rot}) with the help of Stokes-Einstein-Debye theory using probe properties that are available in literature. As it can be seen from Table 5.2, the C_{rot} value varies from 0.4-0.6 which is very similar with the values obtained in conventional solvents.[272] Therefore, other than lowering the viscosity of the medium, nonpolar cosolvent does not play any role on the rotational dynamics of C153.

Table 5.2. Rotational relaxation parameters for C153 in neat RTILs and RTIL-toluene mixture

system	Vis.(cP)	r_0[a]	a_1	τ_1(ns)	a_2	τ_2(ns)	$\langle\tau_{rot}\rangle$(ns)	[b]C_{rot}	[t]C_{rot}
Neat RTIL	128	0.34	0.16	1.01	0.84	5.95	5.16	0.45	0.1-0.7(many solvents)
RTIL-toluene mixture	81	0.36	0.18	0.33	0.82	5.31	4.41	0.60	

[a]r_0 is the initial anisotropy. The [b]C_{rot} values have been calculated by following the procedure from ref. 119. [t]C_{rot} are the literature values of rotational coupling constants of the probe molecules in conventional solvents.[272]

5.3.2. *Effect of Polar Cosolvents*

5.3.2.1. *Steady State Spectral Measurements*

Solute-solvent interactions in neat BMIMTFA as well as BMIMTFA-cosolvent systems have been studied by monitoring absorption and fluorescence measurements. C153 in neat BMIMTFA shows a broad absorption spectrum with a peak at 425 nm**.** The absorption and emission spectra of C153 in BMIMTFA along with emission spectrum of neat RTIL are shown in Figure 5.5. The emission maximum of C153 in this RTIL is found to be 532 nm, which closely matches with that in methanol.[135] The observation indicates that the polarity of BMIMTFA is close to that of methanol. Quite interestingly, the absorption and emission maximum of C153 remains almost unaffected when mole fraction of cosolvents (water and methanol) added to neat RTIL independently is maintained at 0.4. This steady state spectral behavior also illustrates that the local polarity around the probe molecule is not affected by the given amount of highly polar solvents such as water and methanol.
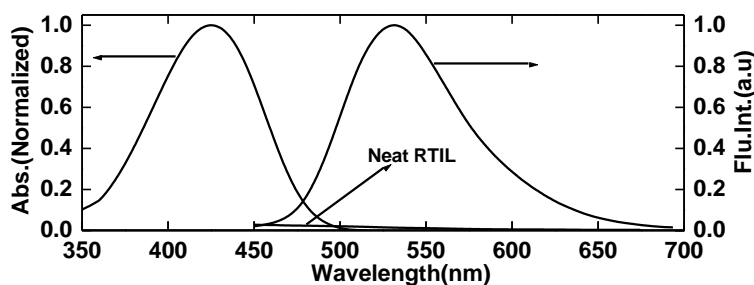
Figure 5.5. Absorption and emission spectra of C153 in BMIMTFA. Emission spectrum of neat RTIL is also shown in the same figure.

In this context, it is pertinent to mention that ionic liquids are microheterogeneous in nature.[76-82] Microheterogeneous natures of ionic liquids[76-82] as well as deep eutectic melts[267, 268] are known to influence medium dynamics considerably. It has been pointed out that these liquids form microscopic polar and nonpolar domains and intermolecular interactions play an important role to their microheterogeneous behavior. In light of these, it is also expected that RTIL-cosolvent mixtures will also be microheterogeneous in nature. In fact, Biswas and

Shirota[284] investigated the microscopic aspects of ionic liquid-water systems by Raman and IR spectroscopy. They have shown that water aggregation is localized at ionic regions. In view of this, understanding the heterogeneity aspects of these media is extremely important. Since water and methanol are expected not to interact with the ionic liquid in the same manner, it is expected that the medium heterogeneity exhibited by RTIL-water and RTIL-methanol would not be same.
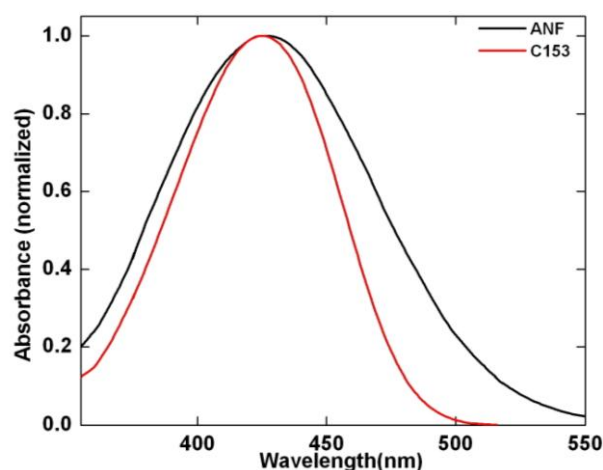
Figure 5.6. Absorption spectra of ANF and C153 in BMIMTFA. Spectra are normalized at their corresponding peak maximum.

In order to explore the structural heterogeneity of the mixed solvent medium we have carried out excitation wavelength dependent fluorescence behaviour of a dipolar probe 2-amino-7-nitrofluorene (ANF) which has shorter excited state lifetime (τ) ~100 ps[79] than C153 in conventional solvents. In this context, it is mentioned that the full width at half maximum (FWHM) as estimated from the absorption spectrum of ANF is found to be higher (5421 cm^{-1}) than that C153 (4168 cm^{-1}) in BMIMTFA (Figure 5.6). This observation indicates a distribution of the molecules in the ground state having multiple solvation sites, and hence different energies. The more inhomogeneous broadening of absorption in case of ANF points out that the presence of ensemble of energetically different species in the ground state is more favoured in present medium. We did not find any change in absorption maxima of ANF with the change in this RTIL and RTIL-cosolvent systems. Excitation wavelength dependent

fluorescence behavior of ANF in RTIL-water and RTIL-methanol mixtures is shown in Figure 5.7. As can be seen from Figure 5.7, the variations of the λ_{max} of the fluorescence spectrum with the variation of the excitation wavelength are quite different for RTIL-water from that of RTIL-methanol. For example, the shift of λ_{max} of the fluorescence is found to be higher (3400 cm^{-1}) in case of RTIL-water system when compared to that (1797 cm^{-1}) in RTIL-methanol system. We would like to mention here that this observation of red shift of $\lambda_{em.}$ (max) of the dipolar molecules when excited at long-wavelength edge of the first absorption band, is known as "red-edge effect"(REE).[192, 193]. The measured excited state lifetime (τ) values for ANF and C153 in BMIMTFA are found to be ~80-120 ps and 3.5-4.0 ns (Table 5.3) which are very much comparable with conventional solvents.[79] Interestingly, it is found that measured excited state lifetimes (80-120 ps) are found to be two to three times shorter than the measured average solvation time (200-350 ps) (Table 5.4). The REE effect in RTILs have been rationalized by considering existence of a distribution of energetically different solvated probes in the ground state and a slower rate of their excited-state relaxation processes than the excited lifetime (80-120 ps).[79] The results obtained in the present study provide supports in favor of the spatial heterogeneity that exists in these RTIL-cosolvent mixtures. This observation also indicates that possibly the interplay of varying nature of intermolecular hydrogen-bonding interaction that exists between the anionic moiety of the RTIL and water and methanol is primarily responsible for the observed excitation wavelength dependent fluorescence behavior (REE) of the two mixtures.
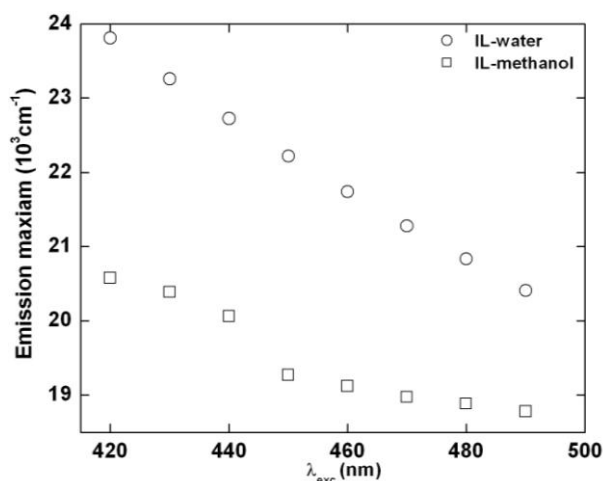
Figure 5.7. Emission maxima (cm^{-1}) vs. $\lambda_{exc.}$ (nm) plots of ANF in RTIL-cosolvent systems at room temperature.

Table 5.3. Time-resolved fluorescence lifetime decay parameters for ANF and C153 in BMIMTFA, BMIMTFA-H$_2$O and BMIMTFA-CH$_3$OH systems.[a]

probe	systems	τ_1(ns)	τ_2(ns)	τ_3(ns)	$\langle\tau\rangle$(ns)[b]
ANF	BMIMTFA	0.11(98.5%)	0.68 (1.5%)	-	0.118
	BMIMTFA-H$_2$O	0.06(98.2%)	0.65(1.6%)	4.54(0.2%)	0.078
	BMIMTFA-CH$_3$OH	0.08(97.5%)	0.55(2.3%)	4.04(0.2%)	0.099
C153	BMIMTFA	0.98(30.73%)	5.34(69.27%)	-	4.000
	BMIMTFA-H$_2$O	0.20(19.50%)	1.45(22.40%)	5.33(58.10%)	3.460
	BMIMTFA-CH$_3$OH	0.56(21.50%)	2.29(14.70%)	5.55(63.80%)	4.000

[a] goodness of fit (χ^2) values are in between 1.0-1.2 and [b] experimental error is $\pm$ 5%

5.3.2.2. *Time-resolved Studies*

5.3.2.2.1. *Dynamic Stokes Shift Measurements*

Representative wavelength dependent decay profile is shown in Figure 5.8 for BMIMTFA-H$_2$O system. When emissions are monitored at shorter wavelength regions, only a faster decay is observed, and at the longer wavelengths, the decay profiles consist of a slow rise followed by the usual decay. TRES of C153 in BIMITFA-H$_2$O system at different time intervals are also shown in Figure 5.9. A time-dependent shift of the emission spectra toward lower energy confirms solvent-mediated relaxation of the excited state of the fluorophore.

The representative plots of $C(t)$ versus time for C153 shown in Figure 5.10 for all these system. The average solvation times are estimated to be different for different systems (Table 5.4) and also found out to depend on cosolvent. For example, the average solvation times estimated to be 0.30 ns, 0.22 ns in case of BMIMTFA-H_2O, BMIMTFA-CH_3OH systems respectively (Table 5.4).
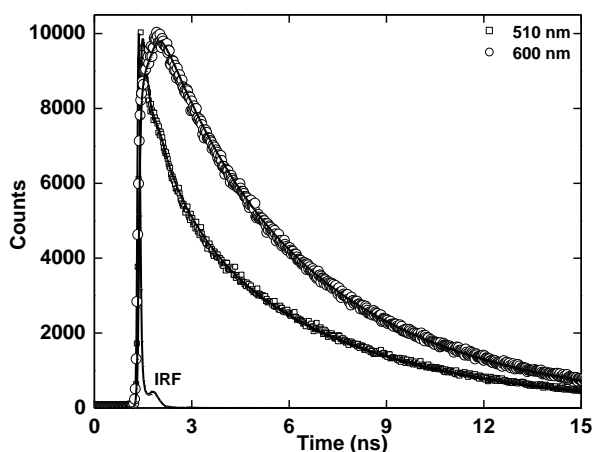
Figure 5.8. Fluorescence decay profile of C153 in BMIMTFA-H_2O system at different monitoring wavelength. The monitoring wavelengths are shown by the corresponding symbol in the same figure. Instrument response function (IRF) is also given in the figure. Symbols denote the experimental data points and solid lines are fit to the data points.
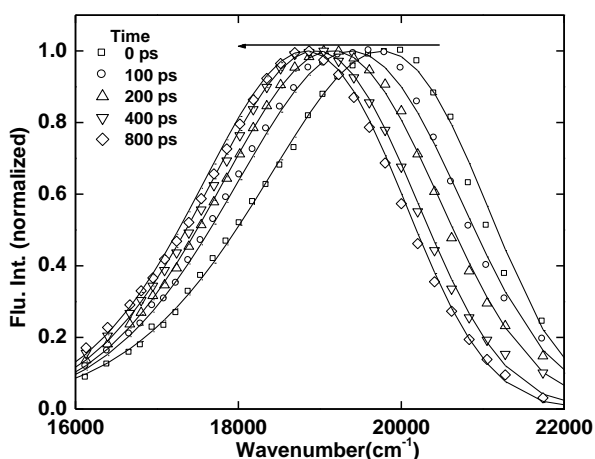
Figure 5.9. Time-resolved emission spectra (TRES) of C153 in BMIMTFA-H_2O system at different time span. Symbols denote the experimental data points and solid lines represent the log normal fit to the data points.

Quite interestingly, the data collected in Table 5.4 also reveal that with the addition of same mole fraction of cosolvent, lowering in viscosity is higher for methanol than that for

water. It points out that methanol separates the cations and anions of RTIL more effectively than water causing relatively more decrease of cohesive energy between ions and eventually this result in more lowering of the bulk viscosity of the RTIL-methanol system.[135] This observation further indicates that RTIL interacts differently with methanol and water. As the medium viscosity profoundly influences solute dynamics, the average solvation time is found to be much less in case of BMIMTFA-CH$_3$OH system (Table 5.4). Table 5.4 also illustrates that the average solvation time drops more (1.64 times) in BMIMTFA-methanol system than in BMIMTFA-water system (1.20 times) even for the same mole-fraction of the respective cosolvents.
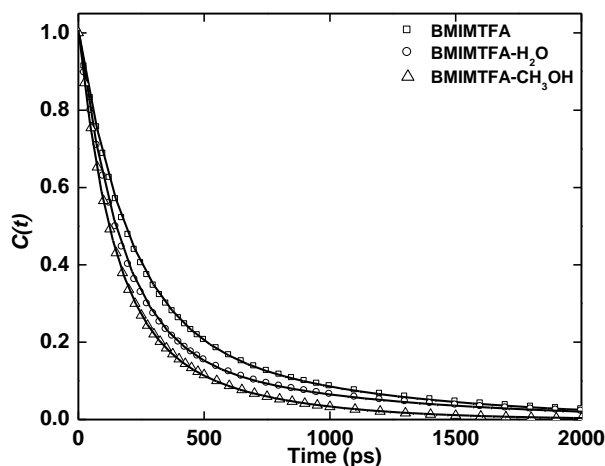
Figure 5.10. Decay of solvent correlation function, *C(t)* of C153 in BMIMTFA, BMIMTFA-H$_2$O, BMIMTFA-CH$_3$OH systems. Symbols denote the experimental data points and solid lines represent the bi-exponential fit to the data points.

Table 5.4. Solvent relaxation parameters of C153 in BMIMTFA, BMIMTFA-H$_2$O and BMIMTFA-CH$_3$OH systems

system	Vis.(cp)	a_1	$\tau_1(ns)$	a_2	$\tau_2(ns)$	$^a\tau_{av.}(ns)$	β	$\tau_{solv.}(ns)$	$\tau_{st}(ns)$	obs. Shift (cm^{-1})
		bi-exponential fit					stretched exponential fit			
BMIMTFA	69	0.26	0.854	0.74	0.198	0.368	0.82	0.296	0.330	999
BMIMTFA- H$_2$O	37	0.19	0.887	0.81	0.168	0.305	0.82	0.235	0.262	1023
BMIMTFA-CH$_3$OH	26	0.29	0.458	0.71	0.128	0.224	0.84	0.192	0.210	899

^{a} experimental error ±5%

5.3.2.2.2. *Rotational Diffusion of C153*

The rotational dynamics of photo excited probe is very sensitive to microenvironment of the probe and local viscosity of the medium.[285] We have carried out time-resolved fluorescence anisotropy decay of C153 in neat BMIMTFA, BMIMTFA-H_2O and BMIMTFA-CH_3OH in order to know the effect of cosolvent addition on the microenvironment of photoexcited probe. Time-resolved fluorescence anisotropy decay (r(t)) is predicted by the following Equation 2.21. The time-resolved fluorescence anisotropy decay profile for BMIMTFA, BMIMTFA-H_2O and BMIMTFA-CH_3OH at $\lambda_{exc.} = 405$ nm is shown in Figure 5.11. The rotational relaxation parameters of C153 in neat RTIL and their cosolvent mixtures at different temperatures are shown in Table 5.5. The anisotropy decay profiles are well fitted by bi-exponential function and rotational relaxation times are calculated according to Equation 2.22.
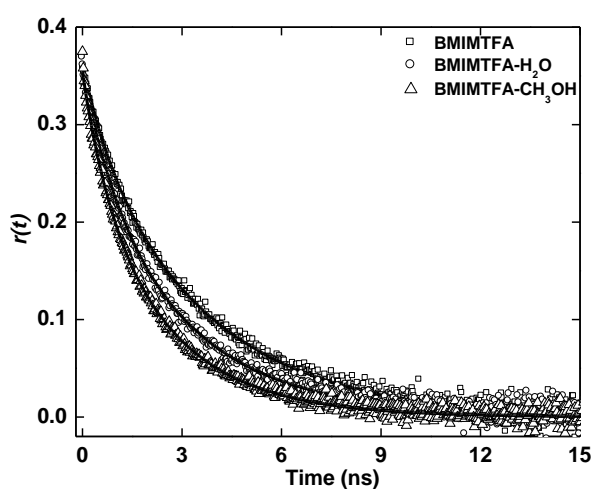
Figure 5.11. Time-resolved fluorescence anisotropy decay of C153 in BMIMTFA, BMIMTFA-H_2O, BMIMTFA-CH_3OH systems at 293K. Symbols denote the experimental data points and solid lines represent the bi-exponential fit to the data points.

It can be seen from Table 5.5 that average rotation time of C153 in neat RTIL is 3.16 ns and C153 rotates faster as cosolvents are added to the neat ionic liquid. The faster rotation of C153 upon addition of cosolvents can be attributed to the lowering of viscosity of the medium. However, quite interestingly, Table 5.5 also shows a more drop in average

rotational time (1.98 ns) in RTIL-methanol system than that (2.52 ns) of RTIL-water system. This observation perhaps indicates that BMIMTFA-CH$_3$OH and BMIMTFA-H$_2$O systems have different structural organizations. In this context, it is pertinent to mention that ionic liquids with alkyl chain C$_4$ or longer are known to be spatially heterogeneous in nature having polar and nonpolar domain[76, 77,103]. Nonpolar domain is believed to be formed mainly by aggregation of apolar alkyl chains, and polar domain forms because of the cations and anions.[76, 77, 103] In light of this one can also reasonably assume that in case of the present ionic liquid, BMIMTFA, butyl chain would be responsible to form a nonpolar domain and the imidazolium cations and TFA anion would give rise to polar domain.

The nonpolar and polar domains are interconnected and give rise to organized network.[285] It is also expected that water and methanol would interact differently with the ionic liquid and thereby perturb the organized network of ionic liquid which will eventually lead to a change in the microviscosity of the medium. As a result, rotational dynamics of C153 is expected to be influenced which is also observed in the present case (Table 5.5).

Table 5.5. Rotational relaxation parameters of C153 in BMIMTFA, BMIMTFA-H$_2$O and BMIMTFA-CH$_3$OH systems at different temperatures

systems	Temp.(K)	Vis.(cP)	[a]r_0	a_1	τ_1(ns)	a_2	τ_2(ns)	$<\tau_r$ (ns)$>$[b]	[c]$C_{obs.}$
BMIMTFA	293	69	0.37	0.18	0.86	0.82	3.67	3.16	0.52
	298	54	0.36	0.30	1.07	0.70	2.91	2.36	
	303	43	0.37	0.33	0.93	0.67	2.43	1.93	
	308	34	0.36	0.69	1.19	0.31	2.34	1.55	
	313	29	0.36	0.73	1.00	0.27	2.20	1.32	
BMIMTFA- H$_2$O	293	37	0.37	0.29	1.08	0.29	3.11	2.52	0.79
	298	30	0.35	0.20	0.52	0.80	2.30	1.94	
	303	24	0.35	0.29	0.72	0.71	2.02	1.64	
	308	20	0.36	0.53	0.80	0.47	2.20	1.37	
	313	16	0.34	0.54	0.75	0.46	1.69	1.18	
BMIMTFA- CH$_3$OH	293	26	0.37	0.29	0.80	0.71	2.47	1.98	0.84
	298	21	0.32	0.12	0.28	0.88	1.72	1.55	
	303	18	0.32	0.14	0.26	0.86	1.42	1.26	
	308	15	0.33	0.21	0.60	0.79	1.20	1.07	
	313	12	0.31	0.11	0.13	0.89	0.98	0.89	

[a] initial anisotropy and [b] average rotational time. [c] average rotational coupling constant

To get a closer insight on whether the change in the organized structure affects the solute-solvent coupling, we have further analyzed experimentally measured rotation time with the help of well known Stokes-Einstein-Debye (SED) hydrodynamic theory. The slip and stick boundary limit, which have been assigned with the help of SED hydrodynamic theory are shown in the Figure 5.12 along with experimentally measured rotational time of C153 in neat BMIMTFA, BMIMTFA-H_2O and BMIMTFA-CH_3OH systems respectively. Quite interestingly, the last column of Table 5.5 reveals that solute-solvent coupling constant (C_{rot}) values are different for neat RTIL, RTIL-water and RTIL-methanol system. In case of neat RTIL, the C_{rot} values are found to be similar to the conventional solvents[272] whereas for other two mixtures it is found to be higher than for the neat RTILs. The change in the C_{rot} values probably indicates a change in the organized structure of the ionic liquids upon cosolvent addition. Moreover, our observation on different C_{rot} values in presence of same mole fraction of water and methanol indicates that water and methanol induce different heterogeneity to the neat RTIL by virtue of their varying nature of intermolecular interaction with RTIL.
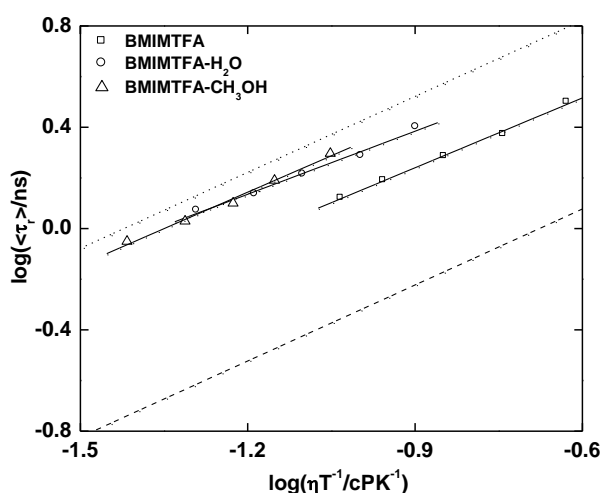
Figure 5.12. log-log plots of rotational relaxation times of C153 vs. η/T in BMIMTFA, BMIMTFA-H_2O and BMIMTFA-CH_3OH system with slip and stick boundary condition parameters. Dashed and dotted lines represent the slip and stick boundary condition for C153. Symbols denote the experimental data points and solid lines represent the fit to the data points respectively

147

5.3.2.3. *Quantum Mechanical Calculations*

To obtain the molecular origin of RTIL-cosolvent interactions, we have optimized the ground state structures of neat BMIMTFA, BMIMTFA-H$_2$O and BMIMTFA-CH$_3$OH systems at B3LYP/6-31++G (d, p) level of theory. This level of theory has recently employed to understand the RTIL-cosolvent interactions by many groups[135, 286-288]. The optimized geometry is identified with lowest energy with no imaginary frequency. As many conformers are possible for neat RTIL, lowest energy geometries are preferred for further (RTIL-cosolvent) calculation. The optimized geometries and structural parameters associated with them are provided in Figure 5.13 and Table 5.6 respectively.

BMIMTFA	BMIMTFA-H$_2$O	BMIMTFA-CH$_3$OH
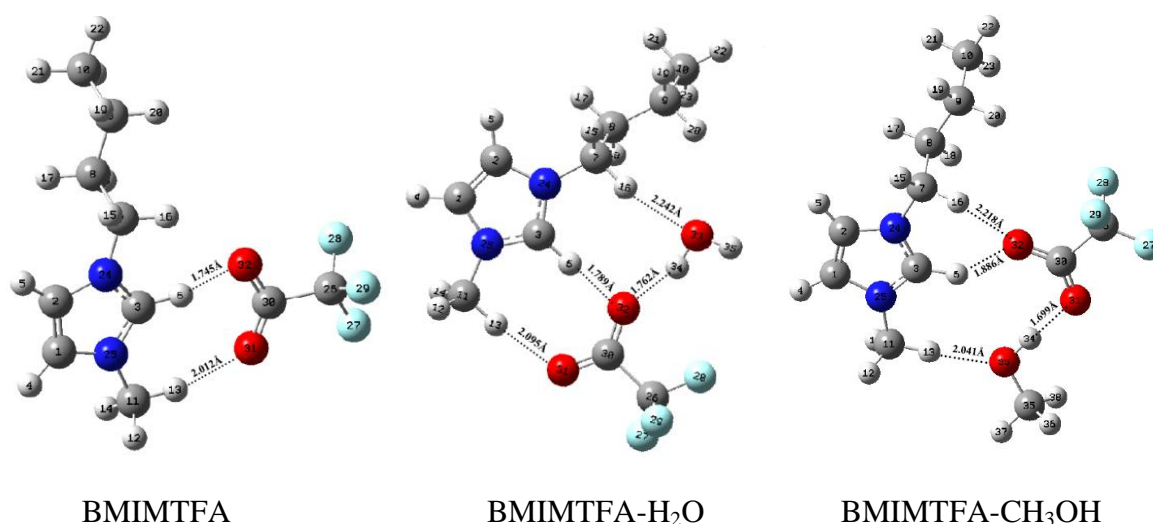
Figure 5.13. Optimized structures of BMIMTFA, BMIMTFA-H$_2$O and BMIMTFA-CH$_3$OH calculated at the B3LYP/6-31++G (d, p) level in the gas phase.

In the B3LYP/6-31++G (d, p) level optimized geometry of neat BMIMTFA the distance between H6-O32, H13-O31 are 1.745 Å, 2.102Å respectively. The van der waals O….H distance is 2.72Å[289] which is higher than the observe distance. Angles among C3-H6-O32 and C11-H13-O31 are found to be 168°, 164° respectively. Considering distance and angle form the optimized geometry, it can be concluded that hydrogen bonding interaction exists between the imidazolium C$_2$-H proton and TFA anion.[250] Methyl proton of imidazolium moiety is also found to make hydrogen bond with TFA anion (Figure 5.13).

Table 5.6. Bond angle and bond distances from B3LYP/6-31++G (d, p) level of optimized structures of BMIMTFA, BMIMTFA-H_2O and BMIMTFA-CH_3OH systems in the gas phase

system	Bond distances	(Å)	Bond angle	(°)
BMIMTFA	H6-O32	1.745	C3-H6-O32	168
	C3-H6	1.112		
	C3-O32	2.842		
	H13-O31	2.102	C11-H13-O31	164
	C11-H13	1.095		
	C11-O31	3.170		
BMIMTFA-H_2O	H34-O32	1.762	O33-H34-O32	160
	O33-H34	0.984		
	O33-O32	2.708		
	H16-O33	2.242	O33-H16-C7	154
	C7-H16	1.093		
	O33-C7	3.260		
	H6-O32	1.789	O32-H6-C3	177
	C3-H6	1.106		
	C13-O32	2.894		
	H13-O31	2.095	O31-H13-C11	173
	C11-H13	1.096		
	C11-O31	3.185		
BMIMTFA-CH_3OH	H34-O31	1.699	O33-H34-O31	177
	O33-H34	0.994		
	O33-O31	2.756		
	H13-O32	2.041	C11-H13-O33	175
	C11-H13	1.096		
	C11-H33	3.134		
	H6-O32	1.886	C30-O32-H6	128
	C3-H6	1.096		
	C3-H32	2.838		
	H16-O32	2.218	C30-O32-H16	156
	C30-O32	1.257		
	C30-H16	3.408		

Figure 5.13 also demonstrates the H-bonding interactions between RTIL and water and RTIL-methanol respectively. It has been observed that in case of water, the hydrogen atom of water molecule is hydrogen bonded to the O atoms of carboxylate moiety of RTIL with the distance 1.762 Å. A weak C-H…O interaction has also been observed between water oxygen atom and hydrogen atom of butyl chain. However, in case of methanol a shorter distance (1.699Å) between methanol hydrogen and O atoms of carboxylate moiety of IL has been observed. C-H…O interaction between methyl hydrogen and oxygen atom of methanol is

also found to be stronger as the distance between them is observed to be 2.041 Å which is shorter than the C-H…O distance (2.242 Å) in case of the water (Figure 5.13). We could not find any H-bonding interaction between imidazolium C_2-H proton and water/methanol within the 1:1 RTIL- cosolvent combination. It may be due to the fact that anion and water/methanol interaction is relatively stronger than that of imidazolium proton-water/methanol interaction. Steric factors may be also responsible for the absence of H-bonding between C_2-H proton of imidazolium and water/methanol.

All of these data indicate that the methanol is a better proton acceptor than water when it interacts with RTIL. These results imply that the replacement of H of water by methyl strengthens the H-bonding interactions and thus the interaction between methanol and ILs is stronger than the interaction between RTIL and water. In this context, it should be mentioned that geometries in Figure 5.13 gives only most probable geometries of the complexes which only provide us the dominant interaction sites that exist between the constituents of the complexes.

From solute and solvation dynamics studies and the data obtained from theoretical calculations, it is evident from the present study that microscopic structural organizations are quite different for RTIL-water and RTIL-methanol systems. These data also lead us to conclude that the variation in structural reorganization is primarily responsible for the observed photophysical responses of C153 in these two media.

5.4. Conclusion

To understand the effect of nonpolar and polar cosolvents in solute and solvation dynamics in RTILs, steady state and time-resolved fluorescence behavior of C153 have been studied in RTIL and RTIL-cosolvents mixture. To study the effect of nonpolar cosolvent, steady state and time-resolved fluorescence behavior of C153 in a hydrophobic RTIL, MOEMPLFAP and MOEMPLFAP-toluene mixture have been studied. The present ionic liquid is well suited to study the influence of RTIL-cosolvent (nonpolar) interaction on

dynamics of solvation for its ultra hydrophobic nature. Even though the steady state spectral behavior of C153 is not affected by the nonpolar cosolvents, involvement of toluene is clearly manifested in the present time-resolved studies. The addition of toluene to RTIL decreases the average solvation time due to the reduction of viscosity of the media. A significant blue shift of the time-zero maximum of fluorescence spectrum upon addition of toluene indicates a more nonpolar surrounding of C153 in the mixed solvents at the early part of dynamics. The present time-resolved data in RTIL and RTIL-toluene data suggests that nonpolar toluene is effectively penetrated into the cybotactic region of probe molecule due to the favorable hydrophobic interaction between RTIL and toluene. The rotational dynamics of the probe also becomes faster in the presence of toluene due to the lowering of the viscosity of the medium.

While studying the effect of polar cosolvents, steady state and time-resolved fluorescence behavior of C153 and ANF have been carried out in neat BMIMTFA and its mixture with water and methanol. Photophysical investigation reveals that water and methanol affects the solute and solvent dynamics in different ways. To understand the intermolecular interactions that exist between RTIL and RTIL-cosolvent systems, theoretical calculations have also been performed by optimizing the ground state geometries of BMIMTFA, BMIMTFA-H_2O and BMIMTFA-CH_3OH. The present photophysical and theoretical calculations data possibly also indicate that the varying nature of intermolecular interaction between RTIL and cosolvent induces different microscopic structural organization in the two (BMIMTFA-H_2O and BMIMTFA-CH_3OH) binary systems.

Solute Rotation and Solvent Relaxation of Coumarin153 in Moderate and High Viscous Room Temperature Ionic Liquids: An Excitation Wavelength Dependence Study

6.1. Introduction

In recent years the intense interest in room temperature ionic liquids (RTILs) is primarily because of two broad reasons; (I) their potential as a specialty media for advanced devices and industrial processes[3-18] and (ii) scientific curiosity to unravel their structure-property correlation[3-18]. Molecular-level understanding on the intermolecular interactions, structure, and dynamics of new solvent systems are very much essential for that substance to be used in new applications. It is not yet possible to quantitatively describe the connection between dynamics and structures of RTILs. In this regard, microheterogeneous nature of ILs has made it even more challenging to find out the structure-property correlation. So, the studies that focus unraveling the relationship between microheterogeneous nature of RTILs and the dynamical feature of RTILs are the need of the hour.

A limited number of studies have been performed on ILs to understand the microheterogeneous nature of RTILs.[76-82] The multi scale coarse grained structure simulation by Wang and Voth[76] and atomistic simulations by Lopes and Padua[77] indicated nanostructural organization in these media. Recently, optical heterodyne-detected Raman induced Kerr effect studies (OHD-RIKES) provide further evidence in favor of heterogeneous nature of ILs.[78] Samanta and coworkers[79] have also shown microheterogeneous nature of ILs by exploiting excitation wavelength dependence fluorescence behavior of several probes in RTILs. Later, Hu and Margulis[80] by molecular dynamics simulation studies proposed that the red edge excitation wavelength dependent fluorescence behavior of molecules arises from probes trapped in quasi-static solvent cages that relax in time scale longer than the fluorescence lifetime of the probes. Very recently, Maroncelli[81] and Bhattacharya [82] have

independently studied the excitation wavelength dependent solvation dynamics in neat RTILs using femtosecond time-resolved emission spectroscopy. In the similar context, recent time-resolved fluorescence studies by Biswas and coworkers in deep eutectic mixtures containing amide and electrolytes are also noteworthy.[267, 268] They have observed the decoupling of solute rotation and solvation dynamics from the medium viscosity. They have also shown that medium heterogeneity plays an important role for this observed behaviour. Deep eutectic melts consisting of amide and electrolytes–a system that contains the same pieces of solvent-solvent interactions as these ILs and thus understanding gained there may be utilized to explain some of the results obtained in the present study. It may be mentioned that the viscosity-diffusion decoupling has been commonly analyzed by fractional viscosity dependence (η) of the measured average solvation $<\tau_s>$ and rotation $<\tau_r>$ times : $<\tau_x> \propto (\eta/T)^p$ (*x* denoting solvation or rotation, *p* is the exponent and T is the temperature).[267, 268] Since the ILs and eutectic melts are very similar in nature; we are interested to know whether such fractional dependence of viscosity is also observed in case of average solvation and rotational times in ILs. Additionally, we are interested to know the roles of both static and dynamic heterogeneities that they play in governing the viscosity decoupling in these media. In this regard, it may be mentioned that the studies on eutectic melts are mostly based on single excitation wavelength based measurements and hence cannot provide much insights into the temporal heterogeneity of the medium. To the best of our knowledge no such studies that focus investigating the role of heterogeneity in the observed viscosity-diffusion decoupling in RTILs have been carried out.

Keeping all these aspects in mind, we have carried out the temperature as well as excitation wavelength dependence solvation and rotational relaxation of C153 in moderately viscous 1-(2-methoxyethyl)-1-methylpyrrolidinium tris(pentafluoroethyl)trifluorophosphate (MOEMPLFAP) and highly viscous 1-(2-methoxyethyl)-1-methylmorpholinium

tris(pentafluoroethyl)trifluorophosphate (MOEMMOFAP). Thermophysical properties of the two ILs have also been investigated with a view to understand how the structural variation in the cationic moiety affects properties of the ionic liquids. Molecular diagrams of ILs and C153 are provided in chart 6.1.

1-(2-methoxyethyl)-1-methylpyrrolidinium tris(pentafluoroethyl)trifluorophosphate (MOEMPLFAP)

1-(2-methoxyethyl)-1-methylmorpholinium tris(pentafluoroethyl)trifluorophosphate (MOEMMOFAP)
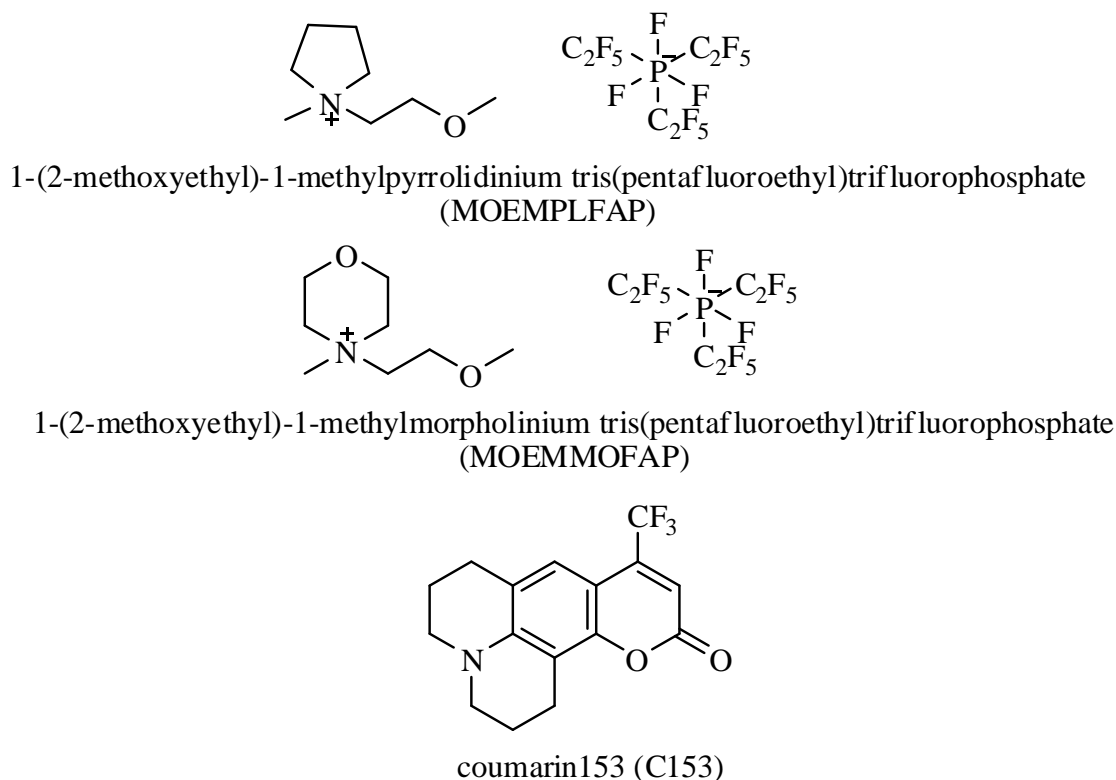
coumarin153 (C153)

Chart 6.1. Molecular diagrams of RTILs and probe under the present study.

6.2. Experiments and Methods

Coumarin153 (C153) (laser grade, Exciton) was used as a probe for solute and solvation dynamics study. RTILs (Chart 6.1) were obtained from Merck, Germany (>99% purity) and used as received. The water and halide contents of the ILs were <100 ppm. For steady state experiments, all samples were excited at 375 nm, 405 nm and 445 nm respectively. Time-resolved fluorescence measurements were carried out using the same TCSPC spectrometer and samples were excited at 375 nm, 405 nm and 445 nm using different picoseconds diode laser. The details of these instrumental techniques, procedure of time-resolved data analysis,

methods for construction of solvent correlation function ($C(t)$) and estimation of solvent relaxation times are discussed in Chapter 2.

6.3. Results and Discussion

6.3.1. *Thermophysical Properties of RTILs*

The properties of the RTILs depend very much on the cations and anions that they are composed of and for that they are also known as designer solvents.[3] In order to know, the effects of cationic moiety in controlling the physicochemical properties of the ILs, thermophysical studies on the present ILs that differ only in their cationic moiety has been carried out. The knowledge about physicochemical properties of the ILs is also expected to be helpful in explaining new experimental observation such as photophysical responses of the systems in proper manner. The measured viscosity and density of the two ILs at different temperatures are provided in Table 6.1. The variation of the viscosity and density of the two ILs at different temperatures are also shown in Figures 6.1(a) and 6.1(b). It is evident that at 293K, viscosity of morpholinium-based system is almost 8 times higher than that of pyrolidinium-based system. This difference in viscosity may be due to presence of oxygen atom in the ring which renders the nitrogen atom more electropositive by virtue of the greater inductive effect of oxygen than carbon atom, which in turn makes the association with the FAP anion more stronger.[155] The fact that N atom of morpholinuim cation is more electropositive than the N atom of pyrrolidinum moiety is supported by calculation of charge densities on the N atom by optimizing (at AM1level[290]) the structures (Figure 6.2) of two cations independently. All the calculations were performed using the GAUSSIAN 03 program package[231]. Quite interestingly, it has been observed that the viscosity of morpholinium-based system is always higher by a factor of 4-8 as compared to pyrrolidinium-based system at all temperatures. The observation indicates that the association between cationic moiety and FAP anion remains always stronger even at higher temperature

(323K) for MOEMMOFAP than for MOEMPLFAP. At all temperatures the measured

densities is found to be slightly higher for MOEMMOFAP than for MOEMPLFAP.
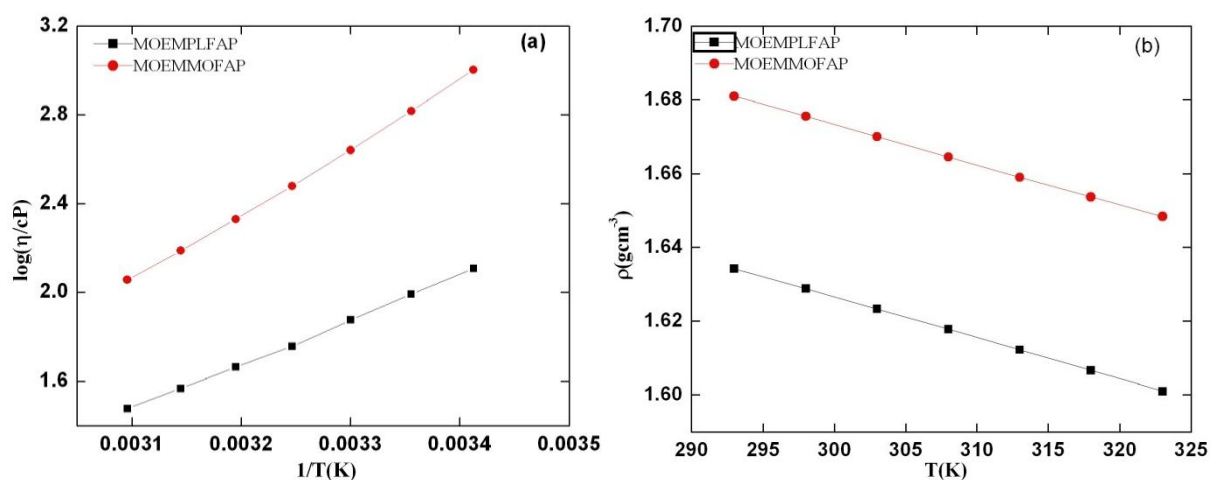
Figure 6.1. (a) Viscosities and (b) densities of MOEMMOFAP and MOEMPLFAP as a function of temperature.

The experimental viscosities (η), densities (ρ) at different temperatures were fitted by

the least-squares method using the following reported equations. [291, 292]

$$\log \eta / cP = A_0 + (A_1/T) \tag{6.1}$$

$$\rho/(g.cm^{-3}) = A_2 + A_3 T \tag{6.2}$$

The values of A_0, A_1, A_2, A_3 and the regression coefficients are collected in Table 6.2.
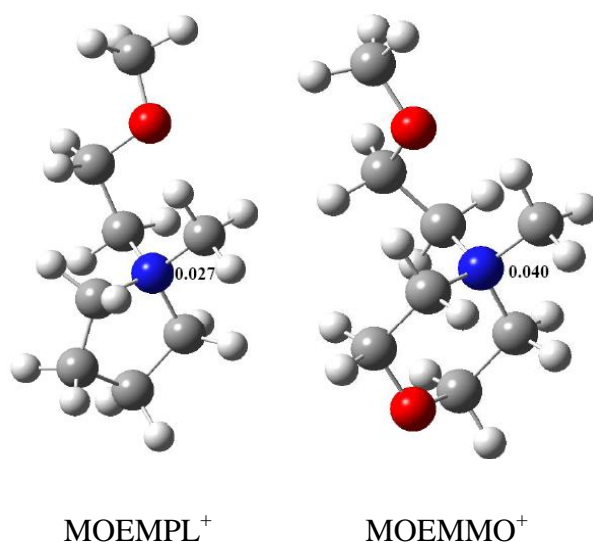
MOEMPL$^+$ MOEMMO$^+$

Figure 6.2. Optimized structures of MOEMPL and MOEMMO cations at AM1of level theory.

Table 6.1. Experimental viscosities and densities for MOEMPLFAP and MOEMMOFAP as function of temperature

Temp.(K)	η/cP		ρ/gm cm^{-3}	
	MOEMPLFAP	MOEMMOFAP	MOEMPLFAP	MOEMMOFAP
293	128	1004	1.634230	1.680979
298	98	657	1.628792	1.675603
303	75	438	1.623288	1.670098
308	57	301	1.617759	1.664575
313	46	214	1.612191	1.659044
318	37	154	1.606593	1.653693
323	30	114	1.600976	1.648369

experimental errors are ±5%

Table 6.2. Fitting parameters for viscosity and density according to equation 6.1 and 6.2

RTILs	A_0	A_1	R	A_2	$A_3 \times 10^{-3}$	R†
MOEMMOFAP	-7.17	2975.72	0.9988	2.00	-1.09	0.9999
MOEMPLFAP	-4.69	1991.15	0.9989	1.96	-1.11	0.9999

†R = regression coefficient

The experimental density values were again used to estimate thermal expansion coefficient (α) of the two ILs by using the following equation[291]

$$\alpha_p = -\frac{1}{p}\left(\frac{\delta p}{\delta T}\right)_p = -\frac{A_3}{A_2 + A_3 T} \tag{6.3}$$

where A_2, A_3 are the fitting parameters from Equation 6.2 and α_p, p and T are the thermal expansion coefficient, pressure and absolute temperature respectively. It may be mentioned that the thermal expansion coefficient (α_P) is also known as volume expansivity.[293] The expansion coefficients of the two ionic liquids are collected in Table 6.3. It can be observed (Table 6.3) that the coefficients of thermal expansion of the ionic liquids do not change appreciably with a change in temperature. The observed thermal expansion coefficient values are found to be similar to those reported for imidazolium, pyridinium, phosphonium, and ammonium based ILs, $(4.8 \times 10^{-4}$ to $6.5 \times 10^{-4})$ K^{-1}.[294, 295]

Table 6.3. Thermal expansion coefficients of the present RTILs as a function of temperature

T/K	$\alpha \times 10^4 \, (K^{-1})^{\dagger}$	
	MOEMPLFAP	MOEMMOFAP
293	6.79	6.48
298	6.81	6.51
303	6.84	6.53
308	6.86	6.55
313	6.88	6.57
318	6.91	6.59
323	6.93	6.61

† Thermal expansion coefficients (α) calculated using Equation 6.3

6.3.2. *Steady State Behavior of C153 in Present RTILs*

The representative absorption spectra of C153 in MOEMPLFAP and MOEMMOFAP are shown in Figure 6.3. The emission spectra of neat RTILs and C153 in two RTILs at different excitation wavelengths are shown in Figure 6.4. Absorption and emission maxima of C153 in MOEMPLFAP and MOEMMOFAP are collected in Table 6.4. A bathochromic shift in both absorption and emission maxima of C153 has been observed on changing the medium from pyrrolinidium to morpholinium systems (Table 6.4). Additionally, one can also observe from Figure 6.4 that the emission maxima of C153 in neat RTILs do not change with the variation of excitation wavelengths ($\lambda_{exc.}$). No significant changes in both absorption and emission maximum of C153 have been observed with the change in temperature (293K to 308K). From the steady state absorption and emission spectral profile, it can be concluded that MOEMMOFAP is more polar in nature than MOEMPLFAP. Interestingly, the full width at half maximum (FWHM) as estimated from the absorption spectrum of C153 is found to be higher (5850 cm^{-1}) in MOEMMOFAP than that (4360 cm^{-1}) in MOEMPLFAP. The observation indicates a distribution of the molecules in the ground state having different energies. The more inhomogeneous broadening of absorption in case of highly viscous ionic liquid points out that the presence of ensemble of energetically different species in the ground state is more favoured in highly viscous medium. To know how the spectral widths (absorption and emission) of C153 in these ILs compare with those from imidazolium IL, we

158

have also measured the FWHM of both the absorption and emission spectra in imidazolium–based ionic liquid, 1-ethyl-3-methylimidazolium tris(pentafluoroethyl)trifluorophosphate (EMIMFAP). In case of absorption, the measured FWHM in EMIMFAP is 4131 cm^{-1}. In case of emission, the FWHM is measured to be 2803 cm^{-1}, 2395 cm^{-1} and 2678 cm^{-1} for MOEMPLFAP, MOEMMOFAP and EMIMFAP respectively. These data probably indicates that morpholinium ILs are more microheterogeneous in nature than the imidazolium-based ILs. In this context we would like to note that a very recent work by Samanta and his coworkers have also pointed out that the morpholinium ILs are more heterogeneous than imidazolium ILs.[117]
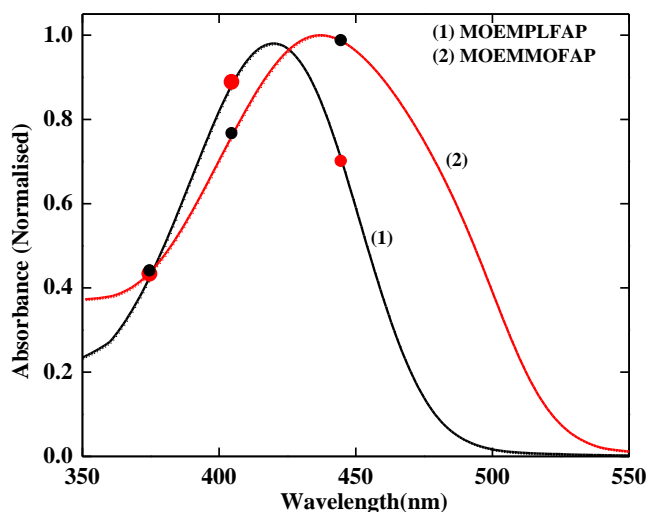
Figure 6.3. Steady state absorption spectra of C153 in (1) MOEMPLFAP and (2) MOEMMOFAP. Spectra are normalized at their corresponding peak maximum. Symbols denote the excitation wavelengths ($\lambda_{exc.}$).

159
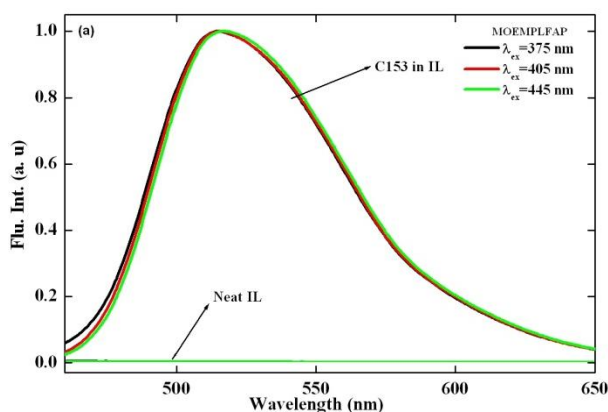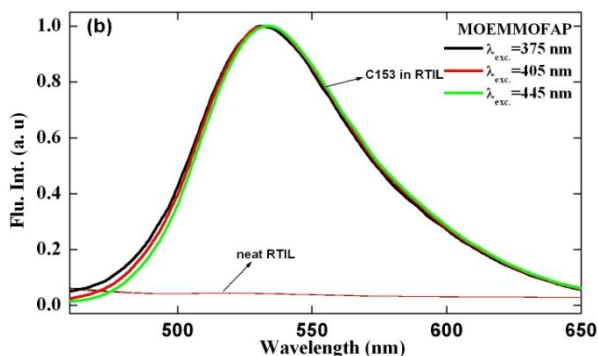
Figure 6.4. Steady state emission of C153 in MOEMPLFAP and MOEMMOFAP at different excitation wavelengths ($\lambda_{exc.}$) at 293K. All emission spectra of C153 are normalized at the corresponding peak. Emission spectra of neat RTILs at the different excitation wavelength ($\lambda_{exc.}$) are also shown in the figure.

Table 6.4. Absorption and emission maxima, Stokes shift of C153 in MOEMPLFAP and MOEMMOFAP

system	$\lambda_{max}^{abs}(nm)^a$	$\lambda_{max}^{flu}(nm)^a$	Stokes shift (cm^{-1})
MOEMPLFAP	420	515	4392
MOEMMOFAP	437	533	4122

^{a}experimental error $\pm$ 1nm

6.3.3. *Solvation Dynamics Study*

Representative wavelength dependent decay profile is given in Figure 6.5 for MOEMMOFAP at $\lambda_{exc.}$ = 405 nm at 293K. The time-resolved emission spectra (TRES) of C153 in MOEMPLFAP at different time intervals are shown in Figure 6.6. A time-dependent shift of the emission spectra toward the lower energy indicates solvent-mediated relaxation of the excited state of the fluorophore (Figure 6.6). In this context, it is also observed that full width at half maxima (FWHM) of the TRES are becoming narrower with time which indicates the solvent mediated stabilization of the excited state of the probe, is shown in Figure 6.7.[242] The total shift of time-dependent emission ($\Delta \bar{\nu}$), calculated from the difference between the peak frequencies (in cm^{-1}) of the measured spectra at zero time ($\bar{\nu}(0)$) and infinite time ($\bar{\nu}(\infty)$), is found to be 924 cm^{-1} and 479 cm^{-1} for C153 at $\lambda_{exc.}$ = 405 nm in MOEMPLFAP and MOEMMOFAP respectively (Table 6.5). These data indicate that ~ 40 % dynamics is missed in case of MOEMPLFAP due to the finite time resolution (~75ps) of

our TCSPC set up.[226] The missing component for highly viscous IL by employing Fee and Maroncelli method[226] is found to be higher. The higher missing component in case of highly viscous IL is probably due to underlying change the in vibronic structure of the solute.
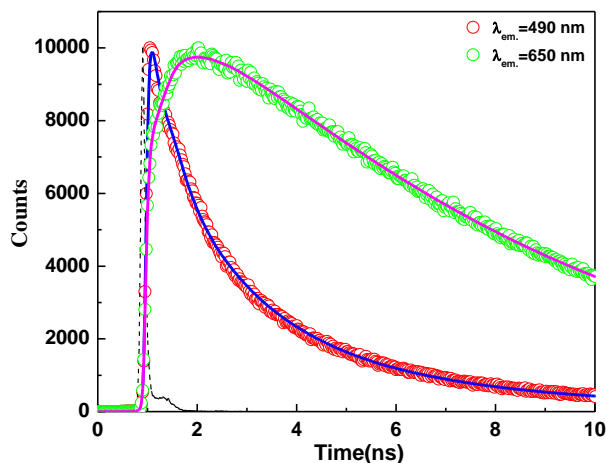
Figure 6.5. Representative emission wavelength dependent decay profiles for C153 in MOEMMOFAP at 293K ($\lambda_{exc.}$ = 405 nm). Circles denote the experimental data points and solid line represent the fit to the data points. Instrument response function (IRF) is also shown in the same figure (dotted lines). The goodness of fit parameter values (χ^2) in these two wavelengths are 1.1 and 1.01 respectively.

The representative plots of *C(t)* versus time for C153 both via bi-exponential and stretched exponential fit to the data are shown in Figure 6.8. Both fits are suitable as both fits provide very similar average solvation times (Tables 6.5, 6.6, 6.7). The average solvation times are estimated to be different for different RTILs (Table 6.5) and also found out to depend on the excitation wavelengths. For example, the average solvation times estimated to be 0.61 ns, 3.10 ns at $\lambda_{exc.}$ = 375 nm and 0.69 ns and 3.65 ns at $\lambda_{exc.}$ = 405 nm in the case of MOEMPLFAP and MOEMMOFAP respectively (Table 6.5). Quite interestingly the data that are collected in Table 6.5 also reveal that even if the average solvation time found to be much higher for morpholinium based ionic liquid to that of pyrrolidinium based system, the change in the average solvation time with respect to the change in the excitation wavelengths are quite similar. On changing the excitation wavelength from 375 nm to 405 nm, the change in the average solvation time is found to be 1.13 and 1.17 times for pyrrolidinium and morpholinium based system respectively. Quite interestingly, data in Table 6.5 also show that

measured average solvation time exhibits stronger excitation wavelength dependence in highly viscous IL, whereas similar sensitivity has not been found in low viscous IL. For low viscous IL, the difference is negligible probably because of rapid inter conversion (low lifetime compared to diffusive timescale of the medium) of the environments probed by the photo-selection; at larger viscosity these distinct environments are relatively longer-lived and thus the measured average solvation time exhibits stronger excitation wavelength dependence. However, missing of the initial fast component in the present experiments may also have some effects on the observed dependence here which cannot be quantified by the present data. The change in average solvation times as a function of excitation wavelengths reflects the microheterogeneous nature of the RTILs. In this context we note that the excitation wavelength dependency on solvation dynamics has also been observed by Maroncelli[81] and Bhattacharyya[82] independently in deferent ionic liquids and the same rationale has been put forward in explaining the observation of excitation wavelength dependence solvation dynamics.

Quite interestingly, although the viscosity of MOEMMOFAP is almost 8 times higher than that of MOEMPLFAP, solvation time is increased only 5.3 times at a particular wavelength. Here, it may be mentioned that average solvation time relates linearly with the viscosity[120] of the medium and hence the present solvation dynamics data in case of highly viscous IL is interesting. To get better understanding on the coupling between average solvation time ($<\tau_s>$) and medium viscosity (η), we have measured temperature dependent average solvation times for both the ILs at 405 nm excitation wavelength (Tables 6.6 and 6.7) and applied the stokes-Einstein relation (SE) which predicts $D^{-1} \propto \eta/T$ where D is the diffusion coefficient and η/T is temperature-reduced viscosity. The similar relationship has also been applied earlier by other authors in eutectic melts for the same purpose.[268] We have fitted the average solvent relaxation time with the $<\tau_s> \propto (\eta/T)^p$ relationship (Equations 6.4

and 6.5). Figure 6.9 depicts the log-log plots of average solvation times vs η/T in the present RTILs. In both the cases p is found to deviate from unity and deviation is more in case of relatively more viscous ionic liquid (Equations 6.4, 6.5 and Figure 6.9). However, in both cases the fractional dependence of average solvation time on temperature-reduced viscosity is not large, but not negligible. These findings are interesting in a sense that dynamic Stokes shift measurements in ionic liquids showed better linear correlation with viscosity.[120]

C153 in MOEMMOFAP log $(< \tau_s>) = 0.159 + 0.69 \log (\eta/T)$ (N = 4, R = 0.97512)   (6.4)

C153 in MOEMPLFAP   log $(< \tau_s>) = 0.153 + 0.85 \log(\eta/T)$ (N = 4, R = 0.99568)   (6.5)

In these expressions, N and R are the number of data points and regression coefficient, respectively.
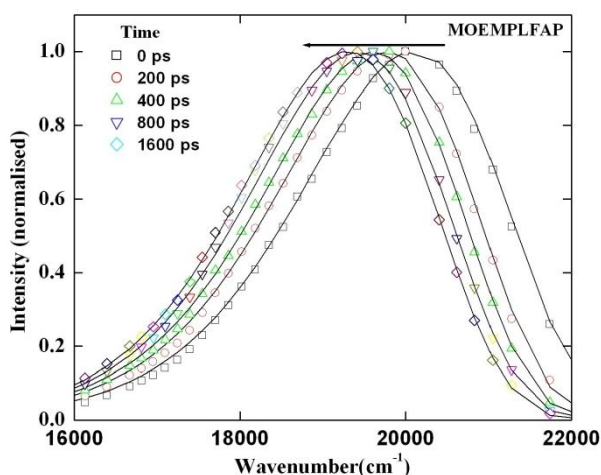
Figure 6.6. TRES of C153 in MOEMPLFAP at 293 K at different time span. Time intervals are indicated by the corresponding symbols. All spectra are normalized at their corresponding peak maximum. $\lambda_{exc.} = 405$ nm.
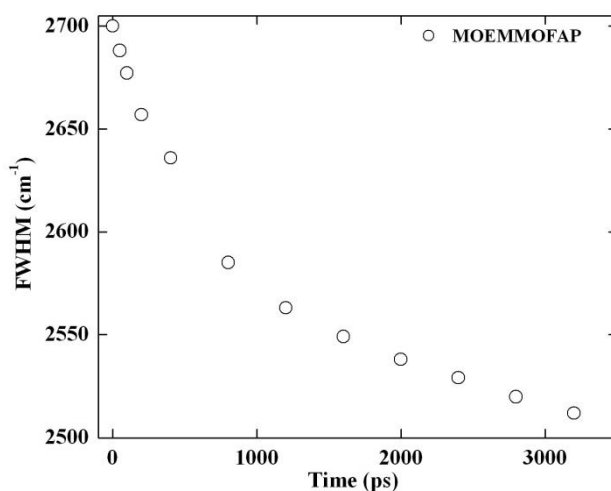
Figure 6.7. Plot of full width half maxima (FWHM), obtained from several time-resolved emission spectra of C153 in MOEMMOFAP at 293K. $\lambda_{exc.} = 405$ nm.
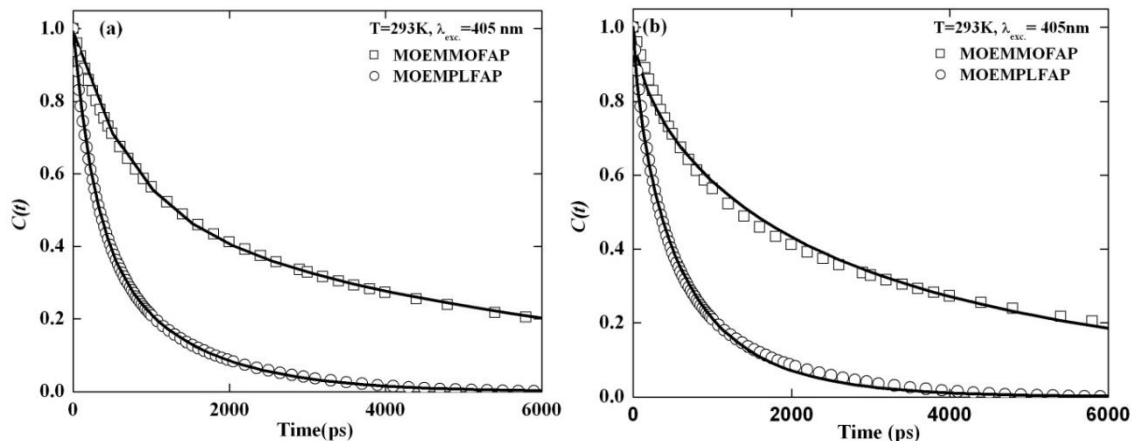
Figure 6.8. (a) Bi-exponential fits and (b) stretched exponential fits to the spectral correlation function, $C(t)$ versus time plot of C153 in MOEMPLFAP and MOEMMOFAP at 293 K. Symbols denote the data points and solid lines represent the corresponding fit to the data points. $\lambda_{exc.} = 405$ nm

Table 6.5. Solvent relaxation parameters of C153 in MOEMPLFAP and MOEMMOFAP at different excitation wavelengths

RTILs	Vis.(cP)	$\lambda_{exc.}$(nm)	a_1	τ_1(ns)	a_2	τ_2(ns)	$\langle \tau_s \rangle^c$(ns)	β	τ_0	$\langle \tau_{st} \rangle$(ns)	Obs. shift(cm^{-1})
					bi-exponential fit[a]				stretched exp. fit[b]		
MOEMPLFAP	128	375	0.44	1.19	0.56	0.15	0.61	0.59	0.39	0.60	808
		405	0.46	1.18	0.54	0.27	0.69	0.76	0.56	0.66	924
		445	0.44	1.21	0.56	0.20	0.64	0.68	0.46	0.60	911
MOEMMOFAP	1004	375	0.47	5.85	0.53	0.67	3.10	0.63	2.18	3.08	483
		405	0.51	6.46	0.49	0.73	3.65	0.64	2.64	3.67	479

[a] bi-exponential fit according to equation 2.13 and [b] stretched exponential fit according to equation 2.15. experimental error $\pm$ 5%

Table 6.6. Solvent relaxation parameters of C153 in MOEMMOFAP as a function of temperature at $\lambda_{exc.} = 405$ nm

Temp.(K)	Vis.(cp)	a_1	τ_1(ns)	a_2	τ_2(ns)	$\tau_{av.}$(ns)	β	$\tau_{solv.}$(ns)	τ_{st}(ns)	Obs.shift (cm^{-1})
		bi-exponential fit[a]					stretched exp. fit[b]			
293	1004	0.51	6.46	0.49	0.73	3.65	0.64	2.64	3.67	479
298	657	0.54	3.75	0.44	0.51	2.25	0.68	1.77	2.30	498
303	438	0.51	3.04	0.49	0.49	1.79	0.70	1.39	1.76	508
308	301	0.57	2.38	0.43	0.35	1.51	0.69	1.19	1.63	613

[a] bi-exponential fit according to equation 2.13 and [b] stretched exponential fit according to equation 2.15. Experimental error $\pm$ 5%.

Table 6.7. Solvent relaxation parameters of C153 in MOEMPLFAP RTIL as a function of temperature at $\lambda_{exc.}$ = 405 nm

Temp.(K)	Vis.(cp)	bi-exponential fit[a]					stretched[b] exp. fit			Obs.shift[†](cm^{-1})
		a_1	$\tau_1(ns)$	a_2	$\tau_2(ns)$	$\tau_{av.}(ns)$	β	$\tau_{solv.}(ns)$	$\tau_{st(ns)}$	
293	128	0.46	1.18	0.54	0.27	0.69	0.76	0.56	0.66	808
298	98	0.50	0.89	0.50	0.24	0.56	0.79	0.48	0.55	913
303	75	0.48	0.71	0.52	0.22	0.45	0.83	0.40	0.44	882
308	57	0.63	0.47	0.37	0.10	0.33	0.78	0.29	0.33	933

[a] bi-exponential fit according to equation 2.13 and [b] stretched exponential fit according to equation 2.15. Experimental error $\pm$ 5%.
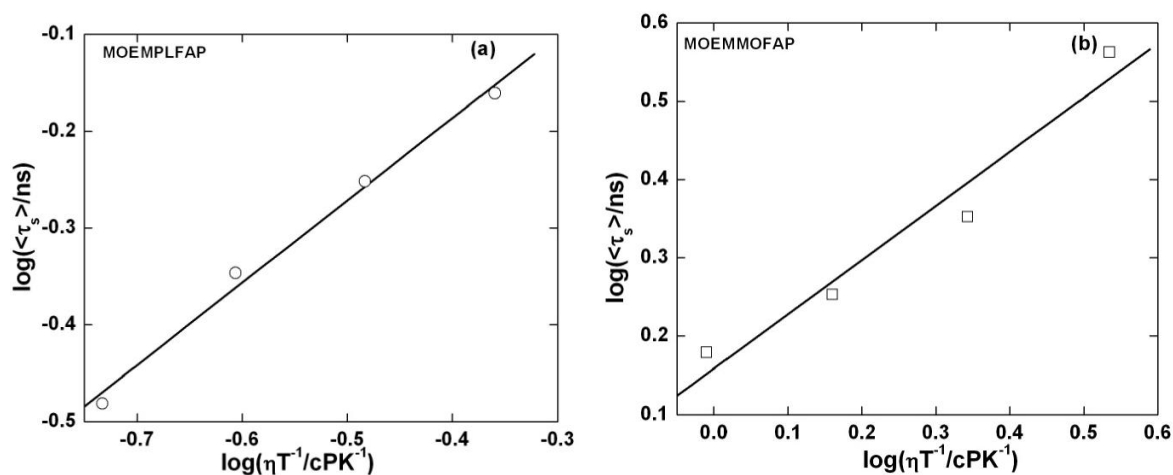
Figure 6.9. log-log plots of average solvent relaxation time ($<\tau_s>$) of C153 vs. η/T in (a) MOEMPLFAP and (b) MOEMMOFAP. Symbols denote experimental data points and solid lines are linear fit to the data.

It is pertinent to mention here that very recently Biswas and coworkers[267] have also observed fractional dependence of average solvation times on viscosity while studying Stokes shift dynamics in eutectic melts. However, they have observed a great degree of nonlinearity in SE relation. The present behavior has been attributed to the presence of pronounced heterogeneity in the medium.[267, 268] The mismatch between the predicted and measured solvation times have also been explained following this argument.[268] The above mentioned results led us to believe that the relatively poorer agreement between the measured average solvation time and expected solvation time in case of highly viscous ionic liquid is perhaps due to the presence of strong heterogeneity of the medium which leads to the substantial decoupling of average solvation time with medium viscosity. It may be mentioned here that

the fractional viscosity dependence of average solvation time that are observed in eutectic melts is similar to the observed viscosity decoupling of diffusion in deeply super-cooled liquids,[296-301] and therefore it was argued that possibly both static and dynamic heterogeneities in these melts may play an important role towards viscosity decoupling of diffusion.[268] The heterogeneity aspect of these RTILs is further investigated by following the excitation wavelength ($\lambda_{exc.}$) dependence of the steady state emission by employing 2-amino-7-nitrofluorene (ANF) which has excited state lifetime (τ) ~100ps[79] in conventional solvents. Fluorescence signature of ANF in the RTILs is expected to be more sensitive to those "transient" domains which could not be distinguished by the C153 due to its relatively longer excited state lifetime (τ = 3-5 ns)[225]. Excitation wavelengths dependent steady state emission behavior of C153 and ANF has been carried out in both ionic liquids. A representative plot which shows the excitation wavelength dependence of emission peak frequency and spectral width (FWHM of emission spectra) of both C153 and ANF is provided in Figure 6.10 in MOEMMOFAP. As can be seen from Figure 6.10(a), the emission peak frequency (ν_m) for ANF shifts by 630 cm^{-1} upon changing the $\lambda_{exc.}$ from bluest end to the most red end of the considered wavelengths, whereas fluorescence maximum of C153 remains almost insensitive to excitation wavelength. A similar result has been found in case of pyrrolidinium IL except for shifts of the emission peak frequency for ANF, which is found to be 430 cm^{-1}. The $\lambda_{exc.}$ dependence of fluorescence spectral width shows usual trend of narrowing down of FWHM with increased solvation for both the probes (Figure 6.10(b)). Figure 6.10(b) also depicts that the extent of narrowing down of fluorescence spectral width is approximately six times as large as that for C153. These data is useful in a sense that it provides an idea about the microscopic structures that induced heterogeneity in these ILs, even though it cannot describe exact domain size. Again, we note that, the observation of red shift of $\lambda_{emi.}$ maximum of the dipolar molecules when excited at the long-wavelength edge of the absorption band, is known

166

as "red-edge effect" (REE)[192, 193]. Samanta and coworkers previously observed that the excitation wavelength dependent shift of the fluorescence maximum of ANF increases with the increase in viscosity of the ILs.[79] The REE is not generally observed in conventional medium of low viscosity. The REE phenomenon in ILs have been explained by considering existence of a distribution of energetically different solvated probes in the ground state and a slower rate of their excited-state relaxation processes.[79] The results obtained in the present study even though cannot pinpoint any domain size or the length scale over which medium particles are correlated, do provide evidences in favour of the spatial heterogeneity that exists in these RTILs. In other words, the observation reflects that high viscosity of the ionic liquid is complementary to microheterogeneity of the medium.
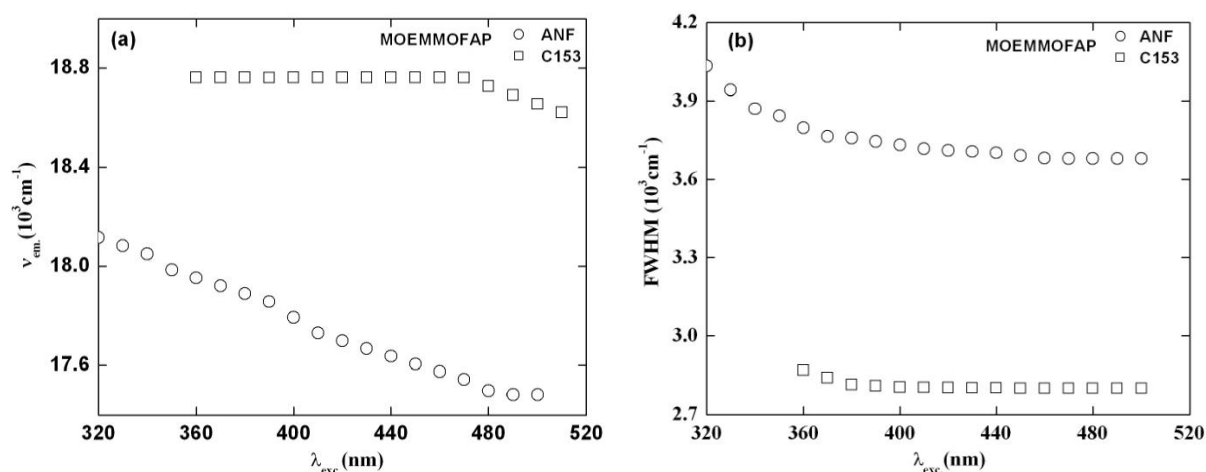
Figure 6.10. Excitation wavelength dependence ($\lambda_{exc.}$), (a) emission peak frequency ($\nu_{em.}$) for ANF and C153 and (b) full widths at half maximum (FWHM) of emission spectra of the two solutes in MOEMMOFAP.

6.3.4. *Rotational Dynamics of C153*

To get further insight into the viscosity-diffusion decoupling, we have performed fluorescence anisotropy studies. The anisotropy results at different $\lambda_{exc.}$ are collected in Table 6.8, and the anisotropy decay curves for C153 in neat RTILs at $\lambda_{exc.} = 405$ nm are shown in Figure 6.11. The initial anisotropies, r_o, are found to vary from 0.31 to 0.36 for C153 in MOEMPLFAP and MOEMMOFAP respectively. The anisotropy decay profiles were fitted by both bi-exponential and single exponential functions of time. It was found that bi-

exponential fits are marginally better than the single exponential fits and average rotational

correlation times, $<\tau_{rot}>$, obtained from the bi-exponential fits were found to be almost

similar to those obtained from the single exponential fits. The uncertainties on $<\tau_{rot}>$ values

are usually in the range of 2-5%, in MOEMPLFAP for all temperature except

MOEMMOFAP where the error is about 10% at low temperature because the recovered

reorientation time is higher than the fluorescence lifetime. The uncertainties on the measured

viscosities (η) are about 5%.
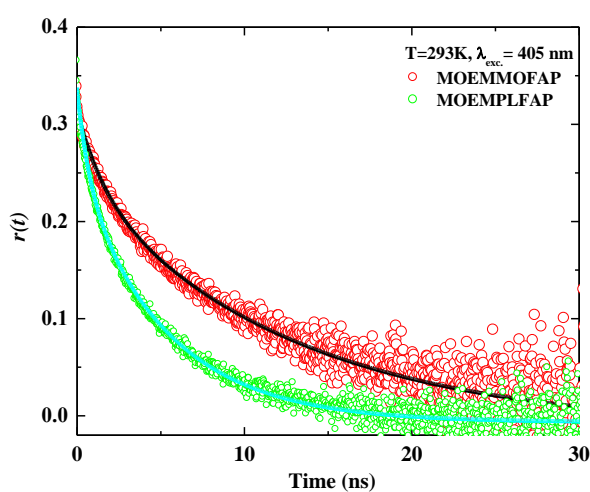
Figure 6.11. Time-resolved fluorescence anisotropy decay for C153 in MOEMMOFAP and MOEMPLFAP at 293K. Solid lines in the same figure represent the bi-exponential fit to the data points.

Table 6.8. Reorientation times of C153 in MOEMMOFAP and MOEMPLFAP at different excitation wavelengths and at 293 K

system	vis.(cP)	$\lambda_{exc.}$(nm)[a]	a_1	τ_1 (ns)	a_2	τ_2(ns)	$\langle\tau_{rot}\rangle$(ns)[b]
MOEMPLFAP	128	375	0.27	1.04	0.72	6.75	5.88
		405	0.20	0.94	0.80	8.26	6.80
		445	0.13	2.34	0.87	6.34	5.82
MOEMMOFAP	1004	375	0.20	1.62	0.80	13.69	11.28
		405	0.26	2.42	0.74	15.70	12.25
		445	0.17	0.48	0.83	15.68	13.10

[a] excitation wavelength, [b] average rotational time.

Interestingly, rotational relaxation data (Table 6.8) reveal that the average rotational

time increases only two times, whereas the viscosity increases almost 8 times upon changing

the medium from MOEMPLFAP to MOEMMOFAP. This observation clearly indicates that the rotational motion of C153 is not becoming as slow as is expected in relatively high viscous, MOEMMOFAP. Quite interestingly, rotational relaxation data (Table 6.8) also reveal that rotation at higher wavelength is slower for the highly viscous IL. In this regard, we would like to recall the earlier observation with regard to solvation relaxation, where solvation time at higher wavelength average is found to be slower for the highly viscous IL (Table 6.5). Hence present observation is interesting. However, at this stage, we are unable to find out the exact origin of this behavior based on the present data. Further work such as computer simulation studies are required to address this issue. No significant differences in average rotational time of C153 at different excitation wavelengths for these ionic liquids have been observed.

To have a better understanding of the rotational diffusion of C153, we have carried out rotational diffusion study of this particular probe in these two RTILs as a function of temperatures at 405 nm excitation wavelength. We have also analyzed the experimentally measured reorientation time with the help of most popularly known Stokes-Einstein-Debye (SED) hydrodynamic theory. The anisotropy results of C153 at different temperature in these medium are collected in Table 6.9. The slip and stick boundary condition, which have been calculated with the help of SED hydrodynamic theory are shown in the Figure 6.12 with experimentally measured reorientation times of C153 in MOEMPLFAP and MOEMMOFAP respectively. Estimated rotational coupling constant (C_{rot}) values are found to be similar to the conventional solvents for both ILs.[272] From the Figure 6.12, it is noticeable that the rotational diffusions of C153 in MOEMPL FAP are in between stick and slip boundaries. However, at lower temperature, in highly viscous MOEMMOFAP the rotational diffusion of C153 significantly departs from SED prediction (Figure 6.12). The departure from the SED

theory predictions is quantified as, $\tau_r \propto (\eta/T)^p$, with a p value 1.10 and 0.48 for MOEMPLFAP and MOEMMOFAP respectively (Equationss 6.6 and 6.7).

C153 in MOEMMOFAP, $\log (<\tau_r>) = 0.90 + 0.48 \log (\eta/T)$ (N = 9, R=0.97224)   (6.6)

C153 in MOEMPLFAP, $\log (<\tau_r>) = 1.21 + 1.10 \log(\eta/T)$ (N = 5, R=0.99799)   (6.7)

In these expressions, N and R are the number of data points and regression coefficients respectively.
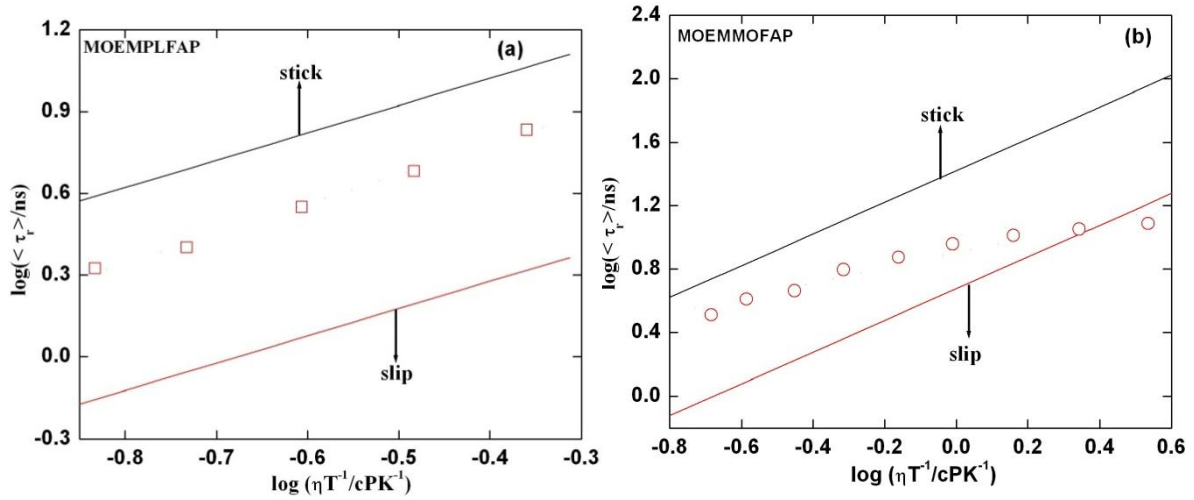
Figure 6.12. log-log plots of rotational relaxation time of C153 vs. η/T in the present RTILs with slip and stick boundary condition parameters.

Table 6.9. Reorientation times of C153 in MOEMMOFAP and MOEMPLFAP as a function of temperature at $\lambda_{exc.} = 405$ nm.

RTILs	temp.(K)	vis.(cP)	a_1	τ_1 (ns)	a_2	τ_2(ns)	$<\tau_{rot}>$(ns)[a]
MOEMPLFAP	293	128	0.20	0.94	0.80	8.26	6.80
	298	98	0.19	1.50	0.81	5.57	4.80
	303	75	0.23	1.08	0.77	4.27	3.54
	308	57	0.26	0.55	0.74	3.21	2.52
	313	46	0.24	0.54	0.76	2.61	2.11
MOEMMOFAP	293	1004	0.26	2.42	0.74	15.70	12.25
	298	657	0.25	2.28	0.75	14.30	11.29
	303	438	0.25	2.21	0.75	12.99	10.27
	308	301	0.21	1.27	0.79	11.16	9.08
	313	216	0.24	1.67	0.76	9.33	7.49
	318	154	0.18	0.81	0.82	7.45	6.25
	323	114	0.21	0.62	0.79	5.66	4.60
	328	85	0.23	0.93	0.77	5.02	4.08
	333	69	0.21	0.83	0.79	3.90	3.25

[a] average rotational time

The observed higher degree of nonlinear behavior for the highly viscous ionic liquid, MOEMMOFAP, is attributed to the pronounced heterogeneity of the medium.[268] These seem to be interesting in a sense that earlier rotational dynamics studies showed better linear correlation with viscosity of the medium.[123] Figure 6.13 showed the deviation of present observation than the earlier reports. In this context, it should be mentioned that similar non linear response of average rotation relaxation time with viscosity have also been observed very recently by Samanta and his coworkers with morpholinium-based ILs and explained the observation on the basis of heterogeneity of the medium.[117] Larger viscosity in an inhomogeneous medium is known to introduce larger decoupling.[298] This arises due to the non Brownian movement such as large angle jumps[302] and the retention of inertia driven motion even much after the onset of the typical diffusion time scale.[303, 304] This alternative dynamic mode significantly reduces the frictional resistance against the diffusing particle arising from the macroscopic viscosity and thus strongly promotes departure from the conventional hydrodynamic description. It is pertinent to mention here that the results obtained from reactive and non-reactive dynamics studies in ionic liquids,[305, 306] and recent measurements in molecular liquids,[307] where ~ 2 nm structural inhomogeneity in an otherwise homogeneous liquid in isothermal condition have been introduced, demonstrates that both the static and dynamic heterogeneities may contribute to probe rotation and medium viscosity. Moreover, the recent work by Biswas and coworkers also explain viscosity-diffusion phenomena in eutectic melts by invoking both static and dynamic heterogeneity.[268] In this context, we would like to mention that solute and solvation relaxation experiments on eutectic melts[268] and super-cooled liquids[298-300] showed a higher p value for rotation than solvation. However, in the present case the observation of the larger value of fraction (p) for solvation than for rotation is interesting. We are not sure about the possible origin of this behaviour at this stage. In this regard, it may be mentioned that the presence of fluorine atoms

sometime causes anomalous photophysical behavior.[308, 309] Since the present ionic liquids also contain fluorine atom in their anionic constituents, the present observation may be linked to those studies. However, further studies are required to rationalize the observed behaviour.

Keeping in mind the latest literature findings and the observation of the higher shift in the excitation wavelength dependent fluorescence both in steady state and time-resolved measurements indicates that static and dynamic heterogeneity of the medium may contribute to the fractional dependence of average rotational time on viscosity in highly viscous ionic liquid.
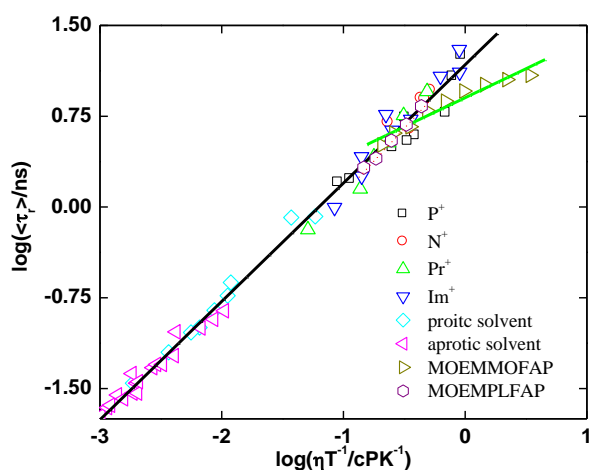
Figure 6.13. log-log plots of rotational relaxation time of C153 vs. η/T in different RTILs. P^+, N^+ Pr^+, Im^+ denoted the phosphonium, ammonium, pyrrolidinium, and imidazolium cation containing RTILs which experimental data are taken from ref. 123. Experimental data for protic and aprotic solvent are taken from ref. 272.

6.4. Conclusion

Time-resolved fluorescence Stokes shift and anisotropy measurements of coumarin 153 are investigated in two hydrophobic ILs, MOEMMOFAP and MOEMPLFAP. Viscosity of the MOEMMOFAP is measured to be eight times higher than that of MOEMPLFAP. In case of highly viscous ionic liquid, the solvation and rotational relaxation times, is not found to be as slow as are expected from the bulk viscosity value. The breakdown of both Stokes Einstein (SE) and Stokes-Einstein-Debye (SED) relationship has been observed. The observation indicates viscosity-diffusion decoupling during solvation and rotational relaxation of C153 in

172

highly viscous IL. The decoupling is also analyzed through fractional viscosity dependence of the measured average solvation $\langle\tau_s\rangle$ and rotation $\langle\tau_r\rangle$ times : $\langle\tau_x\rangle \propto (\eta/T)^p$ (x being solvation or rotation, p is the exponent and T is the temperature). The excitation wavelength dependent fluorescence studies have been carried out to correlate the experimental findings with the medium heterogeneity. The observation seems to suggest that both static and dynamic heterogeneity may play an important role for the observed viscosity-diffusion (d-η) decoupling in highly viscous ionic liquid. However, more studies comprising both theoretical and experimental investigations are required to throw more light on this aspect.

Summary and Future Prospects

Solvation and rotational relaxation dynamics of some well known organic dipolar probes have been investigated in a variety of RTILs in a systematic manner such that a comprehensive and quantitative understanding of the relationship among structure, intermolecular interaction and dynamics in ionic liquids is obtained. Many interesting features with regard to understanding the fundamentals of solvation and rotational dynamics have come out from the present studies which are summarized as follows. (i) Hydrogen bonding interaction even though weak in nature has been found to be responsible for probe dependent solvation dynamics. (ii) Alkyl chain length has no significant effect on average solvation times; average solvation time can be correlated with the medium viscosity. (iii) Orientational motion of organic solute becomes faster with the increase of length of alkyl chains in anion because larger solvent molecules offer lower friction to the rotating solute. (iv) Hindered rotational motion of organic solute (capable of H-bond formation) can be well correlated with the hydrogen bond basicity of anion. (v) Cosolvents, even in trace amount, can affect dynamics of solvation and solute rotation in RTILs in a significant manner. (vi) The highly organized and heterogeneous nature of RTILs is manifested through diffusion-viscosity decoupling (d-η).

The present work provides qualitative and quantitative informations regarding the solvation and rotational dynamics in mono cationic ionic liquids. However, studies on solvation dynamics in dicationic ionic liquids are elusive. Investigation on solvation dynamics in these media can provide information towards understanding the dynamical behavior of dicationic ILs. It would also be interesting to investigate the effect of length of linker alkyl chains between two cationic moieties of dicationc ILs. Studies on the dynamics of solvation in RTILs with different anions having different hydrogen bond basicity would

also be interesting to find a correlation between solvent organization time scale and hydrogen bond basicity of anions.

Although a number of reports are available on intermolecular PET reaction[173-178], limited number of studies on intermolecular PET reactions in RTILs have been performed.[168, 169] We would like to explore the studies on intramolecular PET reactions with different new donor-acceptor systems in a systematic manner. The role of solvation on intramolecular PET process will be explored.

REFERENCES

(1) Wasserscheid, P.; Keim, W. *Angew. Chem. Int. Ed.* **2000**, *39*, 3772.

(2) Seddon, K. R.; Stark, A.; Torres, M. J. *Pure Appl. Chem.* **2000**, *72*, 2275.

(3) Rogers, R. D.; Seddon, K. R. *Science* **2003**, *302*, 792.

(4) Welton, T. *Chem. Rev.* **1999**, *99*, 2071.

(5) Sheldon, R. *Chem. Commun.* **2001**, 2399.

(6) Hayashi, S.; Ozawa, R. Hamaguchi, H. *Chem. Lett.* **2004**, *33*, 1590.

(7) Dupont, J.; de Suza, R. F.; Suarez, P. A. Z. *Chem. Rev.* **2002**, *102*, 3667.

(8) Wasserscheid, P.; Keim, W. *Angew. Chem. Int. Ed.* **2000**, *39*, 3772.

(9) Hough,W. L.; Rogers, R. D. *Bull. Chem. Soc. Jpn.* **2007**, *80*, 2262.

(10) Plechkova, N. V.; Seddon, K. R. *Chem. Soc. Rev.* **2008**, *37*, 123.

(11) Rogers, R. D.; Voth, G. A. *Acc.Chem. Res.* **2007**, *40*, 1077.

(12) Chiappe, C.; Pieraccini, D. *J. Phys. Org. Chem.* **2005**, *18*, 275.

(13) Weingartner, H. *Angew. Chem. Int. Ed.* **2008**, *47*, 654.

(14) Chiappe, C.; Konig, B.; Impareto, G. *Eur. J. Org. Chem.* **2007**, 1049.

(15) Rantwijk, F. V.; Sheldon, R. *Chem. Rev.* **2007**, *107*, 2757.

(16) Seddon, K. R. *Ionic Liquids, Industrial Applications for Green Chemistry, American Chemical Society, Washington DC*, 2002.

(17) Dubreuil, J. F.; Bourahla, K.; Rahmouni, M.; Bazureau, J. P.; Hamelin, J. *Catal. Commun.* **2002**, *3*, 185.

(18) Hallett, J. P.; Welton, T. *Chem. Rev.* **2011**, *111*, 3508.

(19) Walden, P. *Bull. Acad. Imper. Sci.St. Petersberg* **1914**, 1800.

(20) Wilkes, J. S.; Levinsky, J. A.; Wilson, R. A.; Hussey, C. L. *Inorg. Chem.* **1982**, *21*, 1263.

(21) Boon, J. A.; Levinsky, J. A.; Pflug, J. L.; Wilkes, J. S. *J. Org. Chem.* **1986**, *51*, 480.

(22) Wasserscheid, P.; Welton, T. *Ionic Liquids in Synthesis, Wiley-VCH, Weinheim* 2003.

(23) Golding, J. J.; MacFarlane, D. R.; Spiccia, L.; Forsyth, G. B.; Skelton, B. W.; White, A. H. *Chem. Commun.* **1998**, *18*, 1593.

(24) Polyakov, O. G.; Ivanova, S. M.; Gaudinski, C. M.; Miller, S. M.; Anderson, O. P.; Strauss, S. H. *Organometallics* **1999**, *18*, 3769.

(25) Larsen, A. S.; Holbrey, J. D.; Tham, F. S.; Reed, C. A. *J. Am. Chem. Soc.* **2000**, *122*, 7264.

(26) Xu, W.; Wang, L.-M.; Nieman, R. A.; Angell, C. A. *J. Phys. Chem. B* **2003**, *107*,11749.

(27) Davis, J. H. *Chem. Lett.* **2004**, *33*, 1072.

(28) Lee, S. *Chem. Commun.* **2006**, 1049.

(29) Surette, J. K. D.; Green, L.; Singer, R. D. *Chem. Commun.* **1996**, 2753

(30) Santhosh, K.; Samanta, A. *J. Phys. Chem. C* **2012**, *116*, 20643.

(31) Sankaranarayanan, K.; Sathyaraj, G.; Nair, B. U.; Dhathathreyan, A. *J. Phys. Chem. B* **2012**, *116*, 4175.

(32) Ohno, H.; Fukumoto, K. *Acc. Chem. Res.* **2007**, *40*, 1122.

(33) Enomoto, T.; Nakamori, Y.; Matsumoto, K.; Hagiwara, R. *J. Phys. Chem. C* **2011**, *115*, 4324.

(34) Ngo, H. L.; LeCompte, K.; Hargens, L.; McEwen, A. *Thermochim. Acta* **2000**, *357*, 97.

(35) Lewandowski, A.; Swiderska-Mocek, A. *J. Power Sources* **2009**, *194*, 601.

(36) Dzyuba, S.; Bartsch, R. A. *ChemPhysChem* **2002**, *3*, 161.

(37) Carda-Broch, S.; Berthold, A.; Armstrong, D. W. *Anal. Bioanal. Chem.* **2003**, *375*, 191.

(38) Zhang, S.; Sun, N.; He, X.; Lu, X.; Zhang, X. *J. Phys. Chem. Ref. Data.* **2006**, *35*, 1475.

(39) Xu, W.; Cooper, E. I.; Angell, C. A. *J. Phys. Chem. B* **2003**, *107*, 6170.

(40) Hirao, M.; Sugimoto, H.; Ohno, H. *J. Electrochem. Soc.* **2000**, *147*, 4168.

(41) Bonhote, P.; Dias, A.; Papageorgiou, N.; Kalyanasundaram, K.; Gratzel, M. *Inorg. Chem.* **1996**, *35*, 1168.

(42) Karmakar, R.; Samanta, A. *J. Phys. Chem. A* **2002**, *106*, 6670.

(43) Nishida, T.; Tashiro, Y.; Yamamoto, M. *J. Fluorine Chem.* **2003**, *120*, 135.

(44) MacFarlane, D. R.; Meakin, P.; Sun, J.; Amini, N.; Forsyth, M. *J. Phys. Chem. B* **1999**, *103*, 4164.

(45) Fuller, J.; Carlin, R. T.; Long, H. C. D.; Haworth, D. *Chem. Commun.* **1994**, 299.

(46) Law, G.; Watson, P. R. *Langmuir* **2001**, *17*, 6138.

(47) Buzzeo, M. C.; Evans, R. G.; Compton, R. G. *ChemPhysChem* **2004**, *5*, 1106.

(48) Reichardt, C. *Green Chem.* **2005**, *7*, 339.

(49) Aki, S. N. V. K.; Brennecke, J. F.; Samanta, A. *Chem. Commun.* **2001**, 413.

(50) Earle, M. J.; Esperanca, J. M. S. S.; Gilea, M. A.; Lopes, J. N. C.; Rebelo, L. P. N.; Magee, J. W.; Seddon, K. R.; Widegren, J. A. *Nature* **2006**, *439*, 831.

(51) Taylor, A. W.; Lovelock, K. R. J.; Deyko, A.; Licence, P.; Jones, R. G. *Phys. Chem.Chem. Phys.* **2010**, *12*, 1772.

(52) Chambreau, S. D.; Vaghjiani, G. L.; Koh, C. J.; Golan, A.; Leone, S. R. *J. Phys. Chem. Lett.* **2012**, *3*, 2910.

(53) Zhou, Z. B.; Matsumoto, H.; Tatsumi, K. *Chem. Eur. J.* **2005**, *11*,752.

(54) Zhou, Z. B.; Matsumoto, H.; Tatsumi, K. *Chem. Lett.* **2004**, *33*, 1636.

(55) Du, Z. Y.; Li, Z. P.; Guo, S.; Zhang, J.; Zhu, L. Y.; Deng, Y. Q. *J. Phys. Chem. B* **2005**, *109*, 19542.

(56) Bagno, A.; Butts, C.; Chiappe, C.; D'amico, F.; Lord, J. C. D.; Pieraccini, D.; Rastrelli, F. *Org. Biomol. Chem.* **2005**, *3*, 1624.

(57) Widegren, J. A.; Laesecke, A.; Magee, J. W. *Chem. Commun.* **2005**, 1610.

(58) Santhosh, K.; Banerjee, S.; Rangaraj, N.; Samanta, A. *J. Phys. Chem. B* **2010**, *114*, 1967.

(59) Greaves, T. L.; Weerawardena, A.; Fong, C.; Krodkiewska, I.;Drummond, C. J. *J. Phys. Chem. B* **2006**, *110*, 22479.

(60) Hirao, M.; Sugimoto, H.; Ohno, H. *J. Electrochem. Soc.* **2000**, *147*, 4168.

(61) Tokuda, H.; Tsuzuki, S.; Susan, M. A. B. H.; Hayamizu, K.; Watanabe, M. *J. Phys. Chem. B* **2006**, *110*, 19593.

(62) Reichardt, C. *Solvents and Solvent Effects in Organic Chemistry;* VCH: Weinheim, Germany, 1988.

(63) Wakai, C.; Oleinikova, A.; Ott, M.; Weingartner, H. *J. Phys. Chem. B* **2005**, *109*, 17028.

(64) Daguenet, C.; Dyson, P. J.; Krossing, I.; Oleinikova, A.; Slattery, J.; Wakai, C.; Weingartner, H. *J. Phys. Chem. B* **2006**, *110*, 12682.

(65) Paul, A.; Samanta, A. *J. Phys. Chem. B* **2007**, *111*, 1957.

(66) Crowhurst, L.; Mawdsley, P. R.; Perez-Arlandis, J. M.; Salter, P. A.; Welton, T. *Phys. Chem. Chem. Phys.* **2003**, *5*, 2790.

(67) Anderson, J. L.; Ding, J.; Welton, T.; Armstrong, D. W. *J. Am. Chem. Soc.* **2002**, *124*, 14247.

(68) http://www.ccdc.cam.ac.ok/ (accessed Jan 2006).

(69) Dupont, J. *J. Braz. Chem. Soc.* **2004**, *15*, 341.

(70) Hardacre, C.; Holbrey, J. D.; McMath, S. E. J.; Bowron, D. T.; Soper, A. K. *J. Chem. Phys.* **2003**, *118*, 273.

(71) Dieter, K. M.; Dymek, C. J., Jr.; Heimer, N. E.; Rovang, J. W.; Wilkes, J. S. *J. Am. Chem. Soc.* **1988**, *110*, 2722.

(72) Ozawa, R.; Hayashi, S.; Saha, S.; Kobayashi, A.; o Hamaguchi, H. *Chem. Lett.* **2003**, *32*, 948.

(73) Fannin, A. A., Jr.; King, L. A.; Levisky, J. A.; Wilkes, J. S. *J. Phys. Chem.* **1984**, *88*, 2609.

(74) Abdul-Sada, A. K.; Elaiwi, A. E.; Greenaway, A. M.; Seddon, K. R. *Eur. J. Mass Spectrom.* **1997**, *3*, 245.

(75) Gozzo, F. C.; Santos, L. S.; Augusti, R.; Consorti, C. S.; Dupont, J.; Eberlin, M. N. *Chem. Eur. J.* **2004**, *10*, 6187.

(76) Wang, Y.; Voth, G. A. *J. Am. Chem. Soc.* **2005**, *127*, 12192.

(77) Lopes, J.N.A.C.; Padua, A.A.H. *J. Phys. Chem. B* **2006**, *110*, 3330.

(78) Xiao, D.; Rajian, J. R.; Cady, A.; Li, S.; Bartsch, R.A.; Quitevis, E.L. *J. Phys. Chem. B* **2007**, *111*, 4669.

(79) Mandal, P. K.; Sarkar, M.; Samanta, A. *J. Phys. Chem. A* **2004**, *108*, 9048.

(80) Hu, Z.; Margulis, C. J. *Proc. Natl. Acad. Sci. U.S.A.* **2006**, *103*, 831.

(81) Jin, H.; Li, X.; Maroncelli, M. *J. Phys. Chem. B* **2007**, *111*, 13473.

(82) Adhikari, A.; Sahu, K.; Dey, S.; Ghosh, S.; Mandal, U.; Bhattacharyya, K. *J. Phys. Chem. B* **2007**, *111*, 12809.

(83) Tanaka, K.; Toda, F. *Chem. Rev.* **2000**, *100*, 1025.

(84) Kajimoto, O. *Chem. Rev.* **1999**, *99*, 35H.

(85) Seddon, K. R. *Nature (Materials)* **2003**, *2*, 363.

(86) Muzart, J. *Adv. Synth. Catal.* **2006**, *348*, 275.

(87) Shetty, P. H.; Poole, S. K.; Poole, C. F. *Anal. Chim. Acta* **1990**, *236*, 51.

(88) Garlitz, J. A.; Summers, C. A.; Flowers, R. A.; Borgstahl, G. E. O. *Acta Crystallogr., Sect D* **1999**, *55*, 2037.

(89) Lau, R. M.; Sorgedrager, M. J.; Carrea, G.; Van Rantwijk, F.; Secundo, F.; Sheldon, R. A. *Green Chem.* **2004**, *6*, 483.

(90) Lewandowski, A.; Swiderska-Mocek, A. *J. Power Sources* **2009**, *194*, 601.

(91) Armand, M.; Endres, F.; MacFarlane, D. R.; Ohno, H.; Scrosati, B. *Nat. Mater.* **2009**, *8*, 621.

(92) Ding, J.; Zhou, D.; Spinks, G.; Wallace, G.; Forsyth, S.; Forsyth, M.; MacFarlane, D. *Chem. Mater.* **2003**, *15*, 2392.

(93) Qu, J.; Truhan, J. J.; Dai, S.; Luo, H.; Blau, P. J. *Tribol. Lett.* **2006**, *22*, 207.

(94) Janus, E.; Goc-Maciejewska, I.; Lozynski, M.; Pernak, J. *Tetrahedron Lett.* **2006**, *47*, 4079.

(95) Shim, Y.; Duan, J. S.; Choi, M. Y.; Kim, H. J. *J. Chem. Phys.* **2003**, *119*, 6411.

(96) Kobrak, M. N.; Znamenskiy, V. *Chem. Phys. Lett.* **2004**, *395*, 127.

(97) Znamenskiy, V.; Kobrak, M. N. *J. Phys. Chem. B* **2004**, *108*, 1072.

(98) Shim, Y.; Choi, M. Y.; Kim, H. J. *J. Chem. Phys.* **2005**, *122*, 044511.

(99) Bargava, B. L.; Balasubramanian, S. *J. Chem. Phys*. **2005**, *123*, 144505.

(100) Bargava, B. L.; Balasubramanian, S. *J. Chem. Phys.* **2006**, *417*, 486.

(101) Mandal, P. K.; Paul A.; Samanta, A. *J. Photochem. Photobiol*. **2006**, *182*, 113.

(102) Paul, A.; Samanta, A. *J. Phys. Chem. B* **2008**, *112*, 16626

(103) Patra, S.; Samanta, A. *J. Phys. Chem. B* **2012**, *116*, 12275.

(104) E. Binetti, A. Panniello, L. Triggiani, R. Tommasi, A. Agostiano, M. L. Curri, M. Striccoli, *J. Phys. Chem. B*, **2012**, *116*, 3512.

(105) E. Binetti, A. Panniello, R. Tommasi, A. Agostiano, S. Fantini, M. Lucia Curri, M. Striccoli, *J. Phys. Chem. C*, **2013**, *117*, 12923.

(106) Ghosh, A.; Chatterjee, T.; Mandal, P. K. *Chem. Commun.* **2012**, *48*, 6250.

(107) Cha, S.; Shim, T.; Ouchi,Y.; Kim, D. *J. Phys. Chem. B* **2013**, *117*, 10818.

(108) Guo, J. Baker, G. A.; Hillesheim P. C.; Dai, S.; Shaw R. W.; Mahurin, S. M. *Phys. Chem. Chem. Phys.* **2011**, *13*, 12395.

(109) Karmakar, R.; Samanta, A. *J. Phys. Chem. A* **2002**, *106*, 4447.

(110) Karmakar, R.; Samanta, A. *J. Phys. Chem. A* **2003**, *107*, 7340.

(111) Mandal, P. K.; Samanta, A. *J. Phys. Chem. B* **2005**, *109*, 15172.

(112) Mandal, P. K.; Saha, S.; Karmakar, R.; Samanta, A. *Curr. Sci.* **2006**, *90*, 301.

(113) Samanta, A. *J. Phys. Chem. B* **2006**, *110*, 13704.

(114) Paul, A.; Samanta, A. *J. Phys. Chem. B* **2007**, *111*, 4724.

(115) Paul, A.; Samanta, A. *J. Phys. Chem. B* **2008**, *112*, 947.

(116) Samanta, A. *J. Phys. Chem. Lett.* **2010**, *1*, 1557.

(117) Khara, D. C.; Samanta, A. *J. Phys. Chem. B* **2012**, *116*, 13430.

(118) Ingram, J. A.; Moog, R. S.; Ito, N.; Biswas, R.; Maroncelli, M. *J. Phys. Chem. B* **2003**, *107*, 5926.

(119) Ito, N.; Arzhantsev, S.; Maroncelli, M. *Chem. Phys. Lett.* **2004**, *396*, 83.

(120) Ito, N.; Arzhantsev, S.; Heitz, M.; Maroncelli, M. *J. Phys. Chem. B* **2004**, *108,* 5771.

(121) Arzhantsev, S.; Jin, H.; Baker, G. A.; Maroncelli, M. *J. Phys. Chem. B* **2007**, *111*, 4978.

(122) Jin, H.; Li, X.; Maroncelli, M. *J. Phys. Chem. B* **2007**, *111*, 13473.

(123) Jin, H.; Baker, G. A.; Arzhantsev, S.; Dong, J.; Maroncelli, M. *J. Phys. Chem. B* **2007**, *111*, 7291.

(124) Roy, D.; Patel, N.; Conte, S.; Maroncelli, M. *J. Phys. Chem. B* **2010**, *114*, 8410.

(125) Roy, D.; Maroncelli, M. *J. Phys. Chem. B* **2010**, *114*, 12629.

(126) Maroncelli, M.; Zhang, X. X.; Liang, M.; Roy, D.; Ernsting, N. P. *Disc. Faraday Soc.* **2012**, *154*, 409.

(127) Zhang, X. X.; Liang, Min.; Ernsting, N. P.; Maroncelli, M. *J. Phys. Chem. B* **2013**, 117, 4291.

(128) Zhang, X. X.; Liang, M.; Ernsting, N. P.; Maroncelli, M. *J. Phys. Chem. Lett.* **2013**, *4,* 1205.

(129) Chakrabarty, D.; Chakraborty, A.; Seth, D.; Hazra, P.; Sarkar, N. *Chem. Phys. Lett.* **2004**, *397*, 469.

(130) Chakrabarty, D.; Chakraborty, A.; Seth, D.; Sarkar, N. *J. Phys. Chem. A* **2005**, *109*, 1764.

(131) Chakraborty, A.; Seth, D.; Chakrabarty, D.; Setua, P.; Sarkar, N. *J. Phys. Chem. A* **2005**, *109*, 11110.

(132) Chakrabarty, D.; Hazra, P.; Chakraborty, A.; Seth, D.; Sarkar, N. *Chem. Phys. Lett.* **2003**, *381*, 697.

(133) Seth, D.; Sarkar, S.; Sarkar, N. *J. Phys. Chem. B* **2008**, *112*, 2629.

(134) Pramanik, R.; Rao, V. G.; Sarkar, S.; Ghatak, C. ; Setua, P.; Sarkar, N. *J. Phys. Chem. B* **2009**, *113*, 8626.

(135) Sarkar, S.; Pramanik, R.; Ghatak, C.; Setua, P.; Sarkar, N. *J. Phys. Chem. B* **2010**, *114*, 2779.

(136) Chowdhury, P. K.; Halder, M.; Sanders, L.; Calhoun, T.; Anderson, J. L.; Armstrong, W. D.; Song, X.; Petrich, J. W. *J. Phys. Chem. B* **2004**, *108*, 10245.

(137) Carlson, P. J.; Bose, S.; Armstrong, D. W.; Hawkins, T.; Gordon, M. S.; Petrich, J. W. *J. Phys. Chem. B* **2012**, *116*, 503.

(138) Kashyap, H. K.; Biswas, R. *J. Phys. Chem. B* **2008**, *112*, 12431.

(139) Kashyap, H. K.; Biswas, R. *J. Phys. Chem. B* **2010**, *114*, 254.

(140) Kashyap, H. K.; Biswas, R. *J. Phys. Chem. B* **2010**, *114*, 16811.

(141) Kashyap, H. K.; Biswas, R. *Indian J. Chem.* **2010**, *49A*, 685.

(142) Daschakraborty, S.; Biswas, R. *J. Phys. Chem. B* **2011**, *115*, 4011.

(143) Daschakraborty, S.; Biswas, R. *Chem.Phys. Lett.* **2011**, *510*, 202.

(144) Das, S. K.; Sarkar, M. *Chem. Phys. Lett.* **2011**, *515*, 23.

(145) Das, S. K.; Sarkar, M. *J. Mol. Liq.* **2012**, *165*, 38.

(146) Das, S. K.; Sarkar, M. *J. Lumin.* **2012**, *132*, 368.

(147) Das, S. K.; Sarkar, M. *ChemPhysChem* **2012**, *13*, 2761.

(148) Das, S. K.; Sahu, P. K.; Sarkar, M. *J. Phys. Chem. B* **2013**, *117*, 636.

(149) Das, S. K.; Sahu, P. K.; Sarkar, M. *J. Fluoresc.* **2013**, *23*,1217.

(150) Khara, D. C.; Samanta, A. *Phys. Chem. Chem. Phys.* **2010**, *12*, 7671.

(151) Fruchey, K.; Fayer, M. D. *J. Phys. Chem. B* **2010**, *114*, 2840.

(152) Mali, K. S.; Dutt, G. B.; Mukherjee, *J. Chem. Phys*. **2008**, 128, 054504.

(153) Dutt, G. B. *J. Phys. Chem. B* **2010**, *114*, 8971.

(154) Dutt, G. B. *Indian J. Chem.* **2010**, *49A*, 705.

(155) Karve, L.; Dutt, G. B. *J. Phys. Chem. B* **2011**, *115*, 725.

(156) Karve, L.; Dutt, G. B. *J. Phys. Chem.B* **2012**, *116*, 1824.

(157) Karve, L.; Dutt, G. B. *J. Phys. Chem. B* **2012**, *116*, 9107.

(158) Das, S. K.; Sarkar, M. *J. Phys. Chem*. *B* **2012**, *116*, 194.

(159) Gangamallaiah V.; Dutt, G. B. *J. Phys. Chem. B* **2012**, *116*, 12819.

(160) Gangamallaiah, V.; Dutt, G. B. *J. Phys. Chem. B* **2013**, *117*, 5050.

(161) Gangamallaiah V.; Dutt G. B. *J. Phys. Chem. B* **2013**, 117, 9973.

(162) Khara D. C., Kumar J. P., Mondal N., Samanta A. *J. Phys. Chem. B* **2013**, *117*, 5156.

(163) B. Li, M. Qiu, S. Long, X. Wang, Q. Guo, A. Xia, *Phys. Chem. Chem. Phys*. **2013**, *15*, 16074.

(164) Lockard, J. V.; Wasielewski, M. R. *J. Phys. Chem. B* **2007,** *111,* 11638.

(165) Santosh, K.; Samanta, A. *J. Phys. Chem. B* **2010,** *141,* 11638.

(166) Li, X.; Maroncelli, M. *J. Phys. Chem. A* **2011,** *115,* 11638.

(167) Santosh, K.; Samanta, A. *ChemPhyschem* **2012,** *13,* 1956.

(168) Wu, H.; Wang, H.; Xue, L.; Shi, Y.; Li. X. *J. Phys. Chem. B* **2010,** *114,* 14420.

(169) Lee, H. Y.; Issa, J. B.; Isied, S. S.; Castner, E. W. Jr.; Pan, Y.; Hussey, C. L.; Lee, K. So.; Wishart J. F. *J. Phys. Chem. C* **2012**, *116*, 5197

(170) Bhattacharya, B.; Samanta, A. *J. Phys. Chem. B* **2008**, *112*, 10101.

(171) Kumar, V.; Pandey, S. *ChemPhysChem* **2013**, *14*, 491.

(172) Kumar, V.; Rai, R.; Pandey, S. *RSC Adv.* **2013**, *3*, 11621.

(173) Skrzypczak, A.; Neta, P. *J. Phys. Chem. A* **2003,** *107,* 7800.

(174) Paul, A.; Samanta, A. *J. Phys. Chem. B* **2007,** *111,* 1957.

(175) Sarkar, S.; Pramanik, R.; Ghatak, C.; Rao, V. G.; Sarkar, N. *Chem. Phys. Lett.* **2011,** *506*, 211.

(176) Das, K.; Mondal, T.; Sen Mojumdar, S.; Bhattacharyya, K. *J. Phys. Chem. B* **2011,** *115,* 4680.

(177) Liang, M.; Kaintz, A.; Baker, G. A.; Maroncelli, M. *J. Phys. Chem. B* **2012,** *116,* 1370.

(178) Koch, M.; Rosspeintner, A.; Angulo, G.; Vauthey, E. *J. Am. Chem. Soc.* **2012**, *134*, 3729.

(179) Castner, E. W. Jr.; Margulis, C. J.; Maroncelli, M.; Wishart, J. F. Ann. Rev. Phys. Chem. **2011**, *62,* 85.

(180) Bagchi, B.; Jana, B. Chem. Soc. Rev. **2010,** *39*, 1936.

(181) Burai, T. N.; Datta, A. *J. Phys. Chem. B* **2009**, *113*, 15901.

(182) De, D.; Datta, A. *Langmuir* **2013**, *29*, 7709.

(183) Kumbhakar, M.; Goel, T.; Mukherjee, T.; Pal. H. *J. Phys. Chem. B* **2005**, *109*, 18528.

(184) Kumbhakar, M.; Goel, T.; Nath, S.; Mukherjee, T.; Pal. H. *J. Phys. Chem. B* **2006**, *110*, 25646.

(185) Singh, P. K.; Kumbhakar, M.; Pal, H.; Nath, S. *J. Phys. Chem. B* **2008**, *112*, 7771.

(186) Bhattacharyya, K. *Acc. Chem. Res.* **2003**, *36*, 95.

(187) Lang, B.; Angulo, G.; Vauthey, E. *J. Phys. Chem. A* **2006**, *110*, 7028.

(188) Birks, J. B. *Photophysics of Aromatic Molecules*; Wiley-Inter-Science: London, 1970.

(189) Demchenko, A. P. *Luminescence* **2002**, *17*, 19.

(190) Demchenko, A. P. *In Topics in Fluorescence Spectroscopy*; Lakowicz, J. R., Ed.; Plenum Press: New York, 1991; Vol. 3.

(191) Lakowicz, J. R.; Nakamoto, S. K. *Biochemistry* **1984**, *23*, 3013.

(192) Valeur, B.; Weber, G. *Chem. Phys. Lett.* **1977**, *45*, 140.

(193) Weber, G.; Shinitzky, M. *Proc. Natl. Acad. Sci. U.S.A.* **1970**, *65*, 823.

(194) Itoh, K.; Azumi, T. *J. Chem. Phys.* **1975**, *62*, 3431.

(195) Chattopadhyay, A.; Mukherjee, S. *Biochemistry* **1993**, *32*, 3804.

(196) Lakowicz, J. R. *Principles of Fluorescence Spectroscopy, 3rd edition*; Springer: New York, 2006.

(197) Dutt, G. B. *ChemPhysChem* **2005**, *6*, 413.

(198) Gierer, A.; Wartz, K. Z. *Naturforsch A* **1953**, *8*, 532.

(199) Dote, J. L.; Kivelson, D.; Schwart, R. N. *J. Phys. Chem.* **1981**, *85*, 2169.

(200) Julliard, M.; Chanon, M. *Chem. Rev.* **1983**, *83*, 425.

(201) Whitten, D. G. *Acc. Chem. Res.* **1980**, *84*, 981.

(202) Kondratenko, M.; Moiseev, A. G.; Perepichka, D. F. *J. Mater. Chem.* **2011**, *21*, 1470.

(203) Wishart, J. F. *Energy & Environmental Science* **2009**, *2,* 956.

(204) Paul, A.; Samanta, A. *J. Phys. Chem. B* **2007,** *111,* 1957.

(205) Liang, M.; Kaintz, A.; Baker, G. A.; Maroncelli, M. *J. Phys. Chem. B* **2012,** *116,* 1370.

(206) Koch, M.; Rosspeintner, A.; Angulo, G.; Vauthey, E. *J. Am. Chem. Soc.* **2012**, *134*, 3729.

(207) Santosh, K.; Samanta, A. *J. Phys. Chem. B* **2010,** *141,* 11638.

(208) Santosh, K.; Samanta, A. *ChemPhyschem* **2012,** *13,* 1956.

(209) Li, X.; Maroncelli, M. *J. Phys. Chem. A* **2011,** *115,* 11638.

(210) Wu, H.; Wang, H.; Xue, L.; Shi, Y.; Li. X. *J. Phys. Chem. B* **2010,** *114,* 14420.

(211) Lee, H. Y.; Issa, J. B.; Isied, S. S.; Castner, E. W. Jr.; Pan, Y.; Hussey, C. L.; Lee, K. So.; Wishart J. F. *J. Phys. Chem. C* **2012**, *116*, 5197.

(212) Yao, H.; Zhang, S.; Wang. J.; Zhou, Q.; Dong, H.; Zhang, X. J. *Chem. Eng. Data* **2012**, *57*, 875.

(213) Fletcher, K. A.; Pandey, S. *J .Phys. Chem. B* **2003**, *107*, 13532.

(214) Birks, J. B. *Photophysics of Aromatic Molecules*; Wiley-Interscience: New York, 1970.

(215) Gilbert, A.; Baggott, J.; Wagner, P. J. *Essential of Molecular Photochemistry*; Blackwell science Inc.: Cambridge, USA, 1991.

(216) Rohatgi-Mukherjee, K. K. *Fundamentals of Photochemistry*; Wiley Eastern Ltd: India, 1986.

(217) Becker, W. *Advanced time correlated single photon counting technique*; Springer: New York, 2005.

(218) Demas, J. N. *Excited state lifetime measurement*; Academic press: New York, 1983.

(219) O'Connor, D. V.; Phillips, D. *Time Correlated Single Photon Counting*; Academic: New York, 1984.

(220) Ware, W. R. *Creation and detection of the Excited State*; Lamola, A. A., Ed.; Marcel Dekker: New York, 1971; Vol. 1, Part A.

(221) Bevington, P. R. *Data Reduction and Error Analysis for the Physical Sciences*; McGraw-Hill: New York, 1969.

(222) McKinnon, A. E.; Szabo, A. G.; Miller, D. R. *J. Phys Chem.* **1977**, *81*, 1564.

(223) O'Connor, D. V.; Ware, W. R.; Andre, J. C. *J. Phys. Chem.* **1979**, *83*, 1333.

(224) Ware, W. R.; Doemeny, L. J.; Nemzek, T. L. *J. Phys Chem.* **1973**, *77*, 2083.

(225) Horng, M. L.; Gardecki, J.; Papazyan, A.; Maroncelli, M. *J. Phys. Chem.* **1995**, *99*, 17311.

(226) Fee, R. S.; Maroncelli, M. *Chem. Phys.* **1994**, *183*, 235.

(227) Rechthaler, K. *Chem. Phys.* **1994**, *189*, 99.

(228) Becke, A. D. *J. Chem. Phys.* **1993**, *98*, 5648.

(229) Lee, C.; Yang, W.; Parr, R. G. *Phys. Rev. B* **1998**, *37*, 785.

(230) Forster, J.P.; Weinhold, F. *J. Am. Chem. Soc.* **1980**, *102*, 7211.

(231) Frisch, M. J.; Trucks, G. W.; Schlegel, H. B.; al., e. GAUSSIAN 03; Gaussian, Inc.: Wallingford, CT, 2004.

(232) Pensado, A. S.; Gomes, M. F. C.; Lopes, J. N. C.; Malfreyt. P.; Padua, A. A. H. *Phys. Chem. Chem. Phys.* **2011**, *13*, 13518.

(233) Harsha, V. R. A.; Kashyap, H. K.; Biase, P. M. D.; Margulis, C.J. *J. Phys. Chem. B* **2010**, *114*, 16838.

(234) Hardacre, C.; Holbrey, J. H.; Mullan, C. L.; Youngs, T. G. A.; Bowron, D. T. *J. Chem. Phys.* **2010**, *133*, 074510.

(235) Masaki, T.; Nishikawa, K.; Shirota, H. *J. Phys. Chem. B* **2010**, *114*, 6323.

(236) Tsuzuki, S.; Matsumoto, H.; Shinoda, W.; Mikami, M. *Phys. Chem. Chem. Phys.* **2011**, *13*, 5987.

(237) Chapman, C.F.; Fee, R.S.; Maroncelli, M. *J. Phys. Chem.* **1995**, *99*, 4811.

(238) Yao, C.; Pitner, W. R.; Anderson, J. L. *Anal. Chem.* **2009**, *81,* 5054.

(239) Ignat'ev, N.; Sartori, P. *J. Flurine Chem.* **2000**, *103,* 57.

(240) Heider, U.; Hilarius, V.; Sartori, P.; Ignat'ev, N.; WO 00/2 Merck, Patent GmbH, Darmstad, Germany, 1969.

(241) Freemantle, M. *Chem. Eng. News* **2004**, *82,* 44.

(242) Paul, A.; Mandal, P. K.; Samanta, A. *J. Phys. Chem. B* **2005**, *109*, 9148.

(243) Maroncelli, M.; Fleming, G. R. *J. Chem. Phys.* **1987**, *86*, 6221.

(244) Fleming, G.R. *Chemical Applications of Ultrafast Spectroscopy*, Oxford University Press, New York, 1986.

(245) Eisenthal, K. B. *Acc. Chem. Res.* **1975**, *8,* 118.

(246) Grimme, S. *J*, Comput. Chem. **2006**, *27*, 1787.

(247) Weigend, F.; Ahlrichs, R. *Phys. Chem. Chem. Phys.* **2005**, *7*, 3297.

(248) Weigend, F. *Phys. Chem. Chem. Phys.* **2006**, *8***,** 057.

(249) TURBOMOLE V6.2 2010, a development of University of Karlsruhe and Forschungszentrum Karlsruhe GmbH, 1989-2007, TURBOMOLE GmbH, since 2007; available from http://www.turbomole.com**.**

(250) Rahim, Z.; Barman, B. N. *Acta Cryst. A* **1978**, *34*, 761.

(251) Desmukh, M. M.; Gadre, S. R. *J. Phys. Chem. A* **2009**, *113*, 7927.

(252) Jesus, A. J. L.; Rosadoa, M. T. S.; Reva, I. *J. Phys. Chem. A* **2008**, *112*, 4669.

(253) Steiner, T. *Angew. Chem. Int. Ed.* **2002**, *41*, 48.

(254) Agmon, N. *J. Phys. Chem.* **1990**, *94*, 2959.

(255) Maroncelli, M.; Fee, R.S.; Chapman, C. F.; Fleming, G. R. *J. Phys. Chem.* **1991**, *95*, 1012.

(256) Stoppa, A.; Hunger, J.; Buchner, R.; Hefter, G.; Thoman, A.; Helm, H. *J. Phys. Chem. B* **2008**, *112*, 4854.

(257) Mali, K. S.; Dutt, G. B.; Mukherjee, T. *J. Chem. Phys.* **2005**, *123*, 174504.

(258) Small, E.W.; Isenberg, I. *Biopolymers* **1977**, *16*, 1907.

(259) Sension, R. J.; Hochstrasser, R. M. *J. Chem. Phys.* **1993**, *98*, 2490.

(260) Valeur, B. *Molecular fluorescence, principles and applications*. Wiley-VCH, Weinheim (FRG), Chapter 8, 2002.

(261) Hartman, R. S.; Alavi, D. S.; Waldeck, D. H. *J. Phys. Chem.* **1991**, *95*, 7872.

(262) Edward, J. T. *J. Chem. Educ.***1970**, *47*, 261.

(263) Hu, C. M.; Zwanzig, R. *J. Chem. Phys.* **1974**, *60*, 4354.

(264) Anderton, R. M.; Kauffman, J. F. *J. Phys. Chem.* **1994**, *98*, 12117.

(265) Kim, Y. R.; Hochstrasser, R. M. *J. Phys. Chem.* **1992**, *96*, 9595.

(266) Mannekutla, J. R.; Ramamurthy, P.; Mulimani, B. G.; Inamder, S. R. *Chem. Phys.* **2007**, *340*, 149.

(267) Pal, T.; Biswas, R. *Chem. Phys. Lett.* **2011**, *517*, 180.

(268) Guchhait, B.; Daschakraborty, S.; Biswas, R. *J. Chem. Phys.* **2012**, *136*, 11847.

(269) Kurnikova, M. G.; Balabai, N.; Waldeck, D. H.; Coalson, R. D**.** *J. Am. Chem. Soc.* **1998**, *120*, 6121.

(270) Maciejewski, A.; Kubicki, J.; Dobek, K. *J. Phys. Chem. B* **2003**, *107*, 13986.

(271) Shan, S.; Herschlag, D. *Proc. Natl. Acad. Sci. U.S.A.* **1996**, *93*, 14474.

(272) Horng, M. L.; Gardecki J, Maroncelli, M. *J. Phys. Chem. A* **1997**, *101*, 1030.

(273) Guo, Z.; Lue, B. M.; Thomasen, K.; Meyer, A. S.; Xu, X. *Green Chem.* **2007**, *9*, 1362.

(274) Klamt, A. *J. Phys. Chem.* **1995**, *99*, 2224.

(275) Baker, S. N.; Baker, G. A. Bright, F.V. *Green Chemistry* **2002**, *4*, 165.

(276) Harifi-Mood, A. R.; Habibi-Yangjeh, A.; Gholami, M. R. *J. Phys. Chem. B* **2006**, *110*, 7073.

(277) Ficke, L. E.; Brennecke, J. F. *J. Phys. Chem. B* **2010**,*114*, 10496.

(278) Jarosik, A.; Krajewski, S. R.; Lewandowski, A. *J. Mol. Liq.* **2006**, *123*, 43.

(279) Tokuda, H.; Baek, S. J.; Watanable, M. *Electrochemistry* **2005**, *73*, 620.

(280) Carvalho, P. J.; Alvarez, V. H.; Schroeder, B.; Gil, A. M.; Marrucho, I. M.; Aznar, M. Santos, L. M. N. B. F.; Coutinho, J. A. P. *J. Phys. Chem. B* **2009**, *113*, 6803.

(281) Skillet, M. B.; Yokozeki, A. *J. Chem. Eng. Data* **2009**, *54*, 108.

(282) Cammarata, L.; Kazarian, S. G.; Salterb, P. A.; Welton, T. *Phys. Chem. Chem. Phys.* **2001**, *3*, 5192.

(283) Cislak, F. E.; Hamilton, C. S. *J. Am. Chem. Soc.* **1931**, *53*, 746.

(284) Biswas, R.; Shirota, H. *J. Phys. Chem. B* **2012**, *116*, 13765.

(285) Li, B.; Wang, Y.; Wang. X.; Vdovic, S.; Guo, Q.; Xia, A. *J. Phys. Chem. B* **2012**, *116*, 13272.

(286) Zhang, Q. G.; Wang, N. N.; Yu, Z. W. *J. Phys. Chem. B* **2010**, *114*, 4747.

(287) Wang, N. N.; Zhang, Q. G.; Wu, F. G.; Li, Q. Z.; Yu, Z. W. *J. Phys. Chem. B* **2010**, *114*, 8689.

(288) Zhang, Q. G.; Wang, N. N.; Wang, S. L.; Yu, Z. W. *J. Phys. Chem. B* **2011**, *115*, 11127.

(289) Bondi, A. *J. Phys. Chem.* **1964**, *68*, 441.

(290) Dewar, M. J. S.; Zoesisch, E. G.; Healy, E. F.; Stewart, J. J. P. *J. Am. Chem. Soc.* **1985**, *102*, 3902.

(291) Ziyada, A. K.; Wilfred, C. D.; Bustam, M. A.; Man, Z.;Murugesan, T. *J. Chem. Eng. Data* **2010**, *55*, 3886.

(292) Muhammad, N.; Man, Z. B.; Bustam, M. A.; Mutalib, M. I. A.; Wilfred, C. D.; Rafiq, S. *J. Chem. Eng. Data* **2011**, *56*, 3157.

(293) Muhammad, N.; Man, Z.; Ziyada, A. K.; Bustam, M. A.; Mutalib, M. I. A.; Wilfred, C. D.; Rafiq, S.; Tan, I. M. *J. Chem. Eng. Data* **2012**, *57*, 737.

(294) Gu, Z.; Brennecke, J. F. *J. Chem. Eng. Data* **2002**, *47*, 339.

(295) Taib, M. M.; Ziyada, A. K.; Wilfred, C. D.; Murugesan. *J. Mol. Liq.* **2011**, *158*, 101.

(296) Ediger, M. D. *Annu. Rev. Phys. Chem.* **2000**, *51*, 99.

(297) Sillescu, H. *J. Non-Cryst. Solids* **1999**, *243*, 81.

(298) Ediger, M. D.; Angell, C. A.; Nagel, S. R. *J. Phys. Chem.* **1996**, *100*, 13200.

(299) Moynihan, C. T. *J. Phys. Chem.* **1966**, *70*, 3399.

(300) Angell, C. A. *J. Chem. Phys.* **1967**, *46*, 4673.

(301) Chakrabarti, D.; Bagchi, B. *Phys. Rev. Lett.* **2006**, *96*, 187801.

(302) Shlesinger, M. F.; Zaslavsky, G. M.; Klafter, J. *Nature* **1993**, *363*, 31.

(303) Habasaki, J.; Ngai, K. L. *J. Chem. Phys.* **2008**, *129*, 194501.

(304) Hu, Z.; Huang, X.; Annapureddy, H. V. R.; Margulis, C. J. *J. Phys. Chem. B* **2008**, *112*, 7837.

(305) Kobrak, M. N. *J.Chem. Phys*. **2006**, *125*, 064502.

(306) Kimura, Y.; Fukuda, M.; Suda, K.; Terazima, M. *J. Phys. Chem. B* **2010**, *114,* 11847.

(307) Ueno, K.; Angell, C. A. *J. Phys. Chem. B* **2011**, *115*, 13994.

(308) Kwon, O.-H.; Yoo, T. H.; Othon, C. M.; Deventer, J. A. V.; Tirrel, D. A.; Zewail, A. H. *Proc. Natl. Acad. Sci. U.S.A*. **2010**, *107*, 17101.

(309) Li, M.; Jiang, M.; Zhang, Y.-X.; Fang, Q. *Macromolecules* **1997**, *30*, 470.